RKT 2798

8978-6003-RU-000

170p.

SPACE SYSTEMS ANALYSIS STUDY

SUMMARY REPORT

PREPARED FOR
JET PROPULSION LABORATORIES
CONTRACT NO. 950045

12 MARCH 1962

SPACE TECHNOLOGY LABORATORIES, INC.
A SUBSIDIARY OF THOMPSON RAMO WOOLDRIDGE INC.
ONE SPACE PARK · REDONDO BEACH, CALIFORNIA

8976-6006-RU-000

RKT 2798

SPACE SYSTEMS ANALYSIS STUDY

SUMMARY REPORT

12 March 1962

Prepared for

JET PROPULSION LABORATORY
California Institute of Technology
Contract No. 950045

Approved E. H. Tompkins

E. H. Tompkins
Associate Manager
Systems Analysis Department

SPACE TECHNOLOGY LABORATORIES, INC.
A Subsidiary of Thompson Ramo Wooldridge, Inc.
One Space Park
Redondo Beach, California

• PREFACE

In December 1960, Space Technology Laboratories, Inc., was awarded a one-year contract by the Jet Propulsion Laboratory for a Space Systems Analysis Study. This contract was later extended for an additional eight months, and this report summarizes the work accomplished between January 1961 and March 1962. Further details may be found in the seven formal reports and twenty-four informal memoranda listed under REFERENCES.

Generally, the work performed under the SSAS Contract has been confined to the consideration of advanced missions not yet in the development stage, or to generating new techniques applicable to wide classes of missions. This work falls roughly into two categories: (1) Lunar trajectories and guidance studies and (2) Orbit determination studies. In this Preface, the motivations behind these studies will be explained and the scope of the studies indicated.

LUNAR TRAJECTORIES AND GUIDANCE STUDIES

At the time this study was begun, it was felt that the area of earth-to-moon trajectories and missions had already been thoroughly and exhaustively studied by JPL, STL and others in connection with such specific missions as ABLE-5, RANGER, SURVEYOR, etc. By contrast, the area of lunar return was understood in only a rough and sketchy way. Therefore a concentrated effort was directed toward this problem.

First, it was necessary to be able to generate with ease moon-to-earth trajectories satisfying specified end conditions. For this purpose, the Analytic Lunar Return Program, which is described in Part I, was developed (see References [2] and [4].) The three-dimensional trajectory model used in this program is "analytic" in the sense that it consists of two closed form (conic) trajectories which are joined at the moon's sphere of influence. This feature permits the "split end-point" trajectory problem to be solved rapidly and also permits large numbers of moon-to-earth trajectories to be generated and studied parametrically with ease.

Next, a thorough understanding of moon-to-earth trajectories was gained by analysis and computation to establish the relationships between lunar injection parameters, earth atmosphere re-entry parameters, trajectory

geometry, time of launch, time of flight, etc. The sensitivity of moon-to-earth trajectories to launch errors (miss coefficient analysis) and midcourse corrections was also investigated. Although this work could, in principle, have been performed on existing computer programs (such as the STL Encke Program), a more elaborate and efficient study was possible through use of the specialized Lunar Return Program. As illustrated in Part I, very good agreement was obtained between the results from this program and an "exact" (integrating) program.

In conjunction with the trajectory analysis described above, two moon-to-earth mission analysis studies were also performed and are discussed in Part II. These studies covered, in addition to free flight trajectory analysis,

1) A parametric study of powered flight from the lunar surface (Reference [1]),

2) An analysis of launch guidance errors, and

3) Monte Carlo simulations of tracking and midcourse guidance (Reference [3]).

The two missions considered were a "standard" lunar return, employing all the sophistication necessary for a manned mission, and a "minimal" lunar return, applicable, for example, to a sample return from a landed SURVEYOR spacecraft. Subsequent to the mission simulation work reported in Reference [3] additional work has been done on this problem, using a new noise model for tracking observations, and a more exact error analysis has been made of the minimal mission. Thus Part II is actually a revised version of Reference [3] and for this reason is somewhat longer and more detailed than the other parts.

The lunar return mission studies show that both of the above missions are feasible from the point of view of guidance, using either existing equipment or equipment which is compatible with the present state-of-the-art. For example, for the standard mission, re-entry conditions can be controlled to an accuracy of

$$\sigma_{long} = 0.07^{\circ}\ (4\ \text{n mi}), \qquad \sigma_{lat} = 0.2^{\circ}\ (10\ \text{n mi}), \qquad \sigma_{\beta e} = 0.1^{\circ}$$

using two (attitude controlled) midcourse corrections. For the minimal mission, an accuracy of

$$\sigma_{long} = 0.67^{o} \quad , \qquad \sigma_{lat} = 0.45^{o}$$

can be attained using two (spin stabilized) midcourse corrections. (For the minimal mission, re-entry angle β_e is not controlled by midcourse corrections since it is not a critical parameter.) Velocity requirements for launch and for midcourse correction were also estimated for both missions.

The same earth-moon model as used for moon-earth trajectories, employing the moon's sphere of influence, is currently being used to study circumlunar trajectories. This effort is discussed in Part III and in References [27] and [30]. Two basic categories of circumlunar trajectories are under consideration: free-return, or true circumlunar, and non-free-return, in which a velocity increment ΔV is required in the vicinity of the moon to modify the nominal trajectory and make it return to earth.

Emphasis will be on non-free-return trajectories, of which the free-return examples will be special cases. The motivation for studying non-free-return trajectories is that the free-return type is a very restricted class which may not be compatible with many mission objectives, such as having widest freedom in choosing day, time of launch, and pericynthion altitude, and being able to pass over a specified point on the moon's surface. Non-free-return also includes the case of "aborting" near the moon an arbitrary lunar return trajectory.

ORBIT DETERMINATION STUDIES

The term "orbit determination" is used here to mean the processing of noisy, redundant spacecraft "observations" to obtain (1) an estimate of the trajectory of the spacecraft and (2) a measure of the accuracy of the estimate, such as the covariance matrix of the estimate. In all practical methods of orbit determination, the problem is linearized so that the estimation procedure is a linear operation on observational "residuals"; the various techniques differ in the weights assigned to observations and in the resultant covariance matrix of the estimate.

Work on the statistical theory of orbit determination was conducted in two phases and is described in Part IV (see References [5] and [6].) In the first phase, the question of how to handle correlated observations was studied. When observations are correlated, one is faced with the necessity of choosing among several statistical estimation techniques to select the method most appropriate for trajectory applications. This led to a comparative study of least squares and minimum variance methods. As a result of this study, it was concluded that the most suitable technique, both from the point of view of computational simplicity and accuracy, was a particular form of weighted least squares estimation in which the weights assigned to observations are determined not only by the mean square value of the noise but also by the degree of correlation among observations.

Having decided in phase one on the character of the estimation technique, this technique was expanded in phase two to encompass the many special problems which arise in orbit determination: (1) the handling of a priori data, (2) the separation of parameters into classes, according to whether or not they are being estimated, (3) tracking through a midcourse maneuver, and (4) modifying the equations to make them more suitable for spacecraft on-board computation.

In conjunction with, and in addition to, the above theoretical studies, a new computer program, the Tracking Accuracy Prediction Program - (TAPP, Mod I) was developed, and is discussed in Part V (see Reference [7].) This program was designed not for real time tracking, but as an analytical tool for predicting the results of real time tracking and guidance of spacecraft. Thus, for reasons of simplicity and speed, sequences of conics about the principal bodies in question (earth, moon, sun, planets) were used to compute trajectories instead of the true solutions to the equations of motion. In all other respects, however, the program simulates real time tracking operations, and the fact that "analytic" trajectories are employed should have only a slight effect on the results the program was designed to yield.

In common with other orbit determination or tracking programs, TAPP I determines the covariance matrix of estimates of orbital parameters for various types of observational data, data rates, tracking intervals, and observational

noise models. In addition, however, it has the following features:

(1) It determines the statistical effect on orbit determination of uncertainties in physical constants* and tracking station location coordinates, and of biases in various data types.

(2) It simulates tracking "through" a midcourse correction, assigning an appropriate statistical uncertainty to errors in the execution of the correction.

TAPP I is thus particularly well suited to the design and analysis of advanced space missions and can answer many questions which were previously extremely difficult to analyze - viz., what are the effects of systematic errors, interacting with tracking and midcourse guidance, on the final accuracy of a space mission.

Concurrent with the completion of TAPP I, development has begun on a more powerful version (TAPP Mod II) in which the basic TAPP I program is used to drive a Monte Carlo process capable of a complete statistical tracking and guidance analysis of missions having multiple midcourse and terminal guidance maneuvers.

*GM of earth, sun and other planetary bodies, velocity of light, astronomical unit, etc.

ACKNOWLEDGMENT

The following personnel contributed to the results presented in this Summary Report:

E. H. Tompkins, Project Engineer
H. D. Culver
M. C. Fujisaki
G. J. Hanson
I. Kliger
P. Lipinski
A. S. Liu
T. A. Magness
J. B. McGuire
D. D. Morrison
W. H. Pace
P. A. Penzo
O. Senda
L. J. Skidmore
P. Steiner
C. C. Tonies
J. F. White
L. Wong

7

CONTENTS

		Page
• PREFACE		ii
• LUNAR TRAJECTORIES AND GUIDANCE STUDIES		1
I.	MOON-TO-EARTH TRAJECTORIES	1
	A. Introduction	1
	B. The Analytic Lunar Return Program	3
	The Trajectory Model • Program Application • Independent Parameters • Program Logic	
	C. Trajectory Analysis	6
	Earth Phase • Moon Phase • Sensitivity Coefficient Analysis	
	D. Program Accuracy	33
	Preliminary Study • Correction Scheme • Evaluation of Tau • Final Accuracy	
II.	LUNAR RETURN MISSION ANALYSIS	47
	A. Introduction and Summary of Conclusions	47
	B. The Standard Mission	50
	Mission Description • Transit Trajectory • Powered Flight and Injection Guidance • Midcourse Guidance	
	C. The Minimal Mission	76
	Mission Description • Transit Trajectory • Powered Flight and Injection Guidance • Midcourse Guidance	
	D. Orbit Determination for Return Mission	92
III.	CIRCUMLUNAR TRAJECTORIES	99
	A. Free-Return Circumlunar	99
	Introduction • General Analysis • Independent Parameters • Program Logic • Uses of the Program	

CONTENTS (Continued)

		Page
B.	Non-Free-Return Circumlunar Trajectories	107
	Introduction • Modification of the Analytic Circumlunar Program • Modification of the Analytic Lunar Return Program	
•ORBIT DETERMINATION STUDIES		111
IV.	ORBIT DETERMINATION THEORY	111
A.	Background	111
B.	Correlated Observations	113
C.	Special Topics	119
	A Priori Data • Separation of Parameters • Midcourse Maneuvers • Updated Least Squares	
D.	Examples	128
	Estimating Orbital Parameters • Weighting Correlated Data • Effect of Unsuspected Biases	
V.	TRACKING ACCURACY PREDICTION PROGRAM	137
A.	Introduction	137
B.	General Program Description	138
	Orbit and Ephemeris Computations • Search Routine • Rise-Set Times • Radar Derivatives • Normal Matrix • Tracking Accuracy Output • Midcourse Maneuvers	
•REFERENCES		155

ILLUSTRATIONS

Figure		Page
1-1	Location of Independent Parameters	2
1-2	General Logic Block Diagram	5
1-3	Re-entry Velocity (Altitude = 400,000 feet) versus Total Time of Flight for Various Distances to the Moon	7
1-4a	Earth Phase Velocity at the Sphere of Action versus Total Time of Flight for Various Distances to the Moon	8
1-4b	Earth Phase Flight Path Angle at the Sphere of Action versus Total Time of Flight for Various Distances to the Moon	8
1-5	Allowable Touchdown Cones for a Fixed Re-entry Angle and Two Flight Times	10
1-6	Re-entry Flight Path Angle versus Moon-to-Re-entry In-Plane Angle for Various Total Times of Flight	11
1-7	Touchdown Latitude versus Total In-Plane Angle from Moon to Touchdown for Various Declinations of the Moon	13
1-8	Allowable Re-entry Latitudes versus Time of Lunar Month for Various Flight Times and Re-entry Angles	15
1-9	Earth Phase Inclination with the Equator versus the Declination at Touchdown for Various Declinations of the Moon	17
1-10	Earth Phase Azimuth at Touchdown versus the Declination at Touchdown for Various Declinations of the Moon	18
1-11	Geometry at Moon's Sphere of Influence	19
1-12	Lunar Burnout Velocity (Altitude = 100,000 feet) versus Total Time of Flight for Various Distances of the Moon	21
1-13	Hyperbolic Excess Velocity and Velocity at the Moon's Sphere of Action versus Lunar Burnout Velocity at 100,000 feet Altitude above the Surface of the Moon	23
1-14	Earth-Moon-Probe Angle versus Total Time of Flight for Various Distances of the Moon	24
1-15	Moon Phase Geometry	26
1-16	Inclination of the Hyperbolic Plane versus Longitude Minus Earth-Moon-Probe Angle for Various Launch Site Latitudes (Selenographic)	27
1-17	Lunar Burnout Azimuth versus Longitude Minus Earth-Moon-Probe Angle for Various Launch Site Latitudes (Selenographic)	28

ILLUSTRATIONS (Continued)

Figure		Page
1-18	Launch Site-Asymptote In-Plane Angle (Hyperbolic Plane) versus Longitude Minus Earth-Moon-Probe Angle for Various Launch Site Latitudes (Selenographic)	29
1-19	Lunar Burnout Velocity (Altitude = 100,000 feet) versus Lunar Burnout - Asymptote In-Plane Angle for Various Lunar Burnout Flight Path Angles	30
1-20	Constant Burnout Flight Path Angle Contours	32
1-21	Launch Azimuth and Flight Path Angle Contours Mapped on the Surface of the Moon (Including Lunar Librations)	34
1-22	Sensitivity Coefficients at Re-entry to Burnout Velocity versus Selenographic Burnout Longitude	35
1-23	Sensitivity Coefficients at Re-entry to Burnout Flight Path Angle versus Selenographic Burnout Longitude	36
1-24	Sensitivity Coefficients at Re-entry to Burnout Azimuth versus Selenographic Burnout Longitude	37
1-25	Perturbation Correction Scheme	41
1-26a	Variation of τ with Time of Flight	43
1-26b	Variation of τ with Earth-Moon Distance	43
2-1	Schematic Diagram of the Standard Mission	51
2-2	Trajectory P-4. Equatorial Plane View	53
2-3	Trajectory P-4. Y-Z Plane View	54
2-4	Powered Flight Profile for Trajectory P-4	56
2-5	Single Correction Midcourse Velocity Requirements versus Time of Correction (Standard Mission)	65
2-6	Block Diagram of Monte Carlo Simulation of n Midcourse Corrections	66
2-7	Trajectory S-5. Equatorial Plane View	80
2-8	Trajectory S-5. Y-Z Plane View	81
2-9	Effect on Re-entry Point of Velocity Impulses Applied Along the Spin Axis at Different Times	86
2-10	Midcourse Velocity Requirements for Various Correction Time Pairs	88
3-1	Schematic of Circumlunar Flight	100
3-2	Entry and Exit Corridors at the Moon's Sphere of Influence for Circumlunar Trajectories	102
3-3	General Logic Block Diagram	106

ILLUSTRATIONS (Continued)

Figure		Page
4-1	Updated Least Squares Orbit Determination	127
4-2	Autocovariance Function $R = R_1 + R_2$ for Noise on Goldstone Angular Tracking Data	134
5-1	General Block Diagram	140
5-2	Orbit and Variational Equation Block Diagram	142
5-3	Data Processor Block Diagram	149
5-4	Illustration of the B-Plane Coordinate System	151

12

TABLES

Number		Page
1-1	Comparison of Results from Original Model with Results from an Integrating (Exact) Program	39
1-2	Results of the τ-Corrected Analytic Program	45
1-3	Sensitivity Coefficient Comparison Between the Analytic and Exact Programs	46
2-1	Injection and Re-entry Conditions for Trajectories P-3 and P-4	52
2-2	Uncorrected Re-entry Error as a Function of Source Errors, Autopilot Controlled Powered Flight	58
2-3	Injection Miss Coefficient	60
2-4	Uncorrected Miss Covariance Matrices	61
2-5	Standard Mission: Midcourse Velocity Requirement and Final Accuracy	72
2-6	Effect of Changes in Midcourse Execution Accuracy and Tracking Data Rate	73
2-7	Standard Mission	74
2-8	Burnout and Re-entry Conditions for Trajectories S-1, S-3, S-5	78
2-9	Re-entry Miss Coefficients	79
2-10	Re-entry Error Due to Each Independent Powered Flight Error Source. Trajectory S-1	83
2-11	Parameters of 40 Percent (1σ) Uncorrected Miss Ellipses	84
2-12	Midcourse Velocity Requirements for the Minimal Mission	87
2-13	Final Accuracies for Minimal Mission Utilizing Two Spin Stabilized Midcourse Corrections	90
2-14	Standard Mission. Trajectory P-4. Re-entry uncertainty resulting from 12^h to second midcourse correction	94
2-15	Standard Mission. Trajectory P-4. Re-entry uncertainty resulting from using or not using a priori data in tracking from 12^h to second midcourse correction	94
2-16	Standard Mission. Trajectory P-4. Effects on re-entry uncertainty of degraded angular accuracy, keeping R accuracy fixed	96
2-17	Standard Mission. Trajectory P-4. Effects of unsuspected biases on re-entry uncertainty	97
2-18	Minimal Mission Tracking Results for $\sigma_R = 0.5$ fps, $\sigma_A = \sigma_E = 0.2^o$, one set of observations per 10 minutes	98

TABLES (Continued)

Number		Page
4-1	Initial (Injection) Conditions for Earth-Moon Trajectory Employed in Orbit Determination Study	130
4-2a	Two Noise Correlation Models	131
4-2b	Maximum and Minimum Eigenvalues of the Four Correlation Matrices	131
4-3	Comparison of LS, MV and Uncorrelated Case Standard Deviations of Uncertainty in Orbital Elements at Epoch (Injection) for Lunar Trajectory, Data Sample A	133
4-4	Comparison of LS, MV and Uncorrelated Case Standard Deviations of Uncertainty in Orbital Elements at Epoch (Injection) for Lunar Trajectory, Data Sample B	133
5-1	Typical Noise Model for Terrestrial Tracker	145

14

• LUNAR TRAJECTORIES AND GUIDANCE STUDIES

I. MOON-TO-EARTH TRAJECTORIES

A. Introduction

For the purpose of studying moon-to-earth missions, it is desirable to be able to generate moon-to-earth trajectories by choosing values of the parameters listed below (see also Figure 1-1):

a) selenographic (lunar surface) launch site latitude*

b) launch site longitude*

c) day of launch

d) lunar powered flight control angle from launch to lunar burnout, and lunar powered flight time interval

e) burnout altitude*

f) re-entry maneuver downrange angle, and maneuver time from re-entry to touchdown

g) landing site latitude*

h) landing site longitude

i) re-entry flight path angle*

j) re-entry altitude*

k) total time of flight

It is important to determine (1) the lunar injection conditions and certain auxiliary trajectory variables (such as trajectory plane inclinations) which correspond to the above parameters, (2) the geometric constraints which must exist between all of these variables and parameters, and (3) the sensitivities of terminal variables on earth to the lunar injection conditions. A special computing program, the Analytic Lunar Return

*It should be understood that not all of these parameters may be chosen independently of the others. Asterisks denote a partial set of parameters which can be specified independently.

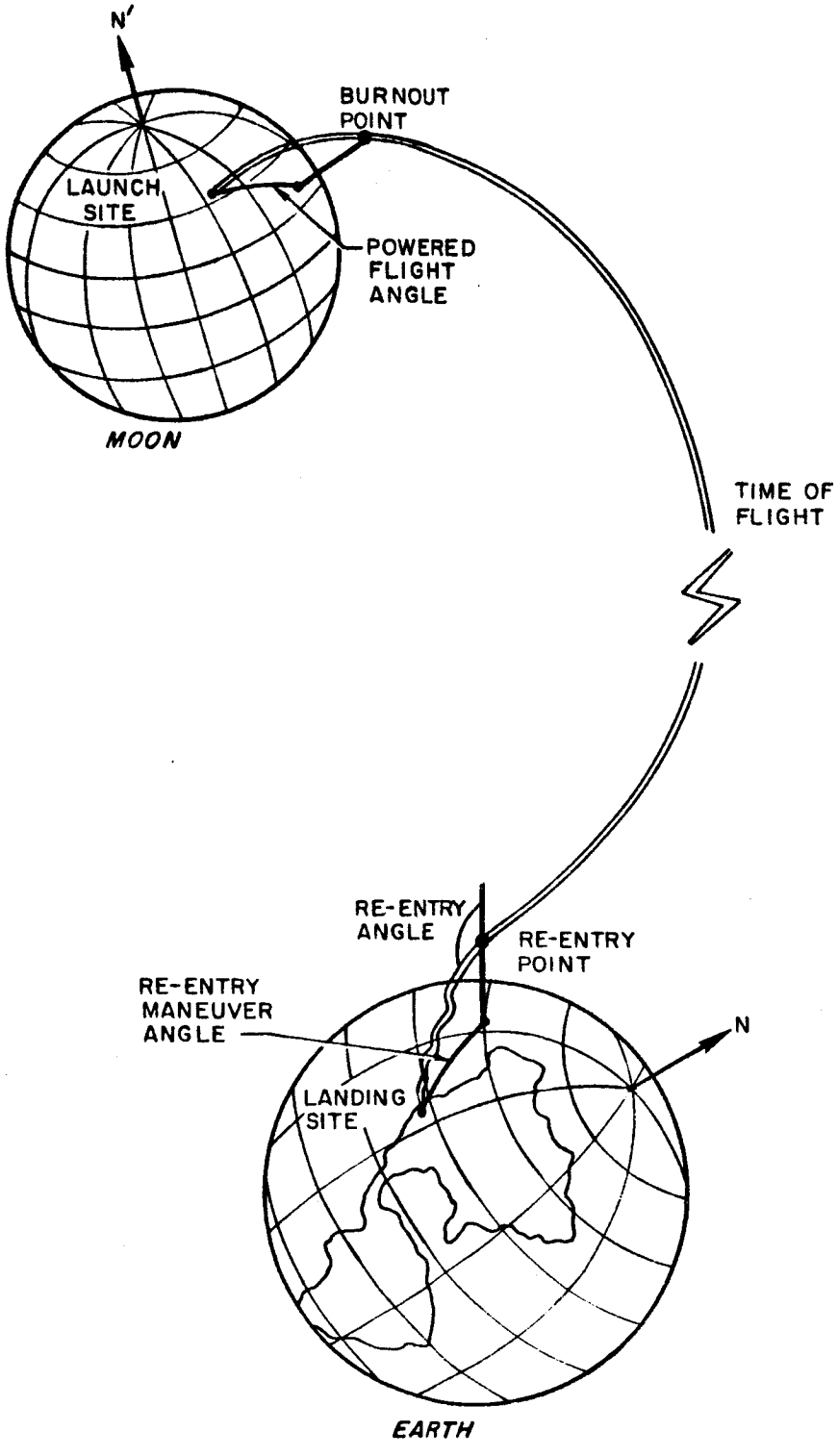

Figure 1-1. Location of Independent Parameters

Program (ALR)[2], was written to facilitate the study of moon-to-earth trajectories from this point of view. In the following sections we shall discuss, in order, the characteristics and logical organization of this program, and the major characteristics of moon-to-earth trajectories as determined with the aid of the ALR program, and the accuracy of the program.

B. The Analytic Lunar Return Program

The ALR Program has the following features:

1) It is "analytic" in that closed form solutions (conics) to the equations of motion are used, yielding a very high computational speed and making it feasible to perform elaborate parametric studies which only an analytic program would allow with reasonable machine time.

2) Search loops are provided to solve the "split-end-point" problem when parameters which are meaningful to the mission analyst are input to the program.

3) When used with the "τ-correction" (see Section D), the program supplies quite accurate approximate lunar burnout conditions for subsequent use with an n-body integration program to determine "exact" trajectories. To aid in this possibility, the lunar ephemeris tape used in the analytic program is the same as that used in STL integrating programs.

4) The Program may be made a part of other analytic programs requiring highest speed, such as a Monte Carlo guidance analysis program [3]. To facilitate this possibility the Program contains a Sensitivity Coefficient Routine which takes lunar burnout or midcourse conditions, introduces incremental changes in each variable, and determines the resulting perturbations at the earth.

5) By varying the size of the burnout or midcourse perturbations, nonlinear effects may be examined. This ability to simulate accurately nonlinear behavior, together with high computational speed, makes practical a Monte Carlo simulation of midcourse guidance freed of the necessity for the usual linearity assumptions.

The analytic model upon which this program is based was first presented by V.A. Egorov in 1956 [32]. In this model, earth-moon space is divided into two regions such that only the moon's gravitational field is effective in one region and only the earth's gravitational field is effective in the remaining region. The dividing surface is defined as the locus of points at which the ratio between the force with which the earth perturbs the motion of a third body and the force of attraction of the moon is equal to the ratio between the perturbing force of the moon and the force of attraction of the earth. This surface is approximately a sphere whose center is coincident with the center of the moon and whose radius is

$$r_s = 0.87\, r_m \left(\frac{m}{M}\right)^{2/5} \doteq 31{,}000 \text{ nautical miles } (57{,}400 \text{ km}),$$

where r_m is the mean earth-moon distance and m/M is the moon-earth mass ratio.

The problem which the program solves is to find the unique moon-phase and earth-phase conics which satisfy the input conditions (specified in the Introduction) and which match in position, velocity and time at the moon's sphere of influence. Rather than attempt to express orbital parameters explicitly as functions of input parameters, the computing technique used is to replace unknown parameters with "trial" values and iteratively solve the equations of motion until input and interface conditions are met, within prescribed tolerances. Figure 1-2 illustrates the general logic of the procedure. This technique has proved quite successful, requiring 4 to 9 iterations to converge.

After the above search is completed, miss coefficients are generated using the Sensitivity Coefficient Routine. This is a separate subprogram which employs explicit expressions and no iterations. It is possible to use explicit equations here because the split-end-point difficulties which complicate the search routine are no longer present.

The τ-correction, described in Section D, is an empirical perturbation made at the moon's sphere of influence to compensate for the moon's perturbing effect on the trajectory during the earth-phase of the trajectory.

GENERAL LOGIC

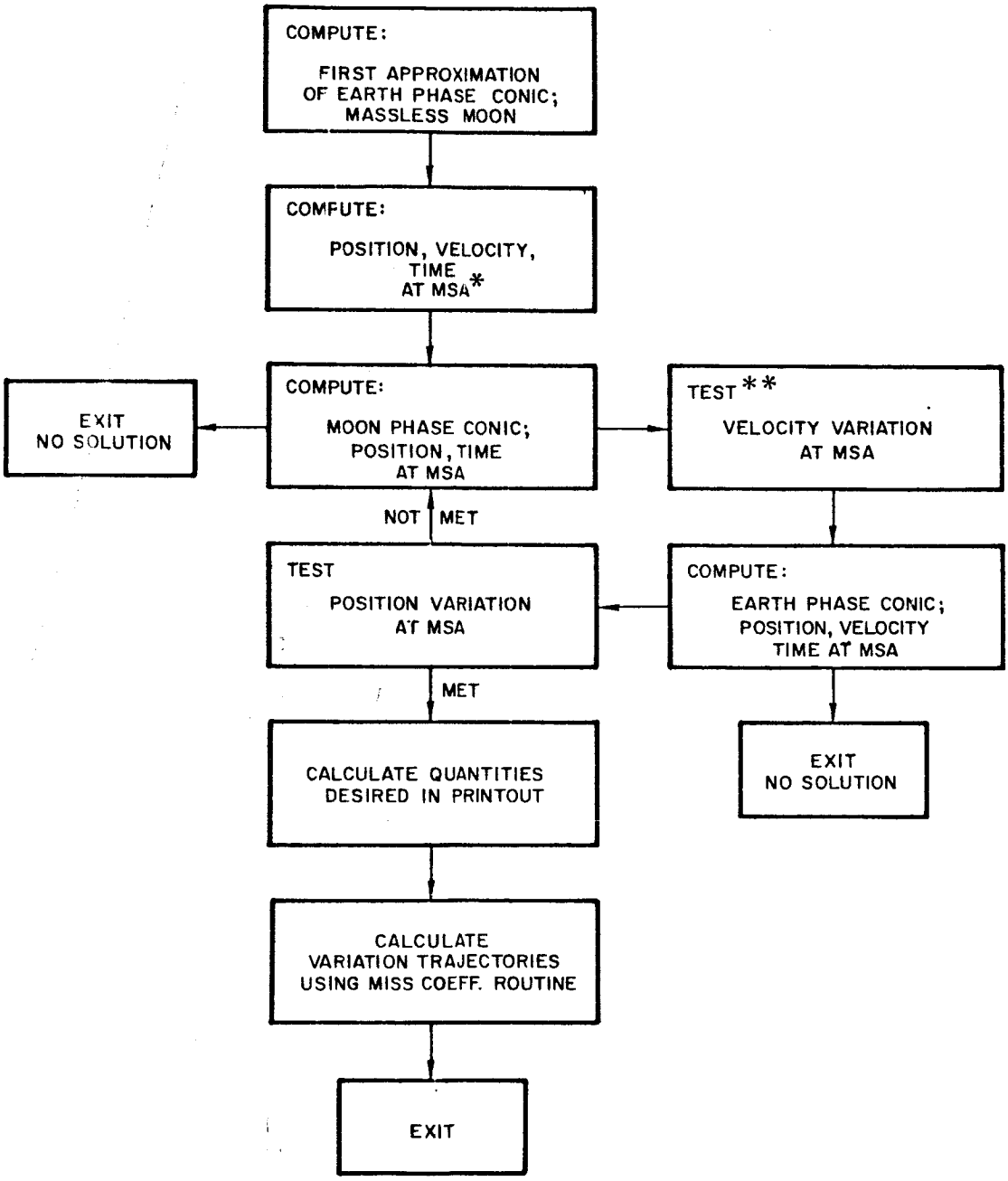

* MSA = MOON'S SPHERE OF ACTION.

** THE SUCCESS OF THIS TEST IS REGISTERED, AND IF THE POSITION TEST IS ALSO SATISFIED, THE PROGRAM EXITS THE SEARCH LOOP.

Figure 1-2. General Logic Block Diagram

C. Trajectory Analysis

1. Earth Phase

Since the moon's sphere of influence is only 31,000 nautical miles in radius, the major part of the trajectory will be the earth-phase conic. Apogee of this conic will be approximately the distance of the moon, or greater, while perigee will be roughly the radius of the earth, or less. Thus, the earth-phase conic will be a portion of a highly eccentric ellipse ($e \geq 0.96$), or else be parabolic or hyperbolic.

Since the trajectory consists almost entirely of the earth-phase conic, this phase may be studied independently of the lunar launch conditions. In performing such studies, it was discovered that many parameters depended primarily on the total time of flight and the distance of the moon.

During a lunar month, the earth-moon distance will vary by about 7.5 earth radii. Thus, for fixed flight times, vehicles launched on those days when the moon is farthest from the earth will have higher (earth phase) energies than those launched when the moon is closest to the earth. This observation is born out by Figure 1-3 which plots the re-entry velocity versus the total time of flight for different earth-moon distances. The effect of the re-entry flight path angle on the re-entry velocity was found to be negligible.

In a similar manner, it is possible to show that the velocity and flight path angle at the moon's sphere of influence will also depend on the time of flight and the distance to the moon. These quantities, however, will also depend upon the re-entry angle; particularly the flight path angle. The flight path angle at the moon's sphere of influence is shown in Figure 1-4b for shallow re-entry (this angle approaches 180 degrees for steep re-entry). The variation of the velocity at the sphere (Figure 1-4a) with the re-entry angle, on the other hand, is significant but small. The indication that steeper re-entry angles have lower velocities may be explained by the fact that these trajectories re-enter on the side of the earth facing the moon, whereas shallow re-entry trajectories come in on the back side of the earth.

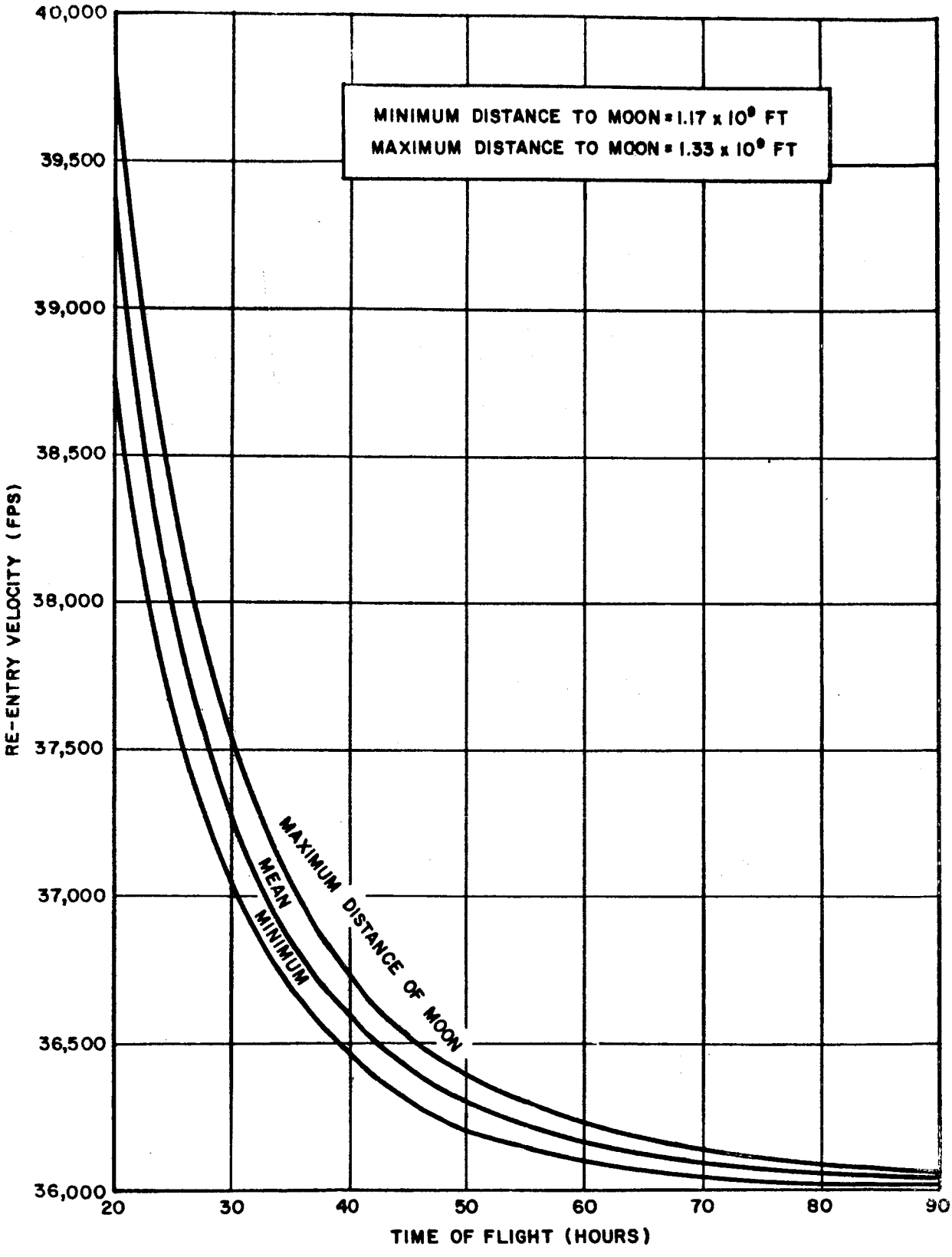

Figure 1-3. Re-entry Velocity (Altitude = 400,000 feet) versus Total Time of Flight for Various Distances to the Moon

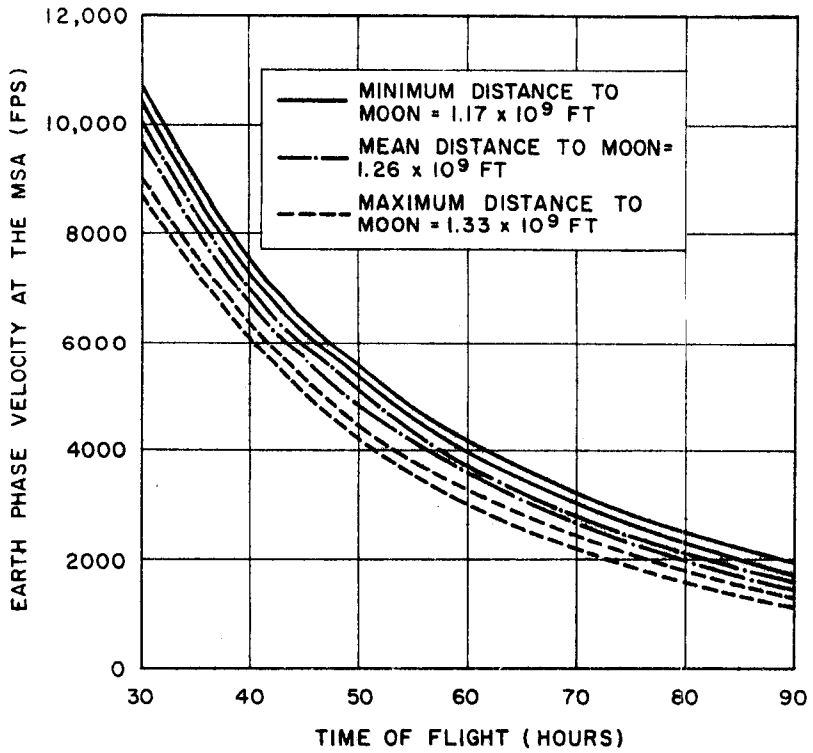

Figure 1-4a. Earth Phase Velocity at the Sphere of Action versus Total Time of Flight for Various Distances to the Moon. The Upper Curves Represent a Re-entry Angle of 96° and the Lower Curves a Re-entry Angle of 175°.

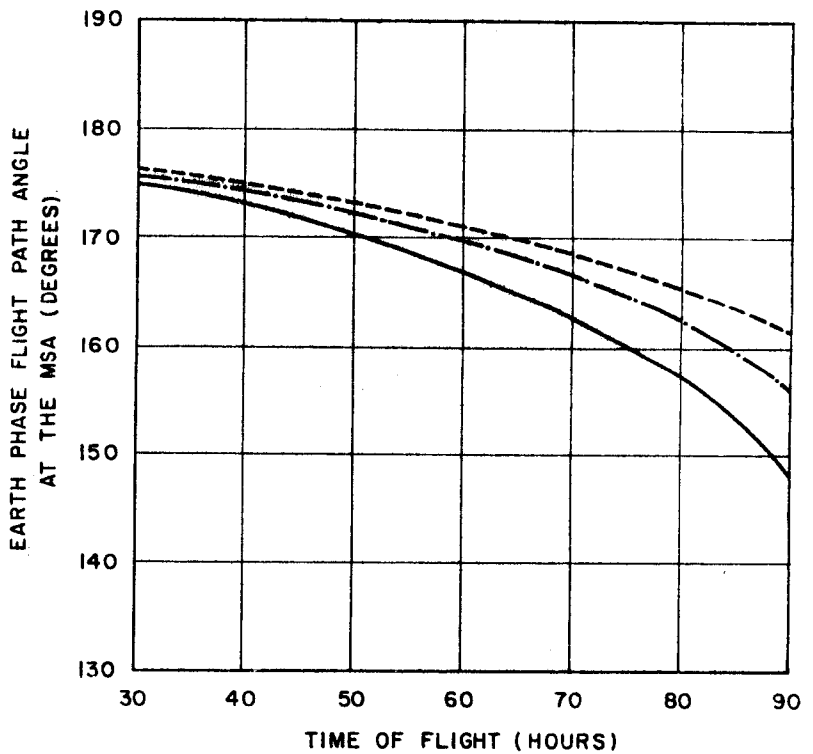

Figure 1-4b. Earth Phase Flight Path Angle at the Sphere of Action versus Total Time of Flight for Various Distances to the Moon. Re-entry Angle = 96°.

The steep re-entry trajectories, then, may have a distance as much as two earth radii less to travel than shallow re-entry trajectories, and therefore require less energy to accomplish this in the same amount of time.

Returning to the first observation that the majority of the lunar return trajectory will consist of the earth-phase conic, it has been shown for a range of analytic trajectories that the declination and right ascension of the moon at launch are within 1.5 degrees of that of the vehicle at the transfer point between the earth and moon phases. The reason for this is that just after lunar burnout, the vehicle very nearly cancels the angular velocity of the moon causing its angular position with respect to an inertial earth centered system to remain nearly fixed out to the transfer point. This fact, and the observation that the in-plane angle between the transfer point and the re-entry point (angle η_{sr} in Figure 1-5) remains essentially dependent only on the time of flight and the re-entry angle, permits us to plot Figure 1-6. This figure will aid in calculating latitude restrictions on the landing site.

On the basis of these observations, it is possible to define what may be called a "touchdown cone" as shown in Figure 1-5. This cone may be generated as follows:

a) For a given total flight time and a given re-entry flight path angle the in-plane angle, η_{sr} will be fixed and may be determined from Figure 6. With the arguments given above, this angle will be essentially the in-plane angle from the moon to re-entry.

b) The re-entry maneuver angle, if nonzero, may now be added to η_{sr} to produce the total in-plane angle from the moon to touchdown.

c) With this total in-plane angle fixed, it is possible to generate all possible earth phase conics which are launched from a certain declination of the moon, i.e., on a certain day, and which have a given total flight time, re-entry flight path angle and re-entry maneuver angle. These trajectories may be generated

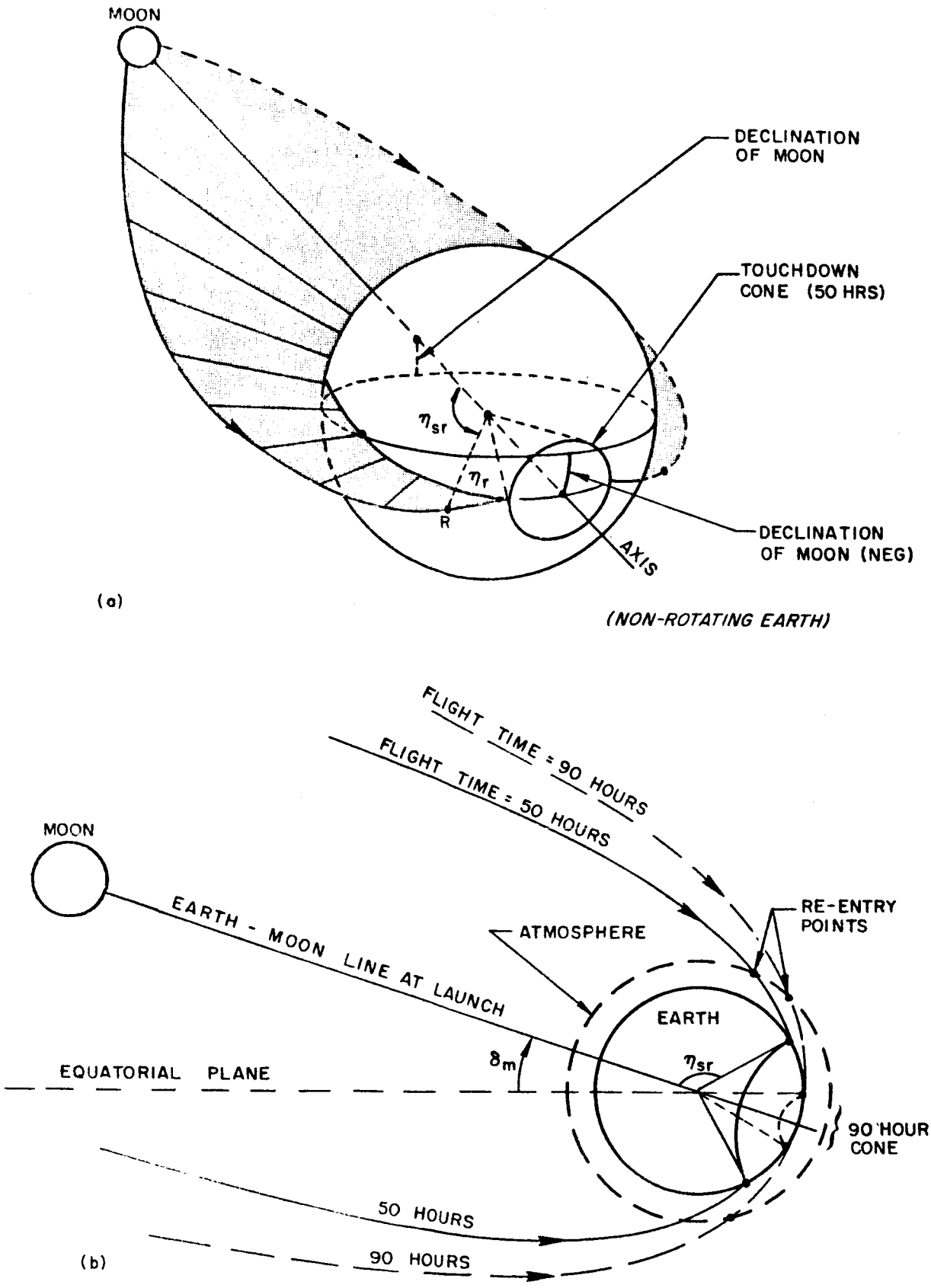

Figure 1-5. Allowable Touchdown Cones for a Fixed Re-entry Angle and Two Flight Times

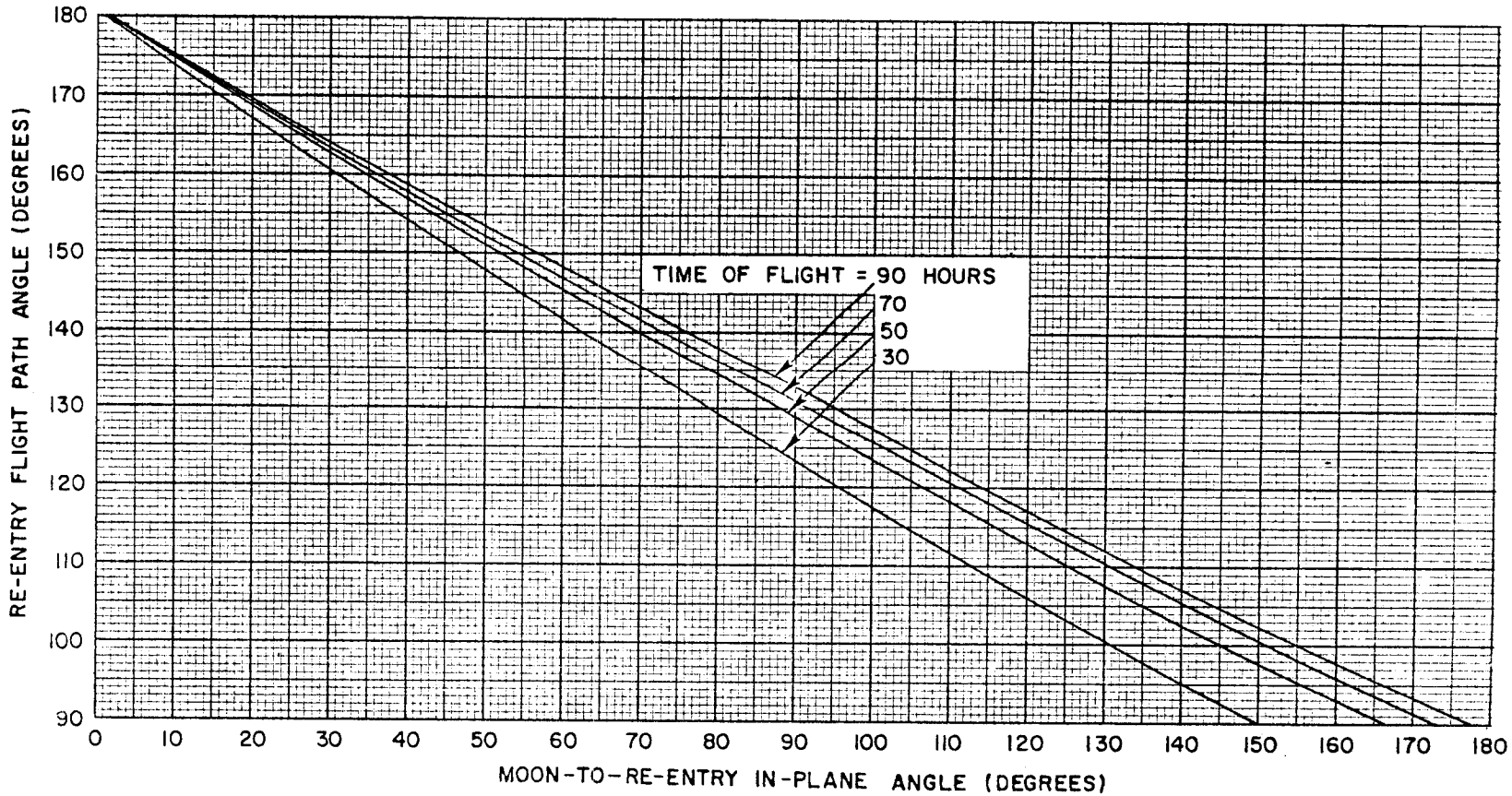

Figure 1-6. Re-entry Flight Path Angle versus Moon-to-Re-entry In-Plane Angle for Various Total Times of Flight

by rotating the in-plane conic about the earth-moon line producing the touchdown cone shown in Figure 1-5a. The two trajectories drawn represent counterclockwise re-entry (in the direction of earth's rotation) and clockwise re-entry.

It is clear that as re-entry progresses from shallow to steep angles, the angular radius of the cone will increase to a maximum of 90 degrees and then decrease, on the moon side of the earth, down to zero for a rectilinear trajectory. The allowable declination for this trajectory will be, as expected, identical to the declination of the moon at launch.

One question which can now be asked is: what restrictions does this process place on allowable landing sites? Certainly there will be no restriction on the landing site longitude since any longitude may be obtained with a given flight time by launching from the moon at the proper time of day. There are restrictions on the allowable landing site latitudes, however, and this is shown in Figure 1-5b. As indicated on this diagram, the landing site must be within a certain angular distance of the earth-moon axis as measured from the center of the earth. The maximum allowable latitude will be attained for the trajectory passing over the north pole whereas the minimum latitude will be for a trajectory passing over the south pole. These are shown in the figure for 50 and 90 hour flight times. Simple linear relationships may be obtained from this figure, giving these extremes of latitude as a function of the total in-plane angle and the declination of the moon. These are presented graphically in Figure 1-7. The manner in which this graph may be used is first, to decide what the total in-plane angle is, based on the total time of flight, the re-entry flight path angle, and the re-entry maneuver angle (with the aid of Figure 1-6, and second, to determine the declination of the moon on the day of launch. The allowable touchdown latitudes will then lie within the parallelogram for the given lunar declination and total in-plane angle.

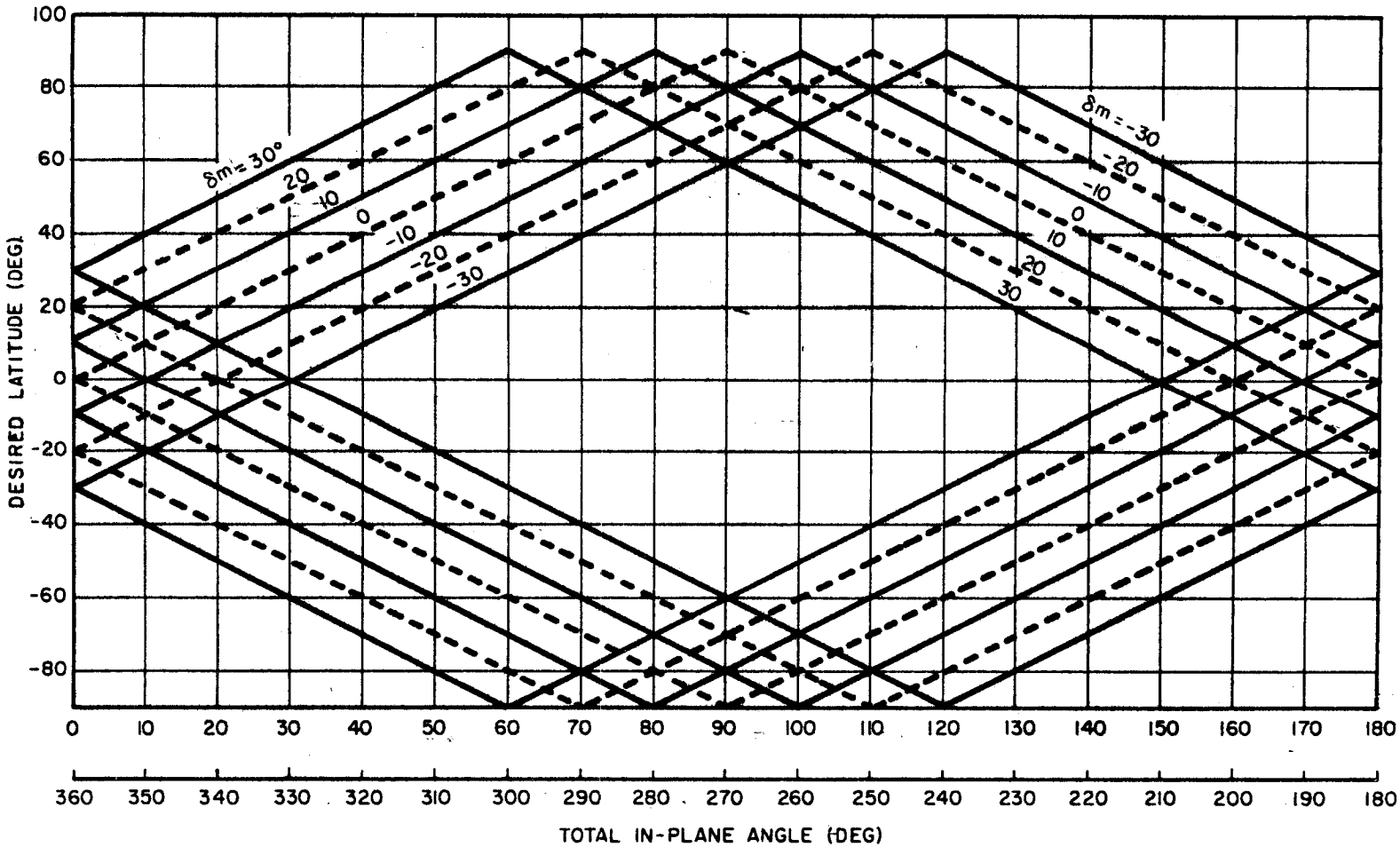

Figure 1-7. Touchdown Latitude versus Total In-Plane Angle from Moon to Touchdown for Various Declinations of the Moon. (Read allowable declinations within the closed figures)

This graph may also be used to answer the following question: for a given landing site latitude, total time of flight and re-entry flight path and maneuver angles, what are the allowable declinations of the moon (which is equivalent to days of the lunar month) for which a trajectory is possible? This question is easily answered by determining what lunar declination parallelograms will cause the desired touchdown latitude to lie within them for a fixed total in-plane angle.

The following two examples are given for illustration.

a) Simple lunar sample return mission:

Total time of flight = 70 hours
Re-entry flight path angle = 175 degrees
Re-entry maneuver angle = 0 degrees

From Figure 1-6, the moon-to-entry in-plane angle will be about 10 degrees. This will also be the moon-to-touchdown angle. If the desired landing site latitude is 20 degrees, then from Figure 1-7, the allowable declinations of the moon will be between 10 degrees to 30 degrees.

b) Apollo manned return mission:

Total time of flight = 70 hours
Re-entry flight path angle = 96 degrees
Re-entry maneuver angle = 40 degrees

From Figure 1-6, moon-to-re-entry in-plane angle will be about 160 degrees. Adding on the maneuver angle will make the total moon-to-touchdown angle equal to 200 degrees. (This angle will produce the same cone as one whose angle is 360 degrees - 200 degrees = 160 degrees). Again if the desired landing site latitude is 20 degrees then, from Figure 1-7, the allowable declinations of the moon will lie between 0 degrees and -30 degrees. For a particular lunar period it is possible, by use of the foregoing graphs, to plot latitude restriction curves such as shown in Figure 1-8. The time period in this case is the month of December in 1963. For a given launch date (which implies a given declination of the moon) and a given time of flight, the allowable re-entry latitudes shall lie

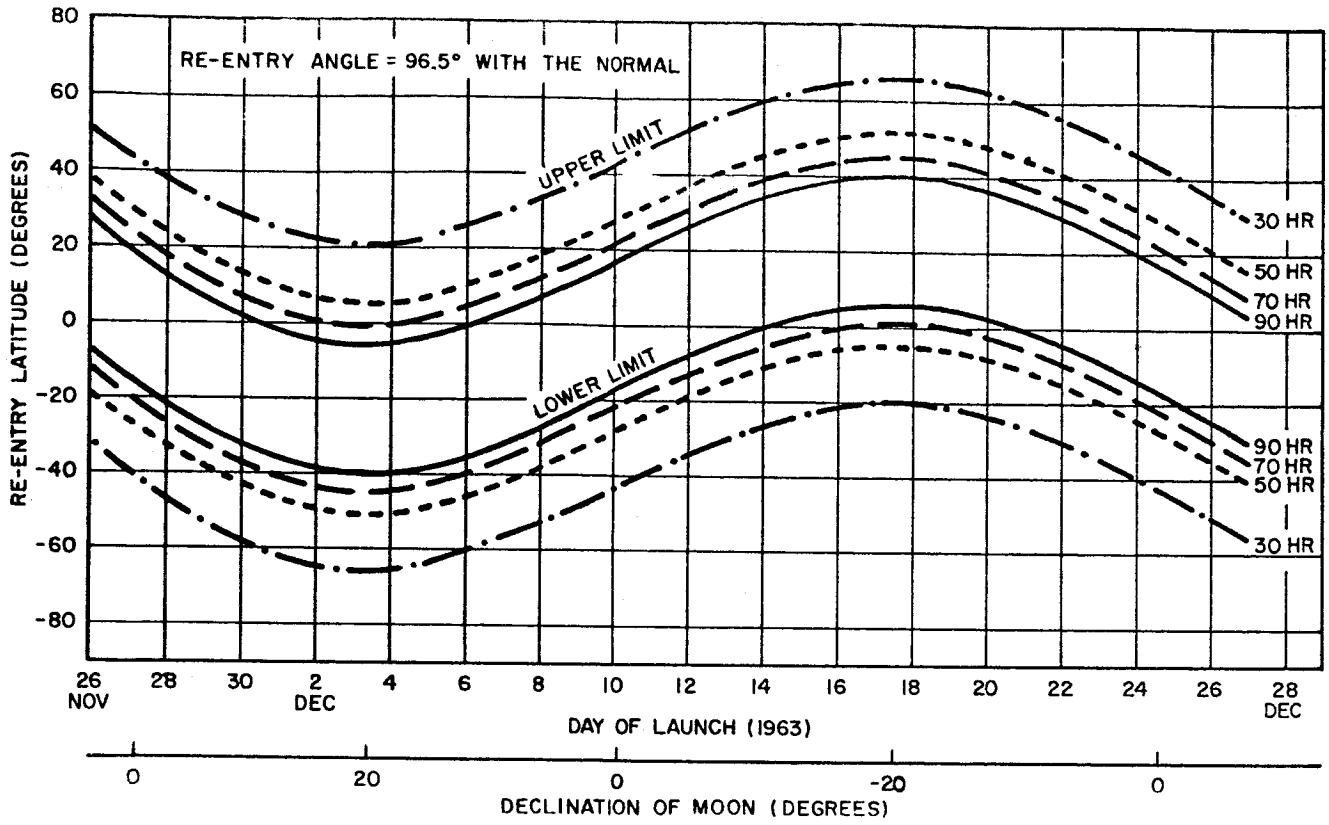

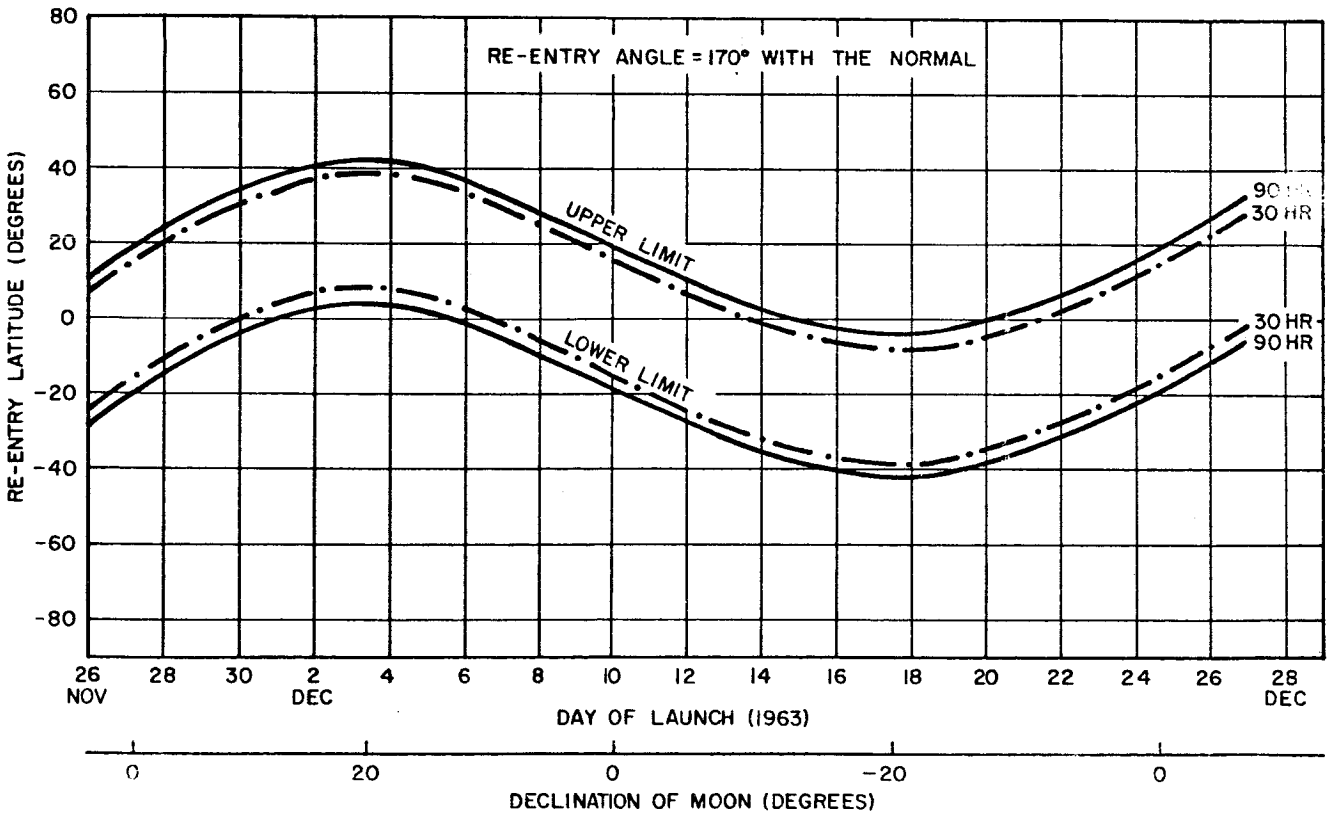

Figure 1-8. Allowable Re-entry Latitudes versus Time of Lunar Month for Various Flight Times and Re-entry Angles

between the two limiting curves. If the re-entry maneuver angle is taken into account, similar graphs may be drawn presenting limitations on landing latitudes.

The reduction of the number of significant variables that enter into the calculation of the earth-phase conic also makes it possible to graphically determine some of the angular quantities involved. For example the declinations of the moon and landing site and the total in-plane angles between these points will determine the orientation of the earth-phase conic. Figures 1-9 and 1-10 present the inclination of the conic and the azimuth at touchdown respectively for specific total in-plane angles. Graphs for a complete range of in-plane angles have been drawn, however, only these are presented for illustrative purposes. For the Standard Return mission presented in Part II where the declination of the moon is -10 degrees, Figures 1-9 and 1-10 indicate the inclination and azimuth to be about 32 and 62 degrees, respectively.

2. Moon Phase

The earth-phase analysis has been based primarily on the fact that many independent parameters at the moon have little affect on the earth-phase conic. To a certain extent, the reverse is also true. Bevore presenting some of the quantitative results generated by the Analytic Program, it is possible to deduce some qualitative properties of the moon-phase by visualizing the class of all earth-phase trajectories for a given flight time and a given re-entry angle. As deduced in the earth-phase analysis, this may be done without involving the shape or orientation of the moon-phase conic. Figure 1-11 shows such a class of trajectories. In this figure, no positions will be designated on the sphere of influence. Instead, only the velocity vector at the sphere, $\bar{v}_s$, projected from the center of the moon, will be drawn. As will be seen later, the directions of these velocity vectors will represent very nearly the direction of the hyperbolic asymptote of the moon-phase conic.

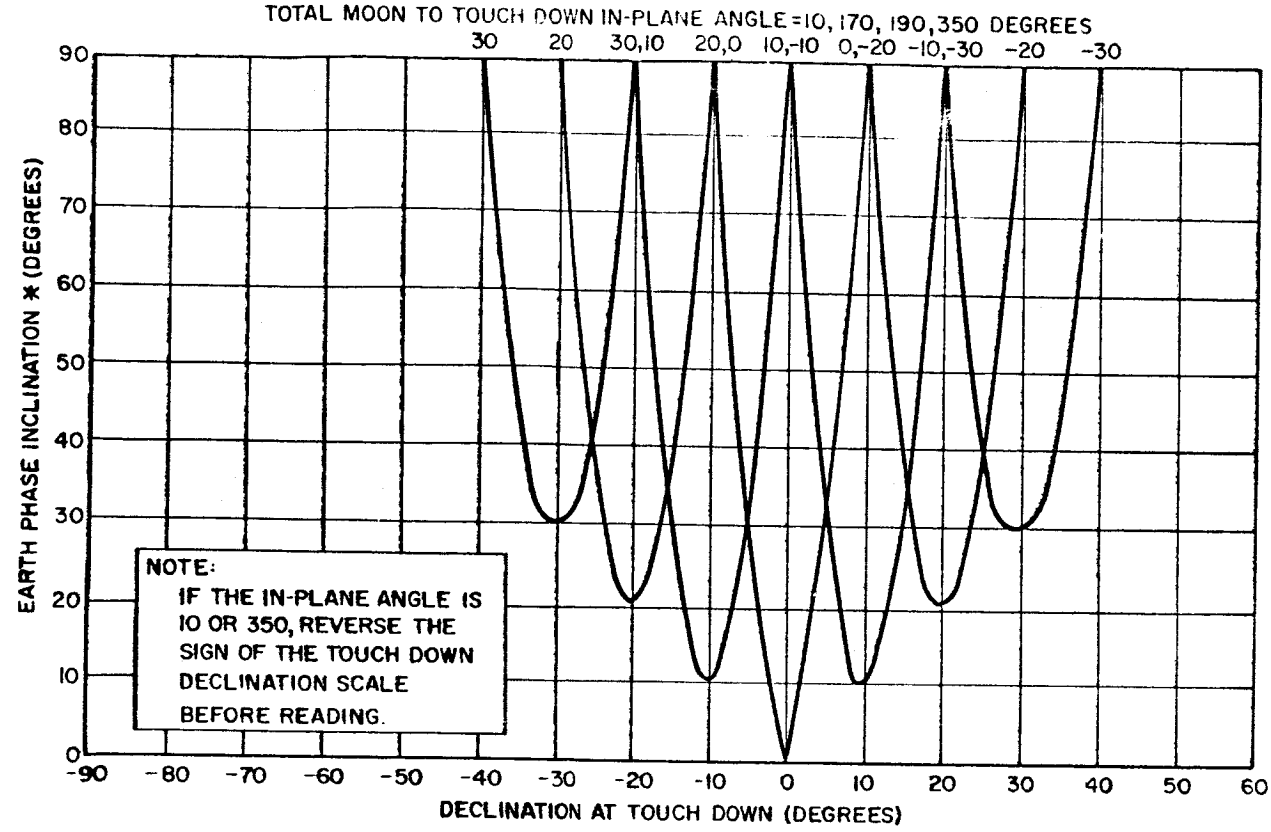

* FOR CLOCKWISE RE-ENTRY, TAKE THE INCLINATION TO BE 180° MINUS THE VALUE GIVEN HERE.

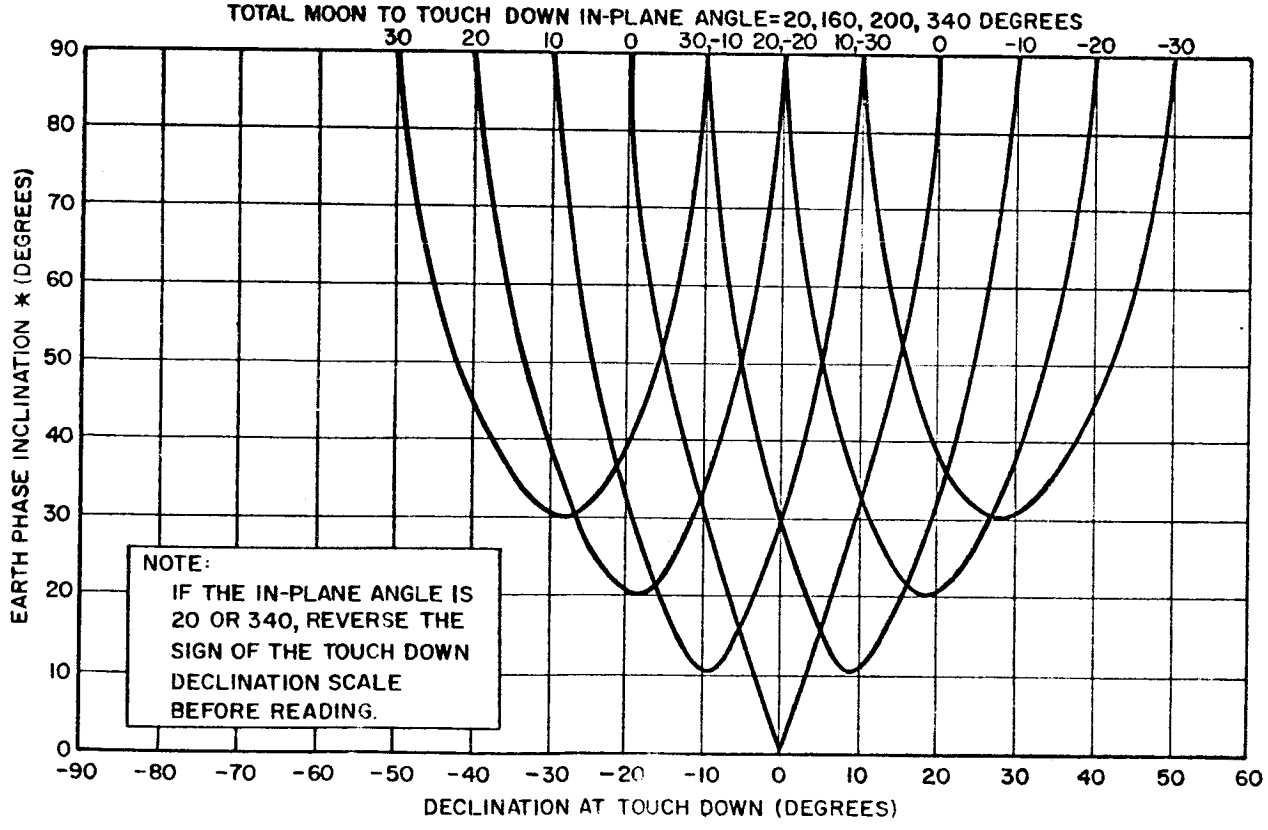

Figure 1-9. Earth Phase Inclination with the Equator versus the Declination at Touchdown for Various Declinations of the Moon

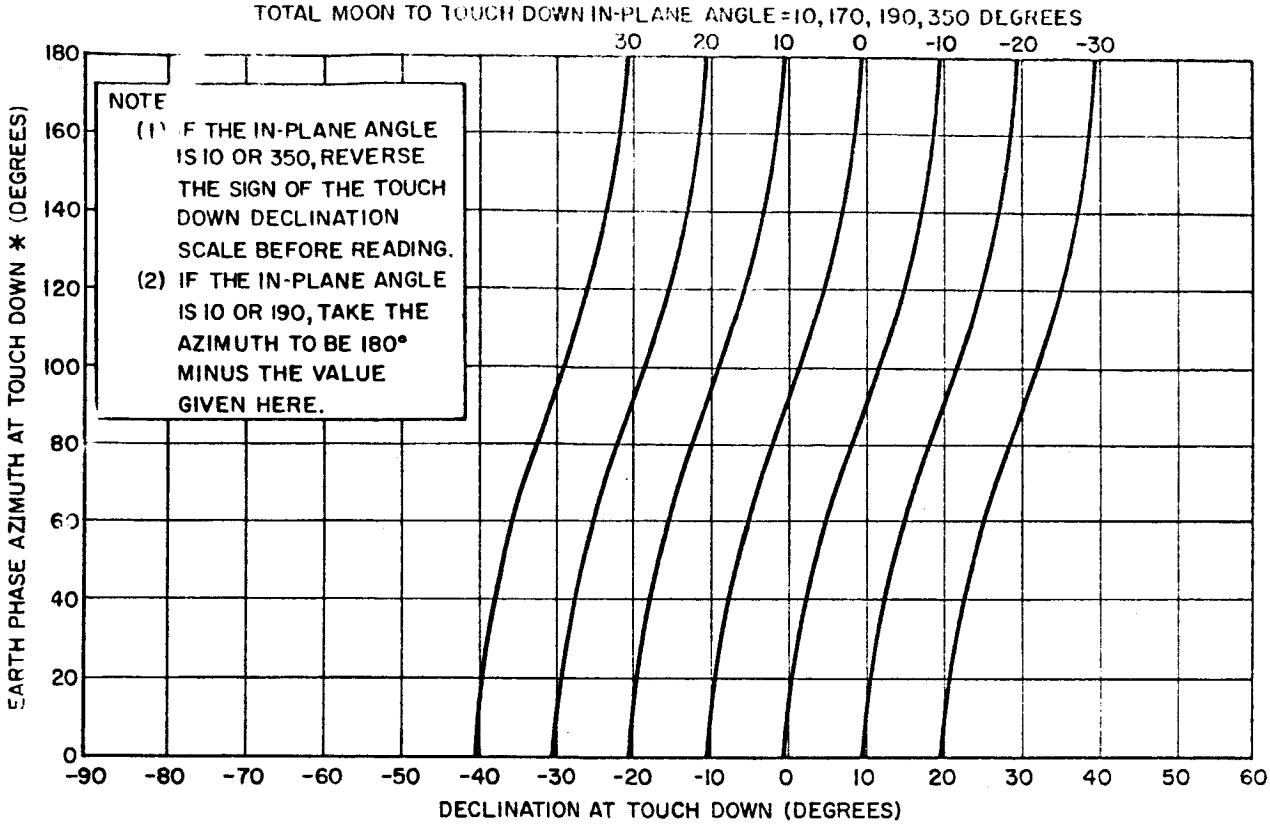

* FOR CLOCKWISE RE-ENTRY, TAKE THE AZIMUTH TO BE THE NEGATIVE OF THE VALUE GIVEN HERE.

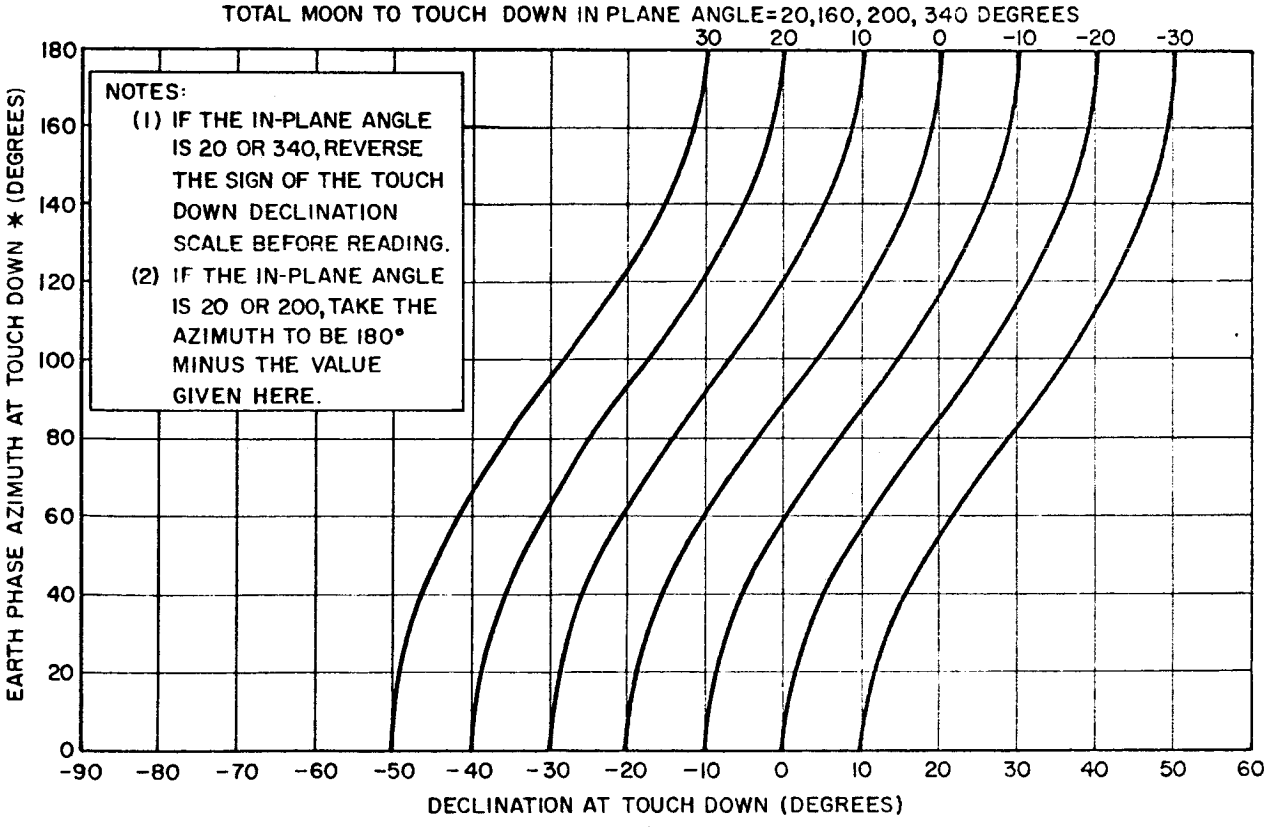

Figure 1-10. Earth Phase Azimuth* at Touchdown versus the Declination at Touchdown for Various Declinations of the Moon

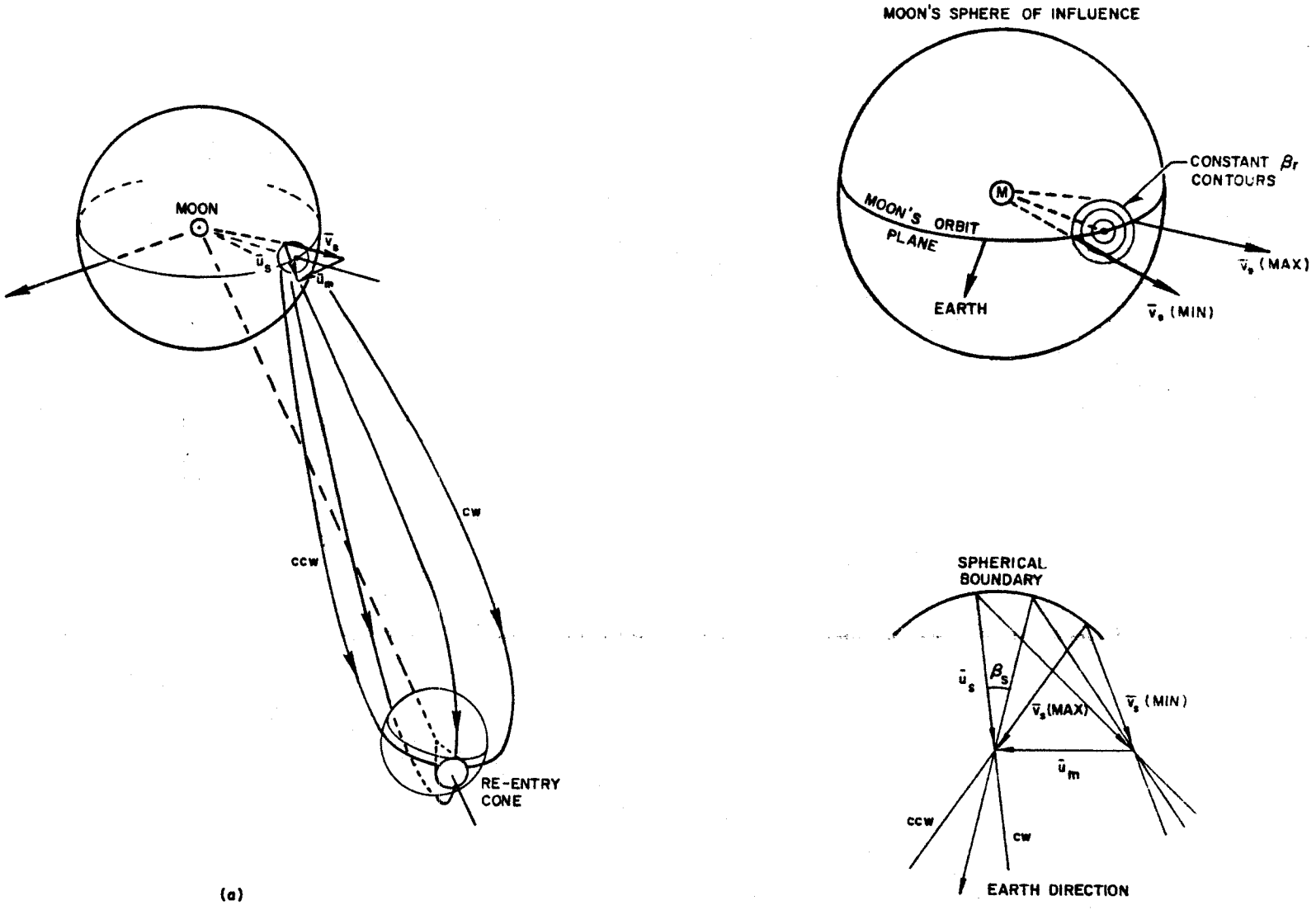

Figure 1-11. Geometry at Moon's Sphere of Influence

Continuing with Figure 1-11a, the earth-phaseconic has been drawn with respect to inertial space where $\bar{u}_s$ and $\bar{u}_m$ are the velocities of the vehicle and the moon respectively at the sphere relative to the earth. For a fixed day of launch, flight time, and re-entry flight path and maneuver angles, it is possible to draw the re-entry cone indicated. Shown on this figure are trajectories which approach the earth in extreme clockwise and counterclockwise manners and over the north and south poles. All other trajectories will form a surface passing through these four. If as assumed above, the time of flight and the re-entry flight path angle are fixed then, as shown in the earth-phase analysis, the velocity magnitude u_s and the flight path angle β_s will be constant. Also, since the vector $\bar{u}_m$ is fixed and the velocity

$$\bar{u}_s = \bar{v}_s + \bar{u}_m \ ,$$

the class of earth-phase velocity vectors may be drawn as radii of a sphere whose radius is u_s and whose center is located at the tip of the $\bar{u}_m$ vector. This is called the spherical boundary in Figure 1-11b where the velocity vector additions for extreme clockwise and counterclockwise re-entry are shown.

On visualizing the class of all possible vector additions, it is seen that the extreme clockwise re-entry will generate the maximum possible moon-phase velocity $\bar{v}_s$ and the extreme counterclockwise re-entry will generate the minimum possible velocity $\bar{v}_s$. Thus, it has been shown that although the energy of the vehicle for various trajectories may be identical in the earth-phase, the energy in the moon-phase will differ. Analysis of extreme clockwise and counterclockwise re-entry trajectories computed by the analytic program indicates that the difference may be considerable. An attempt was made to find the bounds on the energy and this is shown in Figure 1-12. Here the lunar burnout velocity has been plotted against the total time of flight for various distances to the moon. To obtain extreme trajectories a re-entry flight path angle of 96 degrees was chosen for all cases.

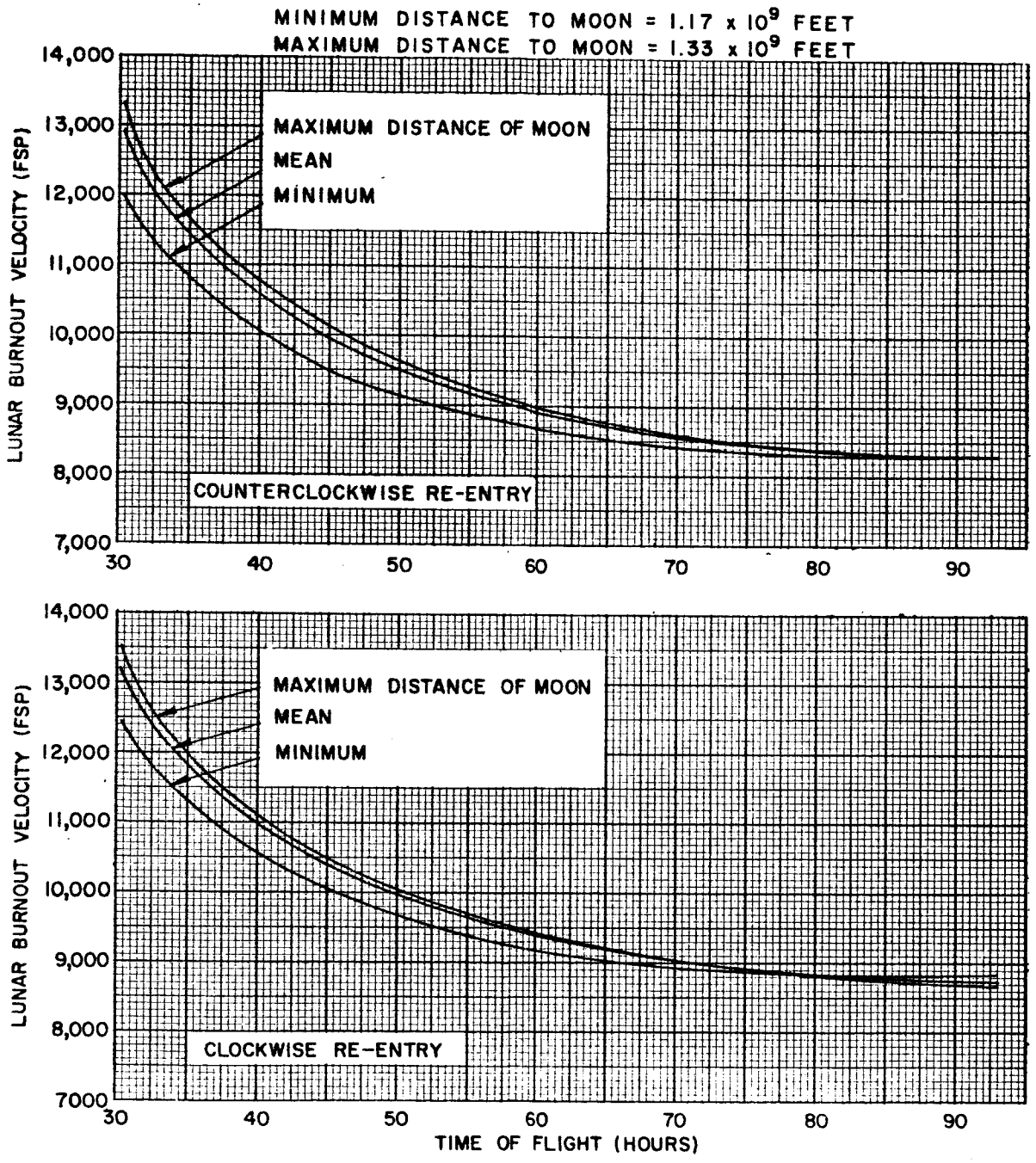

Figure 1-12. Lunar Burnout Velocity (Altitude = 100,000 feet) versus Total Time of Flight for Various Distances of the Moon

By means of the vis-viva integral, it is possible to convert these velocities to equivalent velocities v_s at the sphere of action. The results are shown in Figure 1-11. Also plotted here are the hyperbolic excess velocities, and these are within 100 to 300 fps of the velocities v_s. It can be shown that the direction of the hyperbolic asymptote is within 0.1 degree (order of magnitude) of the direction of $\overline{v}_s$.

Under the basic assumptions concerning the gravitational model, the moon-phase conic may be considered as stationary in inertial space (for an observer on the moon) from the moment that it leaves its surface. Therefore, although the moon will rotate in this system, the direction of the velocity vector $\overline{v}_s$ may be found with respect to the surface of the moon at launch. This angle, measured from the earth-moon line, is presented in Figure 1-14. It is called earth-moon-probe angle (EMP) and will depend upon the same set of parameters on which the magnitude of $\overline{v}_s$ depends. Again the data was taken from analytic runs representing extreme re-entry conditions at the earth ($\beta_r = 96^o$) and for various distances to the moon. It is seen from this graph that this angle varies considerably in going from counterclockwise to clockwise re-entry. Also, as expected from the velocity vector diagram shown in Figure 1-11b, the angle EMP is greater for clockwise re-entry than for counterclockwise re-entry. For example, for a 60 hour total flight time and a mean distance to the moon the angle will vary between 40 degrees (ccw re-entry) and 49 degrees (cw re-entry).

It is well known that except for librations which amount to about 7.5 degrees in the east-west direction and about 6.5 degrees in the north-south direction, the face of the moon directed towards the earth remains relatively fixed. The classical selenographic coordinates set up on the moon are such that the surface's "mean" position on the earth-moon line represents zero latitude and longitude. Also, the moon's axis of rotation lies very nearly perpendicular to its plane of motion around the earth. Thus, its equatorial plane will nearly contain the moon's velocity vector $\overline{u}_m$. This implies that the vector $\overline{v}_s$ will be very close to the selenographic equator and in fact upon observing the results of many

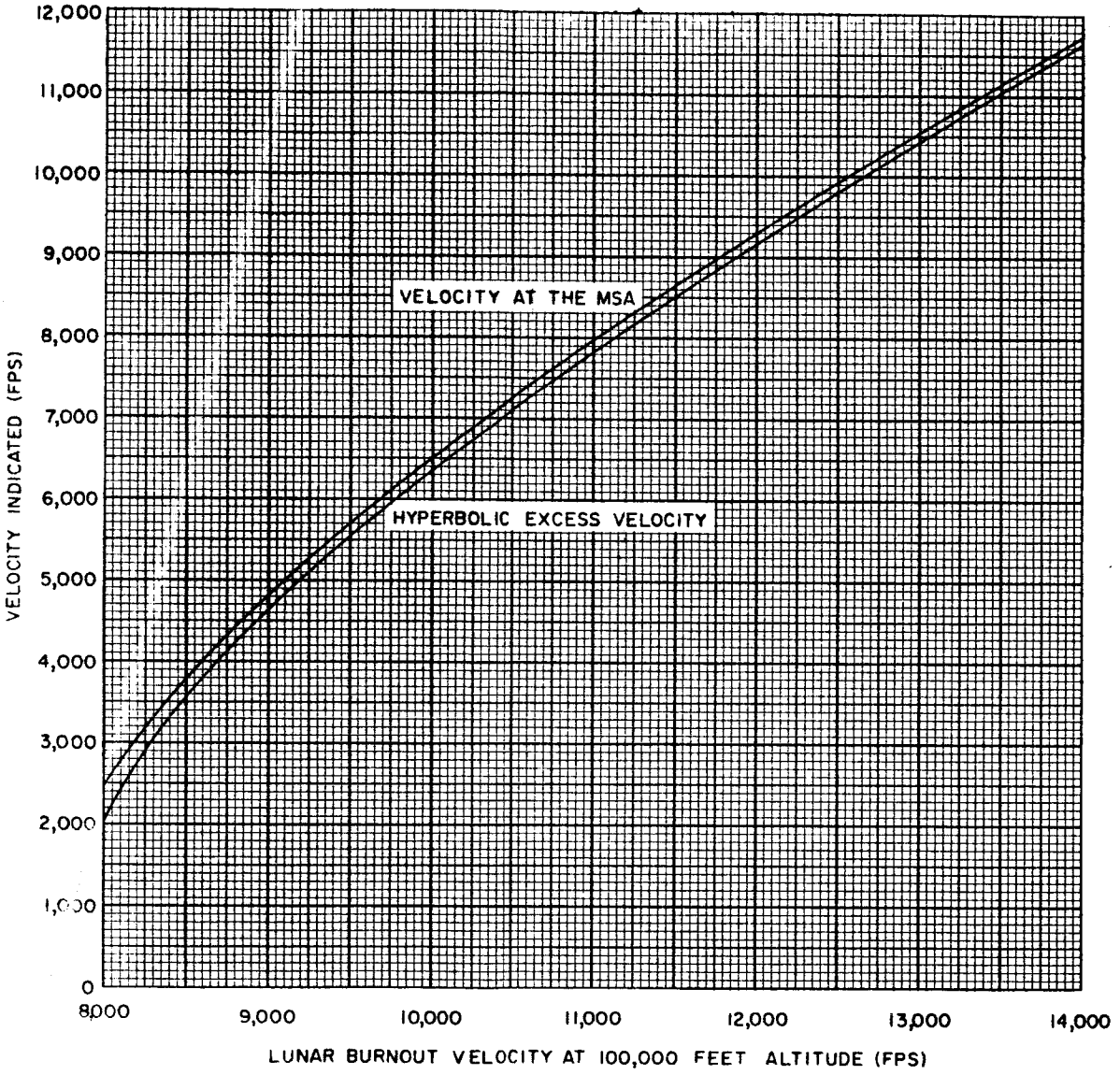

Figure 1-13. Hyperbolic Excess Velocity and Velocity at the Moon's Sphere of Action versus Lunar Burnout Velocity at 100,000 feet Altitude above the Surface of the Moon

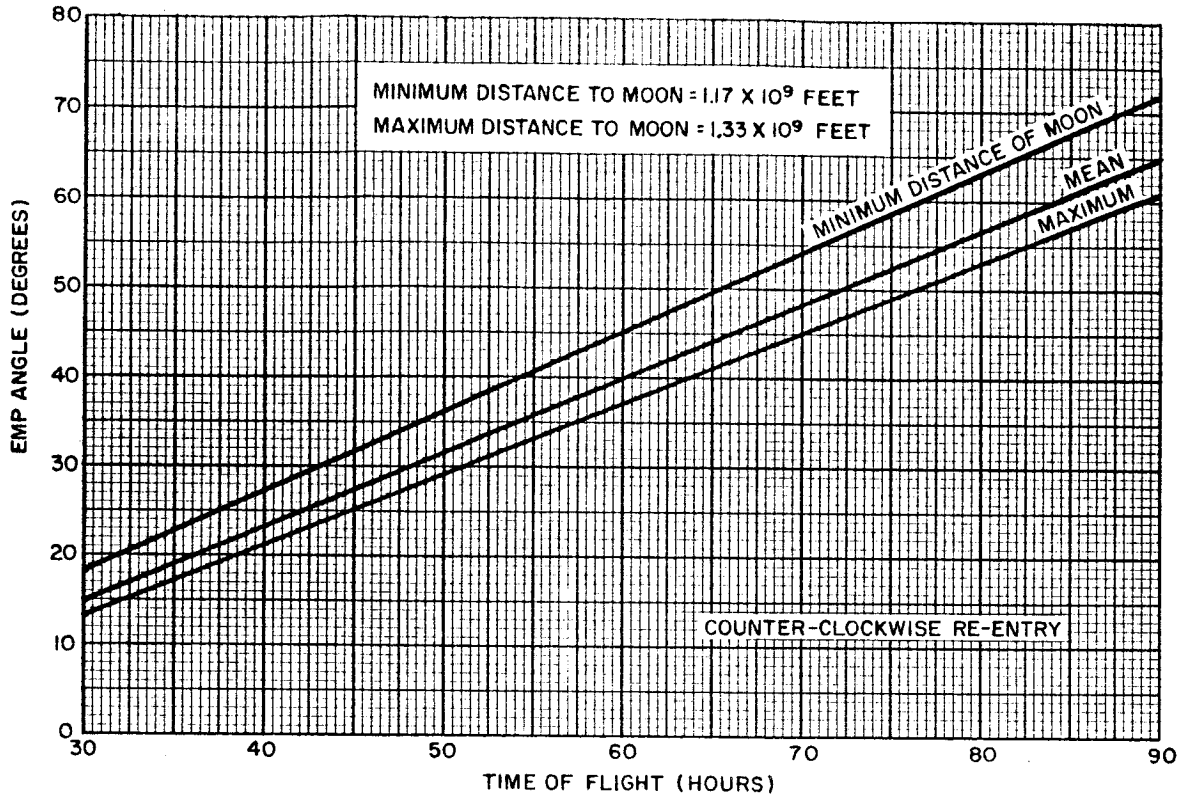

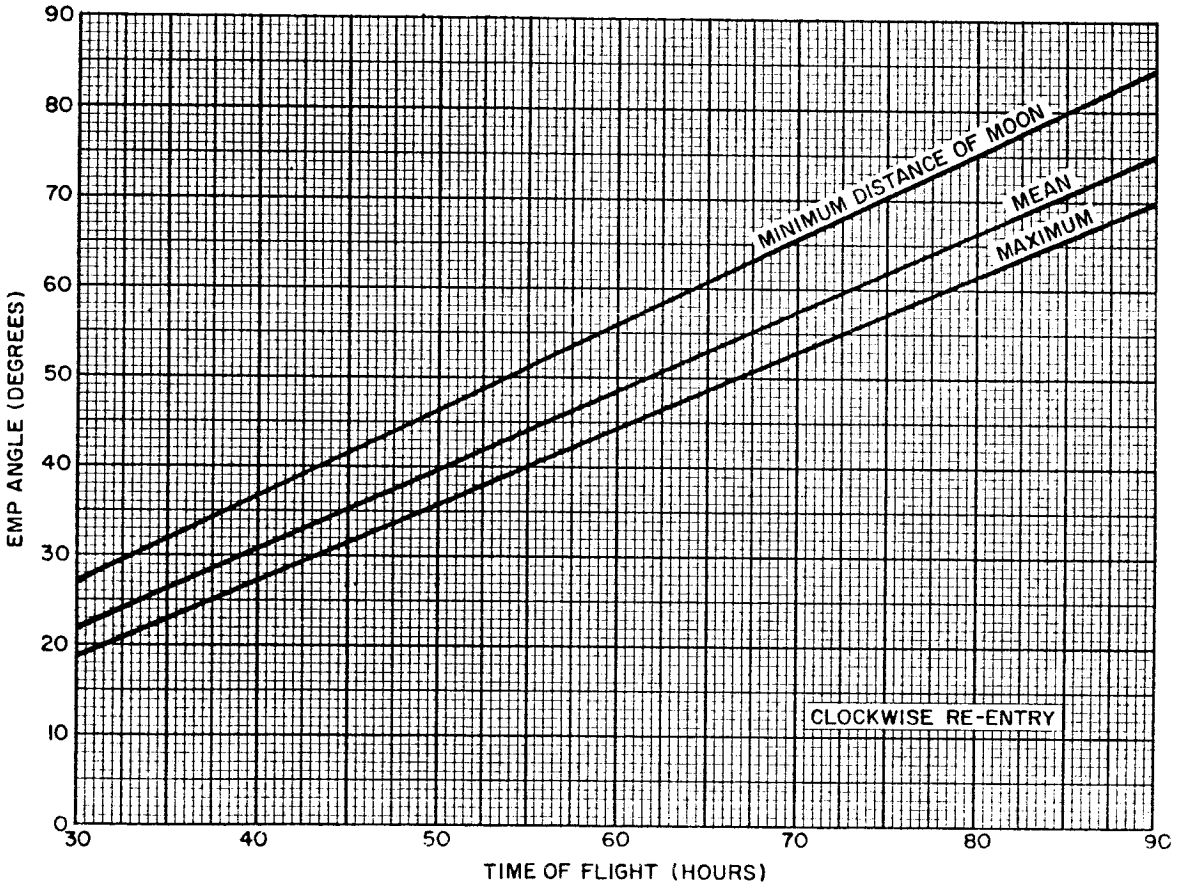

Figure 1-14. Earth-Moon-Probe Angle versus Total Time of Flight for Various Distances of the Moon

analytic runs, it does consistently come within 10 degrees of the moon's equator. Since this angle is of the same order of magnitude as the librations of the moon, and since the librations will be ignored in the qualitative discussion that follows, it will be assumed that the vector $\overline{v}_s$ does in fact lie in the moon's equator.*

We shall consider now a graphical method which may be used to solve approximately for some of the remaining parameters used in the moon phase geometry. This approach has the dual purpose of providing a method for the practical determination of some of the important moon-to-earth parameters while at the same time indicating the parametric relationships involved in the moon phase. The data used in generating these graphs have been obtained in some cases from the analytic program and in others from solutions of simple spherical triangles.

a) First, it is assumed that all the parameters required to solve the earth phase have been decided upon and that the analysis has progressed to the point where the magnitude and direction of the $\overline{v}_s$ vector have been; with the EMP angle representing the direction of this vector relative to the selenographic coordinate system.

b) Then, referring to Figure 1-15, specifying the selenographic latitude and longitude (μ_o and λ_o respectively) will determine the orientation of the moon phase conic since it must pass through the $\overline{v}_s$ vector and the launch site vector. The right spherical triangle shown in this figure with the sides μ_o and $(\lambda_o - EMP)$** may then be solved for the inclination of the moon phase trajectory, the launch azimuth and the in-plane angle from launch to the $\overline{v}_s$ vector. The inclination is given in Figure 1-16 versus the longitude minus the EMP angle for various launch site latitudes.

c) The launch azimuth may be found from Figure 1-17 which is also plotted versus the longitude minus the EMP angle and for various launch site latitudes.

---

*It should be noted that these simplifying assumptions are not made in the Analytic Lunar Return Program, but were only made in the qualitative graphical analysis discussed here and illustrated in Figures 1-16 to 1-20.

**Remember that longitudes measured west of (0, 0) are negative.

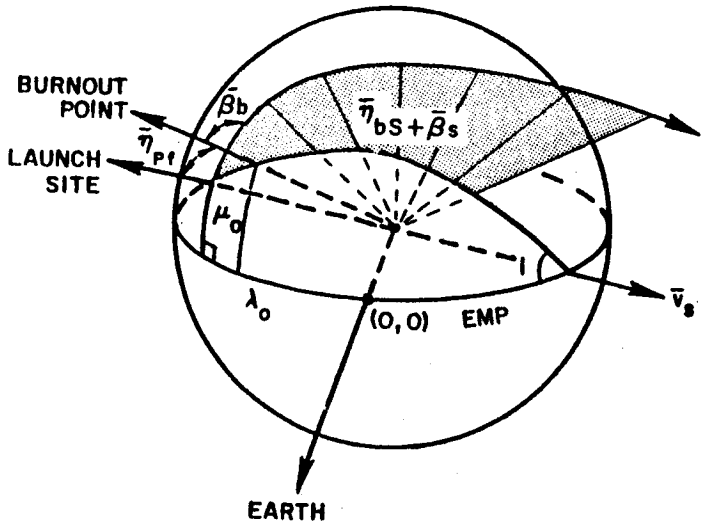

Figure 1-15. Moon Phase Geometry

d) The in-plane angle from the launch site to the vector $\bar{v}_s$ (which also indicates the direction of the hyperbolic asymptote) is composed of the sum of the powered flight angle and the in-plane burnout to asymptote angle; indicated by $\bar{\eta}_{pf} + \bar{\eta}_{bs} + \bar{\beta}_s$ in Figure 1-15. This angle is presented in Figure 1-18 and also plotted versus the longitude minus the EMP angle for various launch site latitudes.

e) The partial in-plane angle $\bar{\eta}_{bs} + \bar{\beta}_s$ may now be used to solve for the burnout flight path angle $\bar{\beta}_b$. The moon phase conic will be completely determined if the burnout parameters of altitude, velocity and flight path angle are specified. Then it is possible to solve for the angle $\bar{\eta}_{bs} + \bar{\beta}_s$ given R_s, the radius of the sphere of influence. These parameters have been plotted in Figure 1-19, for a fixed burnout altitude of 100,000 feet and may be used to solve for $\bar{\beta}_b$.

To illustrate this procedure, consider the following example:

Total time of flight = 90 hours
Distance of the moon at launch $\cong 1.33 \times 10^{10}$ feet (max)
Type of re-entry = counterclockwise
Launch site latitude = 5 degrees
Launch site longitude = 25 degrees
Burnout altitude = 100,000 feet
Powered flight angle = 3 degrees

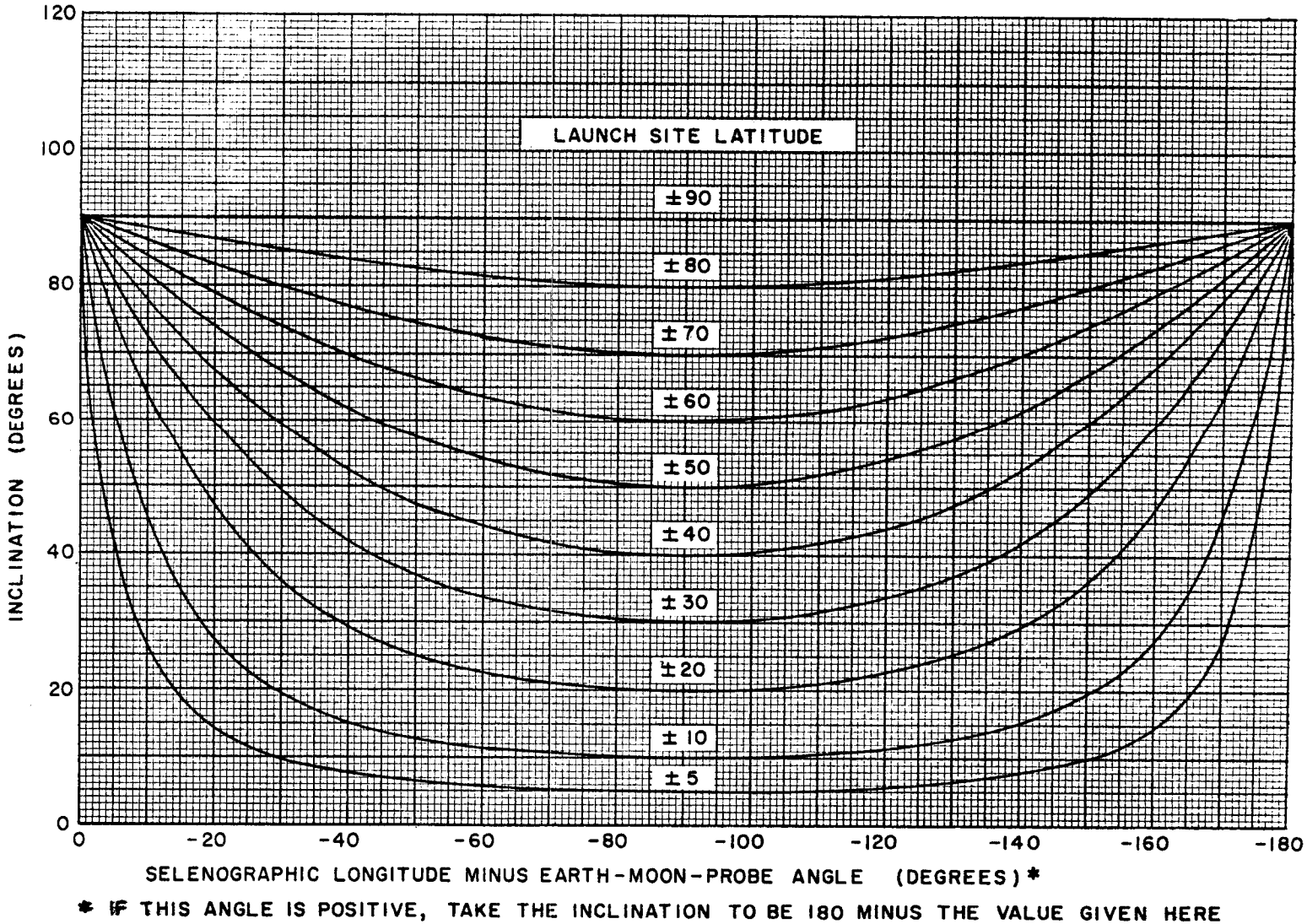

Figure 1-16. Inclination of the Hyperbolic Plane versus Longitude Minus Earth-Moon-Probe Angle for Various Launch Site Latitudes (Selenographic)

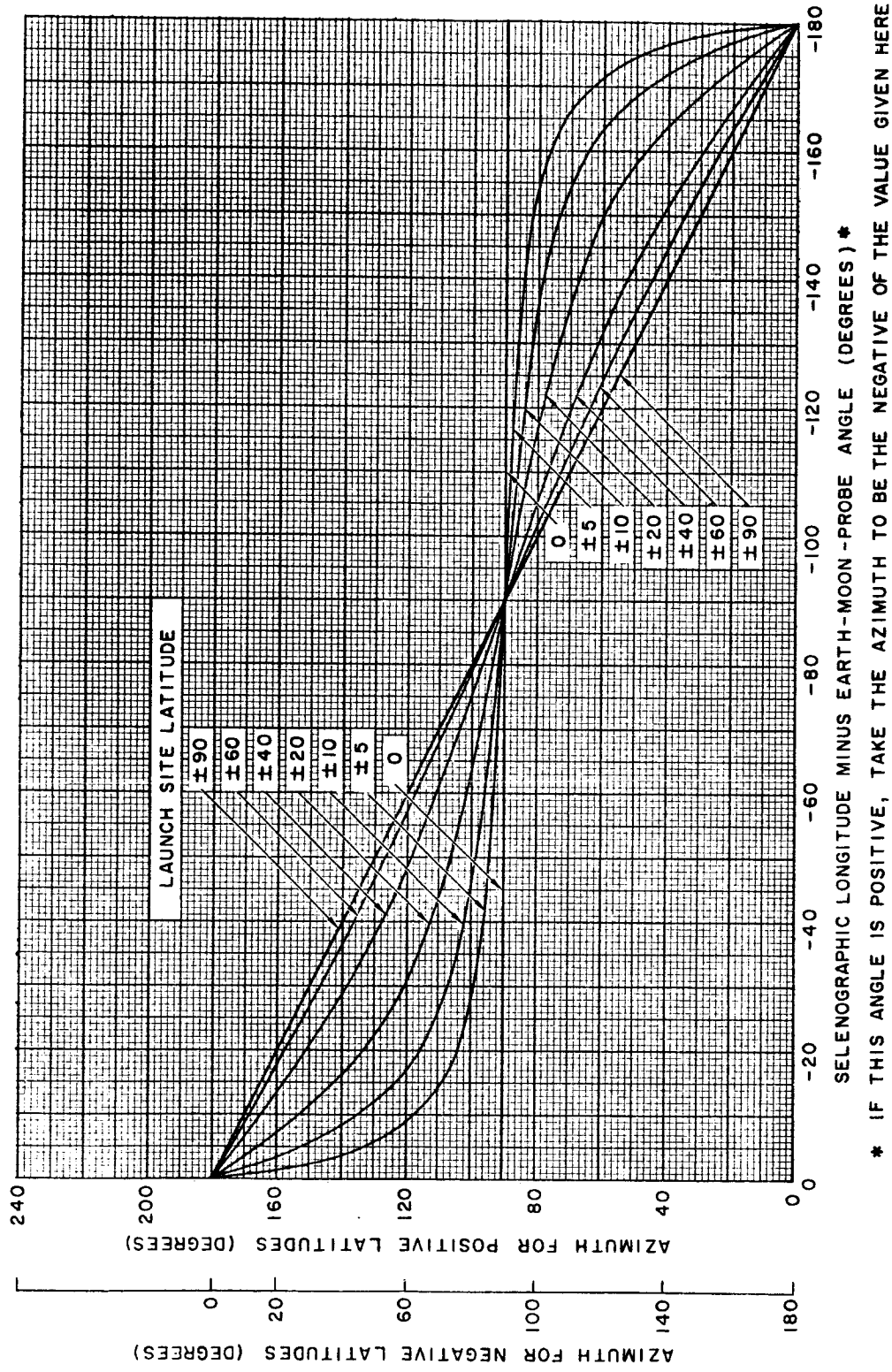

Figure 1-17. Lunar Burnout Azimuth versus Longitude Minus Earth-Moon-Probe Angle for Various Launch Site Latitudes (Selenographic)

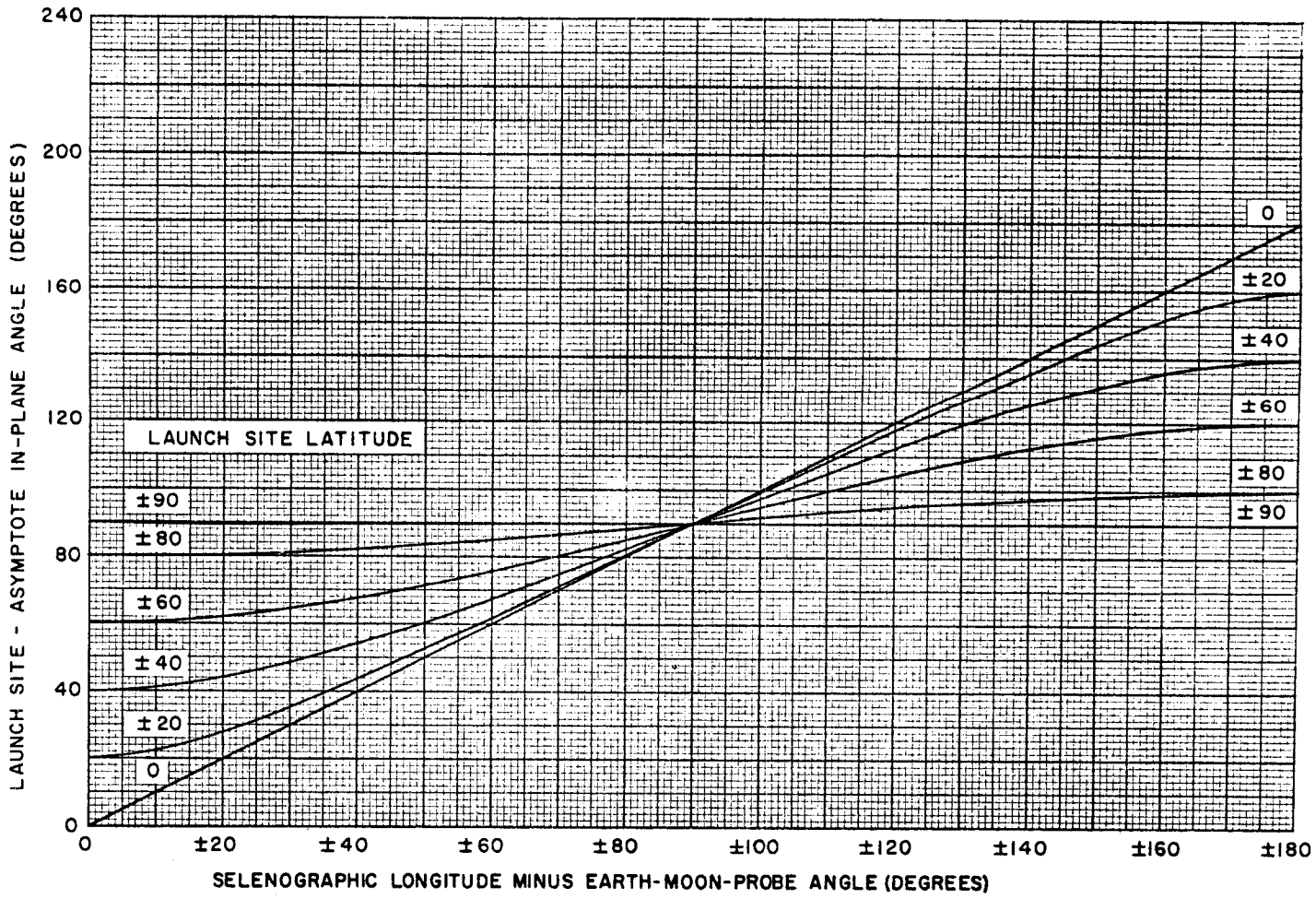

Figure 1-18. Launch Site-Asymptote In-Plane Angle (Hyperbolic Plane) versus Longitude Minus Earth-Moon-Probe Angle for Various Launch Site Latitudes (Selenographic)

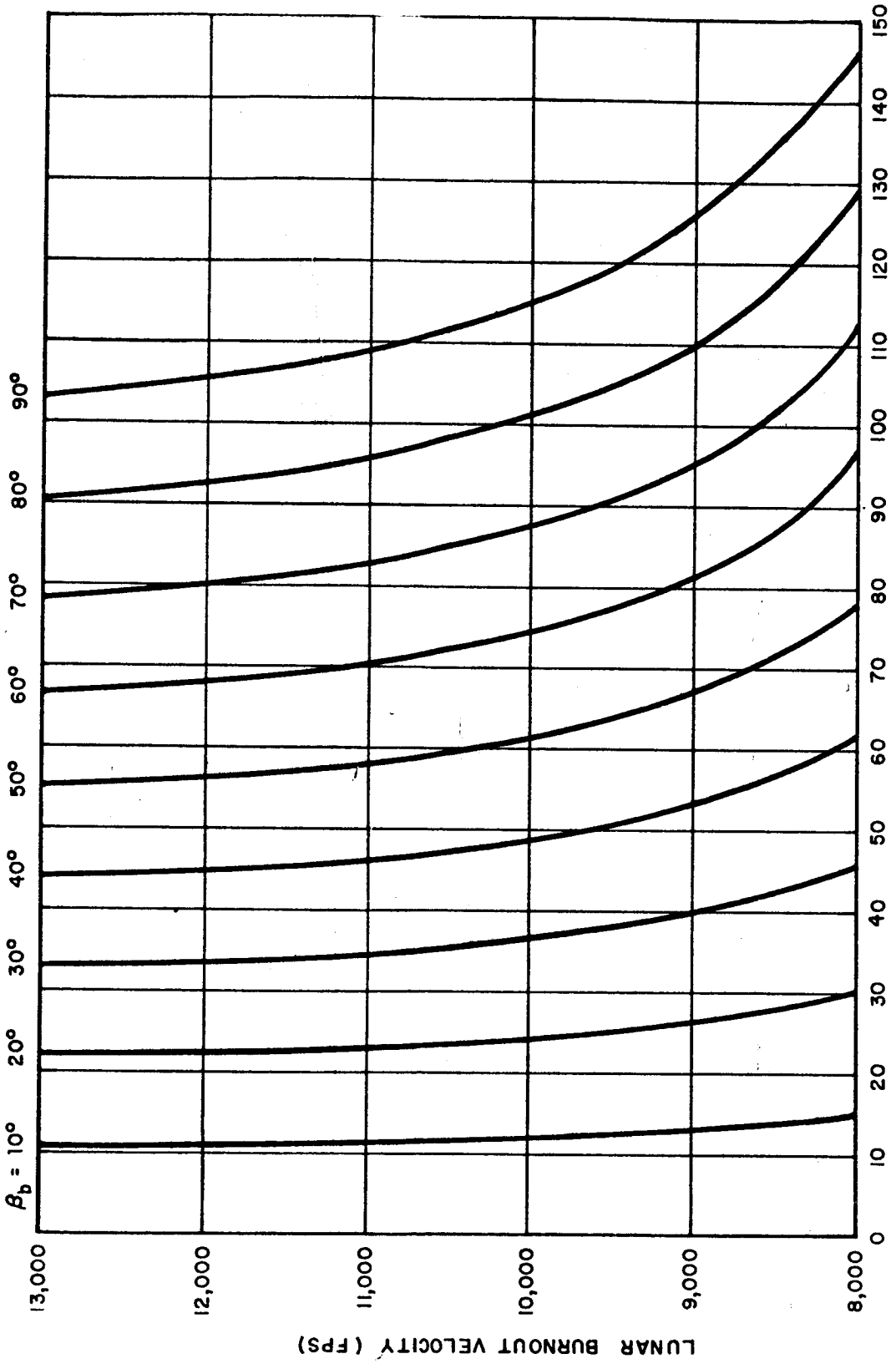

Figure 1-19. Lunar Burnout Velocity (Altitude = 100,000 feet) versus Lunar Burnout - Asymptote In-Plane Angle for Various Lunar Burnout Flight Path Angles

With the information and the foregoing graphs, the following information may be obtained.

Lunar burnout velocity $\cong$ 8250 fps (Figure 1-12)
Velocity at the sphere of action $\cong$ 3200 fps (Figure 1-13)
Hyperbolic excess velocity $\cong$ 2900 fps (Figure 1-13)
Earth-moon-probe (EMP) angle $\cong$ 61 degrees (Figure 1-14)
Longitude - EMP angle = 25 - 61 = -36 degrees
Trajectory inclination = 9 degrees (Figure 1-16)
Launch azimuth = 95 degrees (Figure 1-17)
Launch site - asymptote in-plane angle = 37 degrees (Figure 1-18)
Burnout - asymptote in-plane angle = 37 - 3 = 34 degrees
Burnout flight path angle = 23 degrees (Figure 1-19)

Since it was necessary to specify the day of the month on which the vehicle was launched (except that it must be on a day when the distances to the moon specified above is satisfied) the determination of the moon-phase by this method is independent of the declination of the moon. It has already been made clear that the moon-phase is essentially independent of the terminal conditions at the earth (except for cw or ccw re-entry).

Aside from using these graphs to obtain approximate values of moon-phase parameters in specific situations, it is possible to generate restriction curves as has been done in the earth-phase analysis. Returning to Figure 1-15, for example, itis clear that the in-plane angle $\overline{\eta}_{bs} + \overline{\beta}_s$ is dependent only on the velocity magnitude v_s and the burnout flight path angle $\overline{\beta}_b$. Thus, for a given day of launch and time of flight, and for specific earth phase conditions, the selenographic position and velocity of $\overline{v}_s$ will remain essentially fixed. The in-plane angle $\overline{\eta}_{bs} + \overline{\beta}_b$ will then be only a function of $\overline{\beta}_b$. In this situation it is possible to draw constant $\overline{\beta}_b$ contour curves on the surface of the moon as shown in Figure 1-20 where each point on a given contour is displaced by the corresponding $\overline{\eta}_{bs} + \overline{\beta}_s$ angle from the $\overline{v}_s$ vector.

Such contours have been generated with the analytic program by running trajectories with different launch sites but having all remaining input parameters equivalent. The results of these runs are presented in

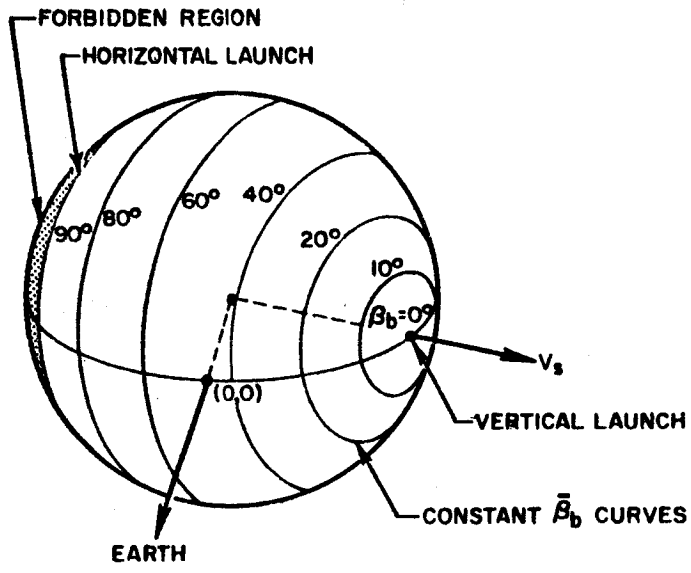

Figure 1-20. Constant Burnout Flight Path Angle Contours

Figure 1-21 which plots, by interpolation, the constant $\overline{\beta}_b (\cong \beta)$ and constant azimuth curves. These curves are not everywhere orthogonal. The restricted region shown here and in Figure 1-20 simply implies that it is impossible to launch a direct ascent moon-to-earth flight from these sites, for the earth-phase parameters considered, without first passing through the pericynthion of the moon-phase conic.

3. Sensitivity Coefficient Analysis

The Sensitivity Coefficient Routine provides a method of computing quite accurate sensitivity coefficients at a very rapid rate (0.1 sec per perturbed trajectory) and therefore makes it possible to generate extensive burnout or midcourse sensitivity data. This data may then be used to show the dependence of sensitivity coefficients on launch site location, energy, time of flight, etc., and the results may be examined for general trends. However, the most meangingful results will be obtained when a specific launch guidance system (i.e., set of burnout errors) is considered, since it is the resultant errors at re-entry or, ultimately, the resulting midcourse correction requirements which are significant, rather than either the burnout errors produced by the guidance system or the sensitivity coefficients. (See Part II).

Figures 1-22, 1-23 and 1-24 are presented to indicate the kind of data that may be generated. Here, the variations in re-entry latitude, longitude, flight path angle and time are found with respect to the lunar burnout velocity, flight path angle and azimuth. An analysis of these graphs, and others, may be found in [5].

D. Program Accuracy

1. Preliminary Study

The usefulness of any analytic model depends directly upon the accuracy with which it yields the true conditions which are being simulated. For this reason, it was necessary to carefully analyze a broad range of results obtained from the model and compare them with exact results. In addition, through study of the behavior of the deviations of the approximate from the true results, it was possible to find a method by which

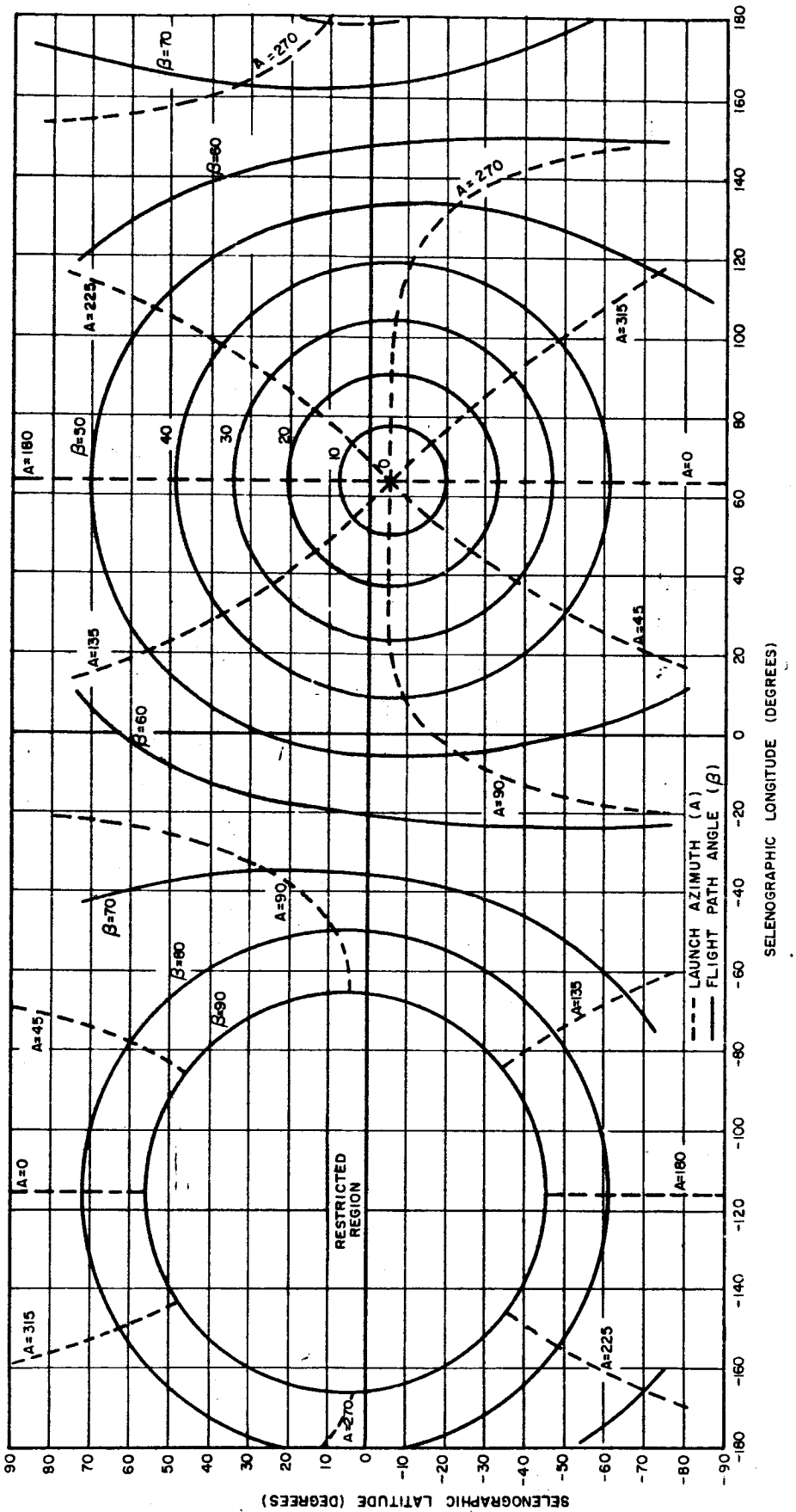

Figure 1-21. Launch Azimuth and Flight Path Angle Contours Mapped on the Surface of the Moon (Including Lunar Librations). Vehicle Launched on December 4, 1963 to Re-enter Gulf of Mexico with a Re-entry Angle of 175°. Total Time of Flight = 70 Hours

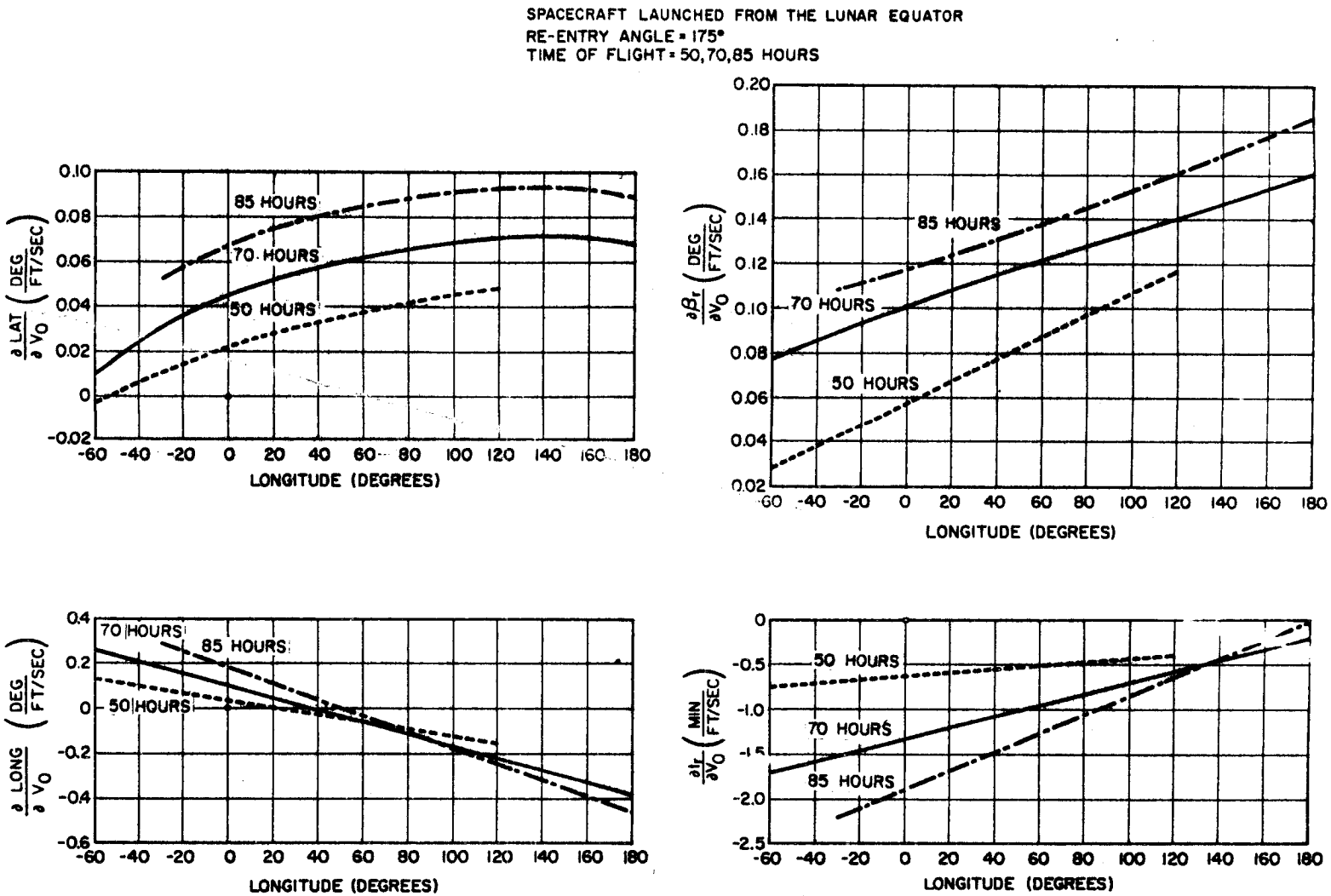

Figure 1-22. Sensitivity Coefficients at Re-entry to Burnout Velocity versus Selenographic Burnout Longitude

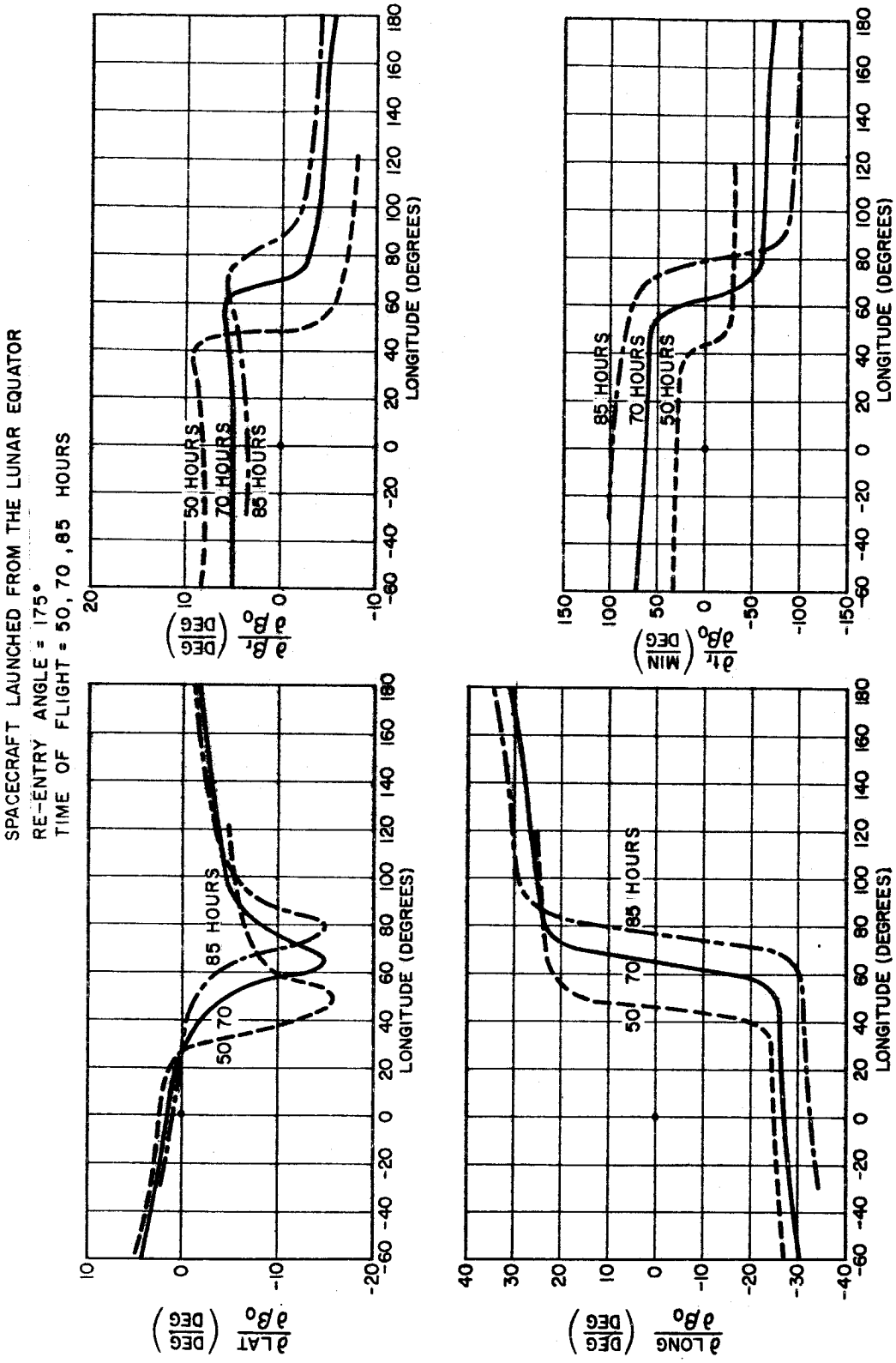

Figure 1-23. Sensitivity Coefficients at Re-entry to Burnout Flight Path Angle versus Selenographic Burnout Longitude

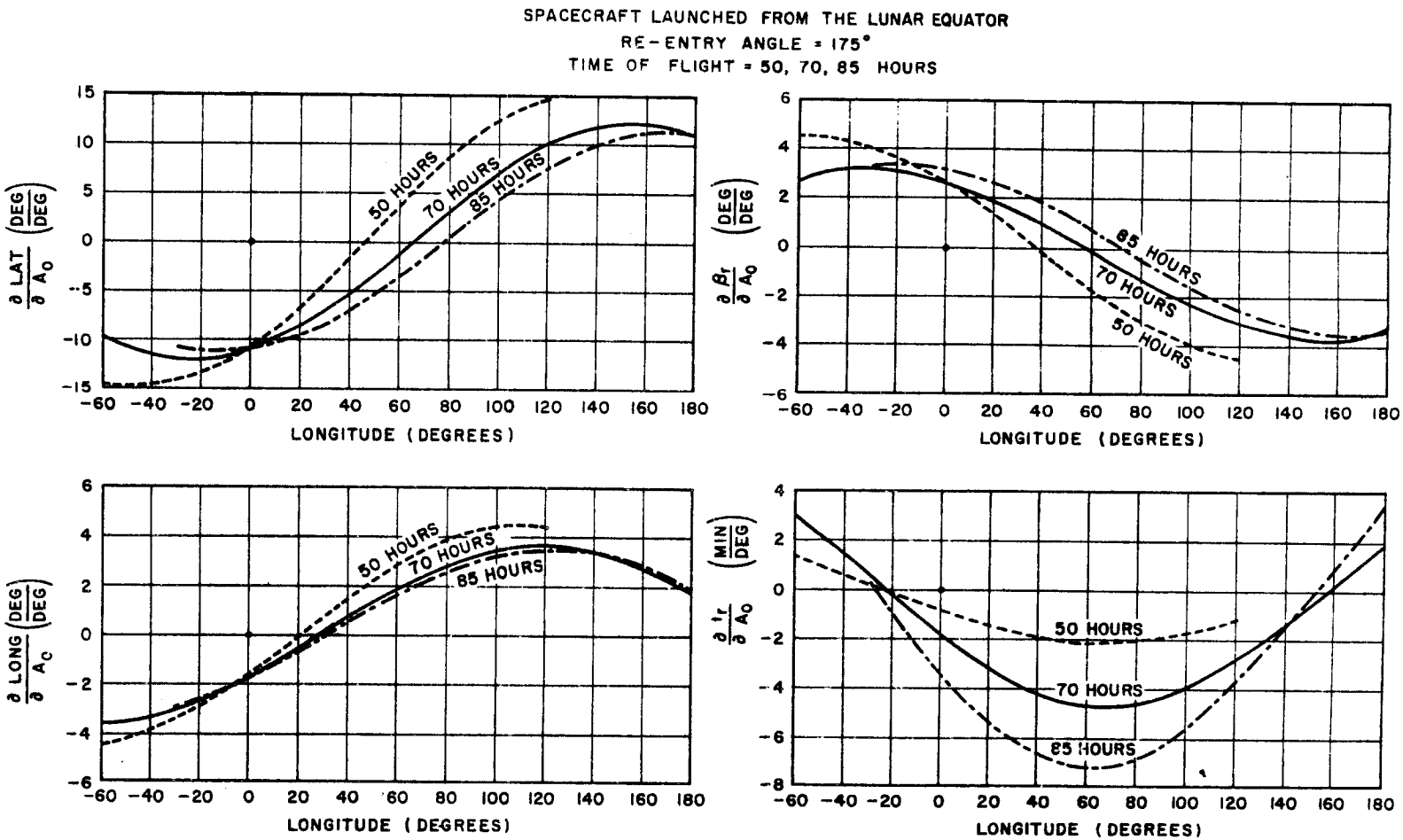

Figure 1-24. Sensitivity Coefficients at Re-entry to Burnout Azimuth versus Selenographic Burnout Longitude

the basic model may be made to yield greater accuracy. This section presents first, a comparison of the results from the original model to those from the exact model; second, the arguments which led to an empirical correction scheme; and finally, a comparison of the true results with those from the corrected model.

The preliminary results obtained from the original model are shown in Table 1. The "exact program" mentioned here solves for the exact trajectory (which includes earth, sun, moon, vehicle and oblateness perturbations) as a function of time by numerically integrating the second order differential equations of motion using Encke's method. Several trends may be noted. First, faster flight times result in greater overall accuracy. This may be expected since the size of the perturbations on the trajectory will be directly proportional to the duration of time in which they act. The second noticable trend is that the greater the re-entry angle (steeper) the more accurate the results. This, of course, is due to the nonlinear effect of the trajectories intersecting the spherical earth. It is expected that the same perturbation acting on a trajectory having a shallow re-entry as acting on one having a steep re-entry may cause the former to miss the earth completely while indicating fair accuracy for the latter. Also, if one looks carefully at the impact longitudes obtained from the exact program, he will notice that in all cases the actual re-entry point is east of the desired re-entry point. A later examination into the nature of the lunar perturbation will explain why this is so. Next, although not enough cases are presented in Table 1 to indicate this, the accuracy is dependent on the lunar date of launch and, in particular, on the distance of the moon from earth. Finally, the one parameter which indicates best results for the cases shown in Table 1 is the total flight time.

To improve the accuracy of the basic model, it was first necessary to determine the specific source and size of the perturbations not accounted for in the analytic model and then attempt a correction. The procedure followed in doing this was to run sample trajectories on the n-body program with and without the sun and oblateness, and with

Table 1-1. Comparison of Results from Original Model with Results from an Integrating (Exact) Program

Analytic Program				Integrating Program*				
Time of Flight (hr)	Re-entry Latitude (deg)	Re-entry Longitude (deg)	Re-entry Angle (deg)	Time of Flight (hr)	Re-entry Latitude (deg)	Re-entry Longitude (deg)	Re-entry Angle (deg)	Perigee (E.R.)
50	30	-104	170	50.2	29.9	-94.1	163.7	----
60	30	-104	160	60.5	23.8	-90.1	149.4	----
60	30	-104	140	60.6	16.4	-90.8	127.5	----
60	30	-104	120	60.7	-5.2	-84.1	97.0	----
60	30	-104	100	60.5	----	----	----	1.28
75	30	-104	140	75.9	4.5	-79.6	116.8	----
75	30	-104	120	75.9	----	----	----	1.08
90	30	-104	170	90.6	19.5	-67.8	148.7	----
90	30	-104	140	91.0	13.6	-76.8	121.4	----
90	30	-104	120	91.0	----	----	----	1.19
90	30	-104	110	89.2	22.9	-21.0	141.0	----**

*All cases shown have counterclockwise re-entry.

**Different launch date.

and without the moon and earth when the vehicle was in the opposing phase. In this manner, it was found that the major part of the perturbations is due to the earth-moon system itself, and, in particular, to the effect of the moon on the earth-phase trajectory.

2. Correction Scheme

After considering several alternatives, it was decided that the best approach would be to correct empirically for the bias type error that existed in all of the runs made with the analytic program. The nature of this bias may be seen more clearly with the aid of Figure 1-25a. As indicated above, the principal perturbation is that due to the moon on the earth-phase trajectory; but, as shown in the figure, the moon at this time has rotated in its orbit and will always lie to the east of the trajectory (as seen from the earth). The bias, then, is simply due to the moon pulling the trajectory eastward. A simple method of correcting this is shown in Figure 1-25b. The earth-phase velocity is first projected into the earth-moon orbit plane and this projection rotated through the empirical angle τ. Thus, only that component of $\bar{u}_s$ which lies in (or parallel to) the moon's orbit plane is rotated. (See Figure 1-25b). This rotation to counteract the undirectional bias will always be counterclockwise. The justification for this correction is the fact that the perturbational effects on the earth-phase trajectory will be primarily in the earth-moon plane and, more strongly, the fact that the correction does yield satisfactory results.

3. Evaluation of Tau

Investigations were next carried out to determine, first, the trajectory parameters on which the correction angle τ depends and second, an empirical expression which approximates this dependence. The procedure used in carrying out these investigations was first to allow τ to be an independent input into the analytic program. The lunar burnout conditions which the program calculated for various values of τ were then fed into the exact program and the results tabulated. Those trajectories whose re-entry conditions, as obtained from the exact program, most closely correspond to the desired entry conditions were considered to have used the optimum correction angle. This study led to the conclusion that τ was a function primarily of flight time and the earth-moon distance.

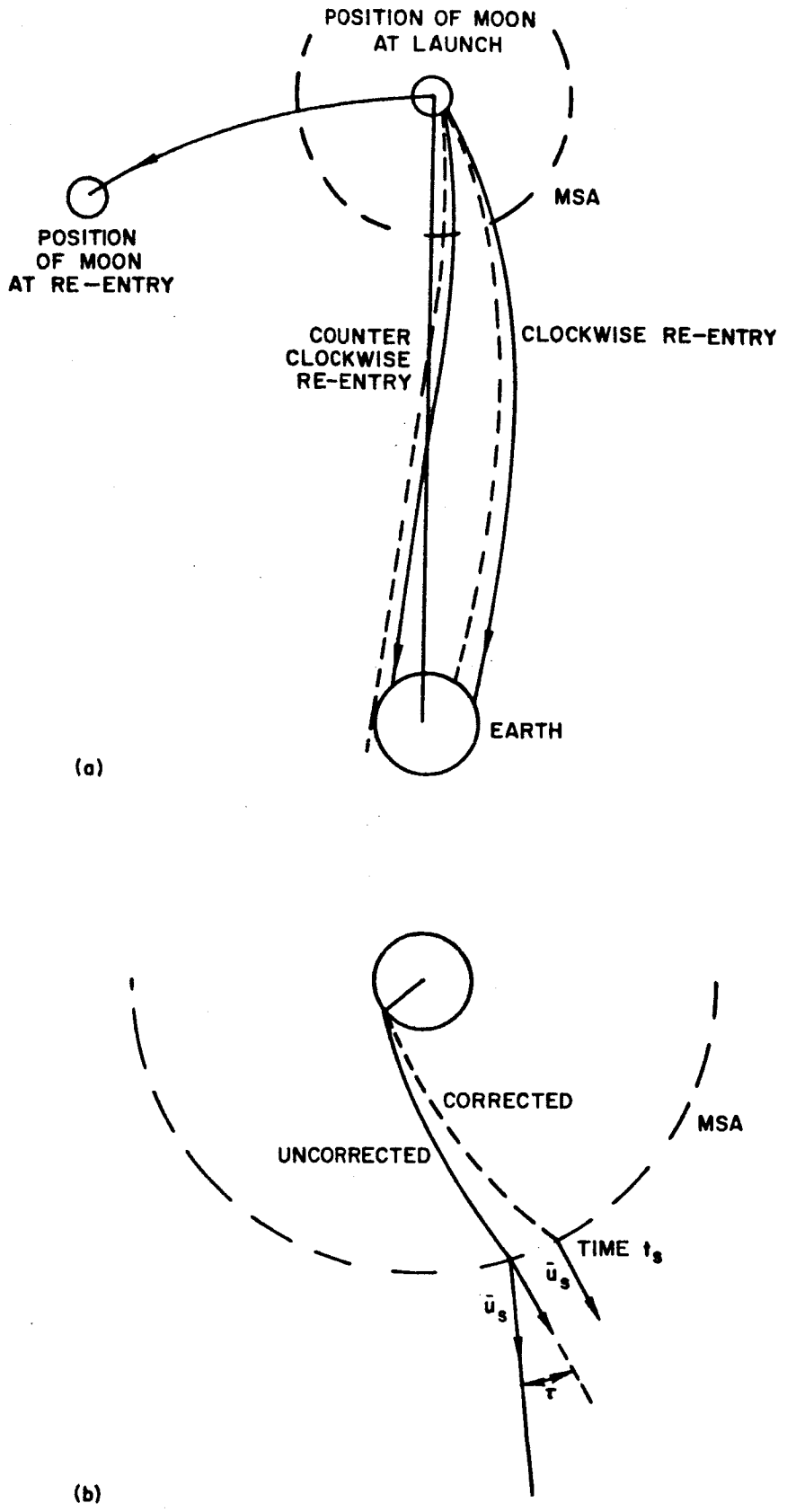

Figure 1-25. Perturbation Correction Scheme

The expression for optimum τ with respect to the time of flight was then determined for the average earth-moon distance. The results are shown graphically in Figure 26a. Also shown in this graph is the variation of τ with the time of flight for clockwise re-entry. The results in this case were sufficiently different as to warrant a separate study. Following the study for clockwise and counterclockwise re-entry, it was found that both sets of empirical data could be easily approximated by quadratic expressions.

Next, effects on τ of the distance to the moon was studied for trajectories having a total flight time of 90 hours. The results in this case, shown in Figure 1-26b, indicates a linear dependence of τ on the earth-moon distance. Again separate studies were required for clockwise and counterclockwise re-entry. The product of the quadratic and linear expressions resulted in the following expressions for the evaluation of optimum τ:

For counterclockwise re-entry and time of flight greater than 45 hours,

$$\tau = (5.5246 - 3.6052 \times 10^{-9} x_m)$$

$$\left(9.881 - 0.69055 \times 10^{-2} T_{mi} + 1.2639 \times 10^{-6} T_{mi}^2\right)$$

For clockwise re-entry and time of flight greater than 35 hours,

$$\tau = (4.7957 - 3.0245 \times 10^{-9} x_m)$$

$$\left(3.1834 - 0.28483 \times 10^{-2} T_{mi} + 0.69247 \times 10^{-6} T_{mi}^2\right)$$

where x_m = distance to the moon in feet, and T_{mi} = time of flight in minutes. The value of τ is taken as zero for flight times shorter than these.

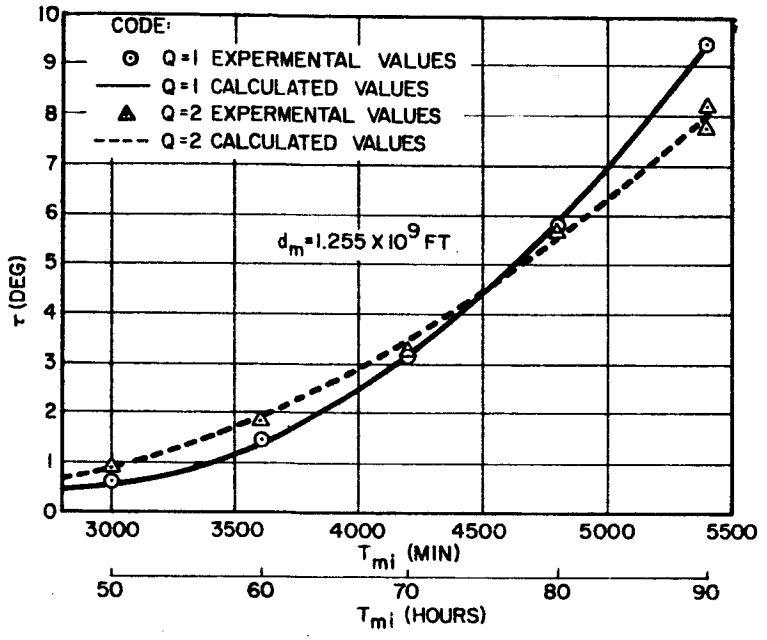

Figure 1-26a. Variation of τ with Time of Flight

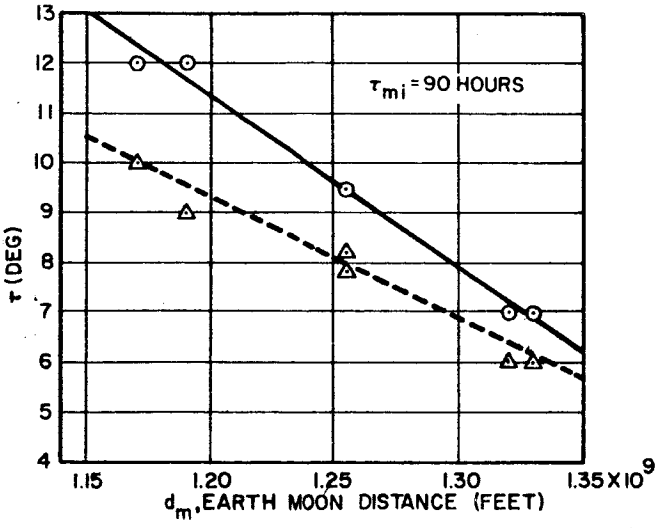

Figure 1-26b. Variation of τ with Earth-Moon Distance

4. Final Accuracy

Incorporating the expressions for τ developed in the last paragraph into the analytic program yields the results shown in Table 2 for a few sample cases. As expected, the results compare most favorably with the exact integration program when the time of flight is the shortest and when the re-entry angle is the steepest and compare the least favorably for long flight times and shallow re-entry. The adjustment required in the burnout conditions of the analytic program to produce the desired conditions on an "exact" program will be of the order of a few tenths of a degree in β and A or a few fps in velocity. This adjustment may be made by incorporating a linear search routine in the exact program.

The final comparison of results that may be made with the exact program are the sensitivity coefficients obtainable from the Sensitivity Coefficient Routine. Table 3 presents these results for two cases; 50 and 90 hour times of flight. The results were obtained from the exact program in exactly the same manner as from the analytic program; i.e., each burnout parameter was varied independently by the increment shown and the trajectory was then integrated to re-entry. The differences between the resulting terminal values and the unperturbed nominal values are those shown in the tables.

Table 1-2. Results of the τ-Corrected Analytic Program

τ-Corrected Analytic Program				Exact Program				
Time of Flight (hr)	Re-entry Latitude (deg)	Re-entry Longitude (deg)	Re-entry Angle (deg)	Time of Flight (hr)	Re-entry Latitude (deg)	Re-entry Longitude (deg)	Re-entry Angle (deg)	Re-entry Direction
50	15	-40	175	50.1	15.7	-36.4	173	ccw
50	15	-40	135	50.1	15.4	-34.1	130.8	ccw
50	-29	184.1	96	49.8	-30.9	178.0	98.5	ccw
60	30	-104	140	60.2	27.7	-103.2	138.0	ccw
60	30	-104	140	60.3	29.9	-107.5	140.0	ccw
90	--	-150	175	90.5	-1.0	-156.9	175.4	ccw
90	30	-104	170	90.2	29.6	-107.3	170.1	ccw
90	30	-104	170	90.6	30.4	-105.6	172.6	ccw
90	15	-40	135	88.9	15.3	-25.3	135.6	ccw
90	30	-104	110	90.7	28.0	-95.2	113.0	ccw
90	30	-104	110	91.4	29.4	-114.4	114.3	ccw
90	-6	173.4	96	88.1	-7.0	176.9	106.7	ccw

Table 1-3. Sensitivity Coefficient Comparison Between the Analytic and Exact Programs

Total Time of Flight = 50 Hours
Re-entry Flight Path Angle = 163 Degrees
Increments*

Terminal Parameters	Δr (50,000 ft)	Δλ (1 deg)	Δμ (1 deg)	Δv (50 fps)	Δβ (1 deg)	ΔA (1 deg)
Re-entry Time	-21.4	19.9	-0.065	-35.2	28.0	0.11
	(-21.3)**	(20.5)	(-0.300)	(-35.1)	(28.8)	(0.30)
Latitude	-0.051	3.33	1.41	0.389	2.69	-15.21
	(0.003)	(3.20)	(1.24)	(0.451)	(2.52)	(-15.1)
Longitude	4.72	-20.2	0.692	4.93	-28.1	-3.52
	(4.50)	(-19.9)	(0.735)	(4.56)	(-27.8)	-3.25
Re-entry Angle	0.291	5.81	-0.49	1.75	8.03	1.59
	(0.386)	(5.70)	(-0.56)	(1.89)	(7.90)	(1.50)

Total Time of Flight = 90 Hours
Re-entry Flight Path Angle = 169 Degrees
Increments

Terminal Parameters	Δr (50,000 ft)	Δλ (1 deg)	Δμ (1 deg)	Δv (50 fps)	Δβ (1 deg)	ΔA (1 deg)
Re-entry Time	-48.4	68.4	-3.6	71.0	100.2	-6.67
	(-44.5)	(71.9)	(-4.3)	(-65.0)	(103.9)	(06.0)
Latitude	1.24	1.13	7.98	1.34	-1.00	-7.05
	(1.17)	(1.00)	(7.86)	(1.22)	(-1.13)	(-7.16)
Longitude	-1.72	-20.8	3.29	-4.67	-30.8	-0.55
	(-2.79)	(-21.1)	(3.17)	(-6.50)	(-30.8)	(0.68)
Re-entry Angle	3.82	1.05	-3.14	4.18	2.43	1.58
	(3.95)	(0.90)	(-2.96)	(4.30)	(2.13)	(1.50)

*The values in the tables represent actual variations in the terminal parameters and have not been divided by the indicated increments.

**Quantities in parentheses are from the Exact Program.

II. LUNAR RETURN MISSION ANALYSIS

A. Introduction and Summary of Conclusions

This section examines the trajectory and guidance problems involved in returning a spacecraft from the lunar surface to earth. Two generalized missions are considered in order to display the guidance requirements, tradeoffs, and problem areas in two extreme cases of current interest:

a) The return of a spacecraft having all sophistication necessary to achieve manned re-entry conditions (the standard mission),

b) A minimal, sample return mission using a small (~250 lb spin-stabilized slant-launched vehicle with or without midcourse correction (the minimal mission).

In both missions, midcourse guidance is assumed to be under earth-based control; however, the method of analysis and many of the results for the standard mission apply equally well when the midcourse guidance is under spacecraft control.

Sections B and C discuss the power flight, injection guidance, transit trajectory, midcourse velocity (fuel) requirement, and final re-entry errors for the two missions. For the standard mission, an autopilot-accelerometer cutoff launch guidance system and a present state-of-the-art inertial guidance system are compared on the basis of re-entry dispersion and midcourse fuel requirement. The relative contributions of the launch guidance errors, tracking errors, and midcourse execution errors are shown. Matrices are included relating each independent launch source error directly to re-entry errors so that the effect of changes in the assumed source errors may be easily seen. For the minimal mission, a comparison is made of accelerometer cutoff and fuel depletion launches and of the re-entry dispersions with and without a midcourse guidance system. Section D illustrates the tracking accuracy attainable from DSIF range rate and angular data for moon-to-earth missions.

For the particular magnitudes of error sources employed in Sections B and C, the following conclusions may be drawn from the study results.

1. Standard Mission

a) Both the autopilot and inertial systems simulated provide accuracy for manned re-entry when used with two midcourse corrections. Typical final re-entry dispersions are (inertial launch guidance, 90 hour flight):

$\sigma_{Lat} = 0.07^{o}$ (4 n mi), $\sigma_{Long} = 0.2^{o}$ (10 n mi), $\sigma_{\text{re-entry angle}} = 0.1^{o}$

(For comparison, a typical manned capsule with an L/D = 0.5 should allow reaching a landing site anywhere within a re-entry footprint 800 nautical miles in width and extending from a point 1500 nautical miles from the sub-re-entry point to a point 3500 nautical miles from re-entry. A re-entry flight path angle spread of 3 degrees can be tolerated, full corridor width.)

b) Compared with an allowable 3 degree re-entry angle corridor width (± 1.5 degrees):

1) Neither guidance system will suffice uncorrected,

2) Both systems are very accurate after two corrections $[\sim 0.1^{o} (1\sigma)]$.

c) The uncorrected miss at re-entry for the inertially guided flight is almost completely caused by launch site uncertainty and initial reference direction errors. These sources (whose assumed dispersions were: lunar latitude of site 0.05^{o} (1σ), lunar longitude of site 0.05^{o} (1σ), altitude 1000 ft (1σ), azimuth direction 0.25^{o} (1σ)) alone produce re-entry errors on a 50-hour flight of:

$$\sigma_{Long} = 12.4^{o}, \sigma_{Lat} = 1.37^{o}, \sigma_{\text{re-entry angle}} = 5.8^{o} .$$

d) Tracking based on DSIF range rate and angular data alone ($\sigma_{\dot{R}} = 0.5$ fps, $\sigma_{A} = \sigma_{E} = 0.2^{o}$) using a data rate of one observation set per minute is sufficient to allow the final re-entry accuracy quoted in a) above.

e) Employing two midcourse corrections, degradations of a factor of 10 in velocity execution accuracy or a factor of 5 in angular orientation accuracy over values typical of present day inertial platform accuracies cause changes of less than 35 percent in re-entry accuracy.

f) The autopilot-controlled flights studied required 2 to 5 times as large a midcourse velocity increment as comparable inertially guided flights. The total midcourse velocity increments required (68 percent probability level) for the two systems and for two flight times are:

50 hr Inertially Guided	38 fps	90 hr Inertially Guided	25 fps
50 hr Autopilot	72 fps	90 hr Autopilot	123 fps

2. Minimal Mission

a) Return trajectories originating near the landing region of a 66-hour earth-to-moon flight were studied as a function of flight time and re-entry angle. The smallest uncorrected dispersion was obtained for a fast (50 hr) trajectory having a steep re-entry angle (80 degrees to the horizontal). The uncorrected re-entry 40 percent error ellipse for this trajectory, with powered flight terminated by fuel depletion, has the parameters:

semi-major axis 7.95°, semi-minor axis 3.86°

b) The use of an accelerometer cutoff system is only weakly effective in reducing re-entry misses because of the dominant re-entry errors produced by the initial pointing and spin-up errors in elevation and azimuth (assumed 0.25° 1σ).

c) The use of two spin-stabilized midcourse corrections of modest execution accuracy and a very simple correction logic is highly effective in reducing the re-entry miss. For a typical 90-hour trajectory (having a larger uncorrected miss than the 50-hour trajectory just discussed) the dispersion in re-entry after correction is

$$\sigma_{Long} = 0.67^{\circ}, \quad \sigma_{Lat} = 0.45^{\circ} \quad .$$

The standard deviations of the two velocity corrections for this trajectory are

$$\sigma_{v_1} = 179 \text{ fps}, \quad \sigma_{v_2} = 207 \text{ fps (correlation coeff} = 0.997).$$

d) Tracking based on DSIF range rate and angular data alone ($\sigma_{\dot{R}}$ = 0.5 fps, $\sigma_A = \sigma_E = 0.2^o$), using a data rate of one set per 10 minutes, is sufficient to allow the above re-entry accuracy.

B. The Standard Mission

1. Mission Description

The mission discussed here will be termed "standard" in the sense that the payload weight is assumed to be large enough to permit any guidance and control equipment to be utilized which is necessary or desirable to insure re-entry conditions suitable for manned flight.

In particular, the mission is characterized by the following features:

a) The lunar powered flight will be performed under either autopilot control or control of an inertial guidance system.

b) The spacecraft is fully attitude controllable at all times. Midcourse corrections may be made in arbitrary directions under attitude controlled conditions.

c) The re-entry flight path angle will be held to 96 degrees (i.e., 6 degree re-entry angle with the horizontal) with close tolerances compatible with manned re-entry conditions employing a re-entry L/D as small as 0.5.

Figure 2-1 shows a schematic diagram of the mission. The powered flight consists typically of a vertical launch, a kickover in the pitch plane if required by final flight path angle, and a constant pitch rate profile, all under control of an autopilot or inertial guidance system. The free flight trajectory is tracked by the DSIF, using range rate, elevation, and azimuth data. A midcourse correction is performed by radio command, based on the results of tracking. This maneuver is designed to correct three components of miss at re-entry -- longitude, latitude, and flight path angle. A second midcourse correction, based on additional tracking data, is made 24 to 48 hours later as a vernier on the first. In the following sections, these phases will be discussed in detail.

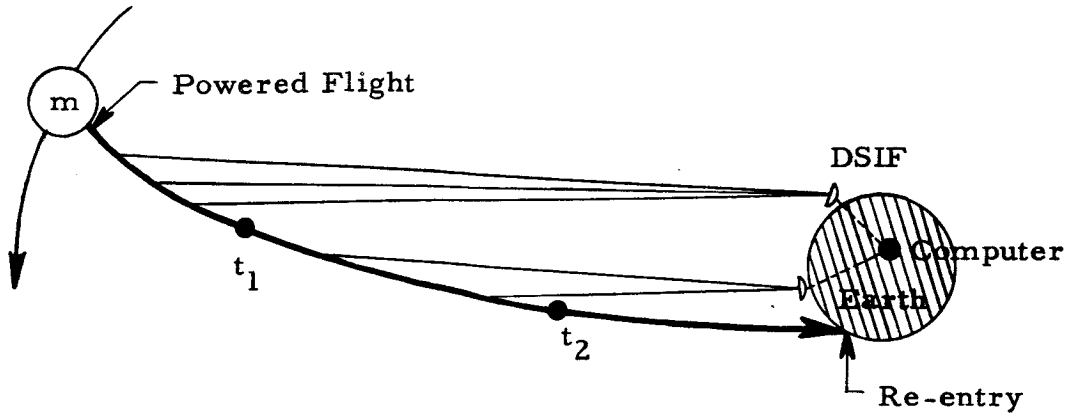

Figure 2-1. Schematic Diagram of the Standard Mission.

2. Transit Trajectory

The return trajectory may be specified by choosing desired values of the following variables:

Selenographic latitude of lunar launch site

Selenographic longitude of launch site

Return flight time

Re-entry latitude

Re-entry longitude

Re-entry angle

Launch date (time of lunar month)

Earth approach direction (i.e., clockwise, or counterclockwise).

From these variables the required injection conditions at the end of the lunar powered flight may be computed. Using the Analytic Lunar Return Program described in Part I, approximate lunar injection conditions were computed for a number of trajectories having different launch site locations and flight times. These conditions were then adjusted slightly to yield the desired re-entry conditions using an integrating (Encke) program. The guidance requirements for two of the trajectories were considered in detail.

Table 2-1 lists the nominal injection and re-entry conditions for trajectories P-3 and P-4. Launch occurs on December 17, 1963 (lunar declination $\sim$ -23 degrees) from a point near the earth-moon line at approximately

$7^{o}W$, $5^{o}N$. After a flight time of 50 or 90 hours, re-entry occurs at approximately $30^{o}N$ latitude with a re-entry angle of 6 degrees with the horizontal at an altitude of 400,000 feet. Figures 2-2 and 2-3 show the P-4 transit trajectory projected on the equatorial plane and on a plane perpendicular to the equator.

Table 2-1. Injection and Re-entry Conditions for Trajectories P-3 and P-4

Injection		
Liftoff time (min after 0^{h} GMT)	180.53	705.32
Selenocentric radius, r_o(ft)	5,733,000	5,733,000
Selenographic latitude, μ_o(deg)	5.14	5.87
Selenographic longitude, λ_o(deg)	-6.98	-7.05
Inertial Velocity (moon frame), V_o(fps)	9546.5	8270.3
Flight path angle (from lunar vertical), β_o(deg)	24.68	45.21
Selenographic azimuth of $\vec{V}_o$, A_o(deg)	88.69	79.43
Re-entry		
Flight time, t_f(hr)	50.23	90.45
Latitude of re-entry point, lat_i(deg)	29.98	29.58
Longitude of re-entry point, $long_i$(deg)	-99.27	-99.26
Re-entry flight path angle, β_i(deg)	95.83	96.00

3. Powered Flight and Injection Guidance

The powered flight sequence consists of the following steps:

a) A set of reference directions in space is established on radio command (or crew control) through one or more astronomical sightings and an accelerometer or pendulum determination of the vertical. In the case of the inertial launch guidance system, these measurements establish the inertial platform reference.

b) Guidance constants or autopilot settings are transmitted from earth to the spacecraft computer.

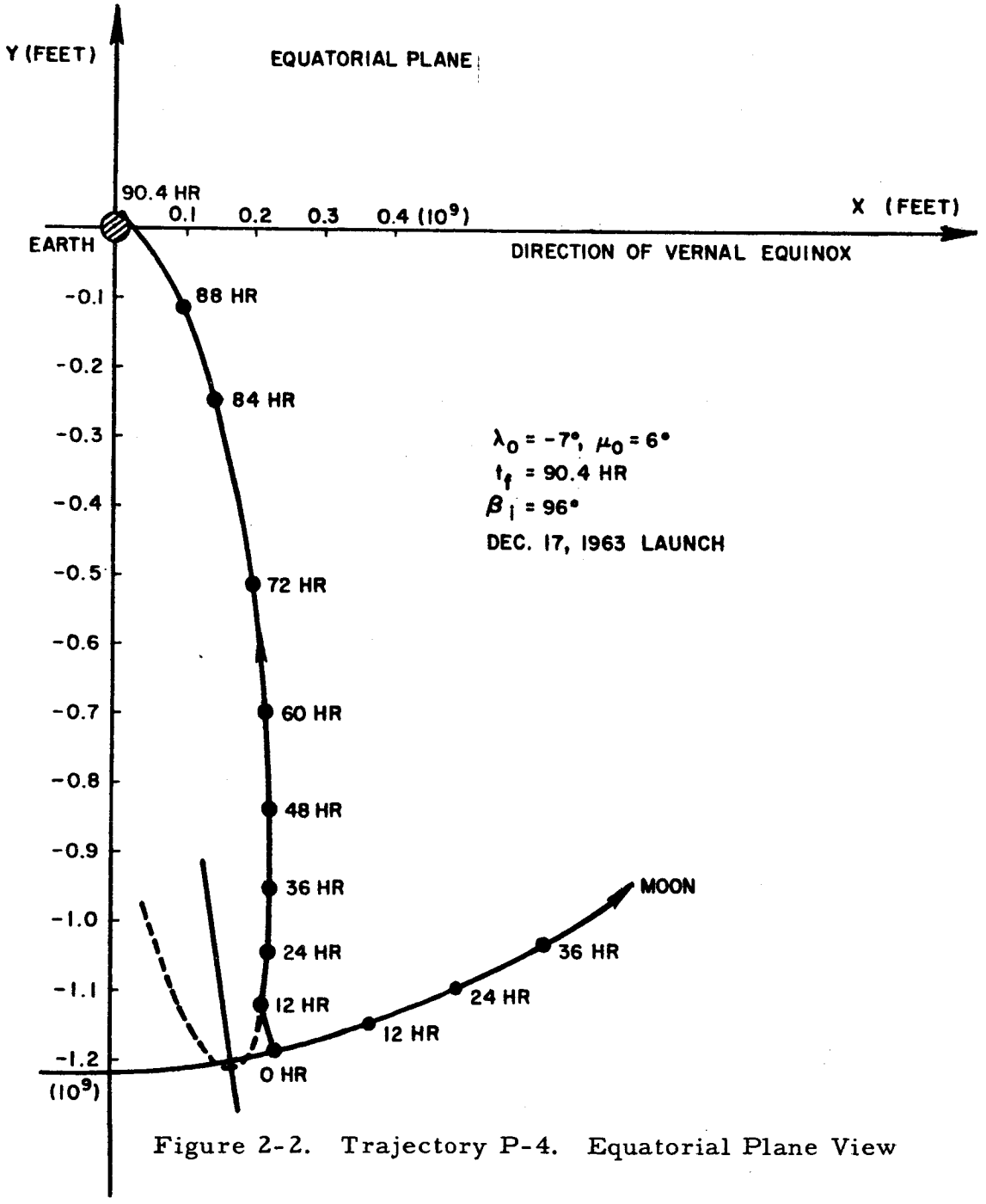

Figure 2-2. Trajectory P-4. Equatorial Plane View

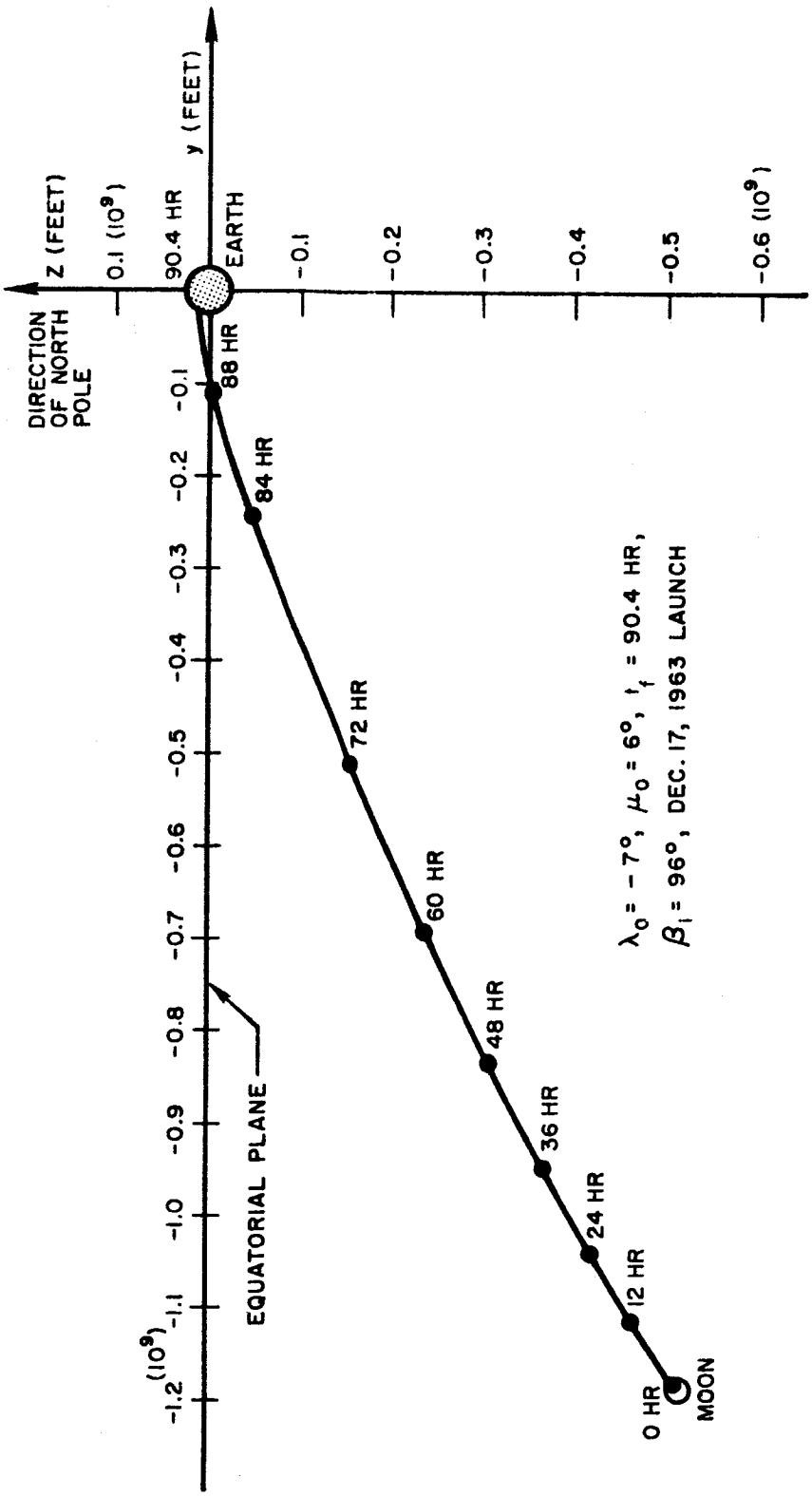

Figure 2-3. Trajectory P-4. Y-Z Plane View

c) On earth command (or crew command) liftoff occurs. A launch window may be mechanized by varying the burnout conditions as a function of liftoff time, as with direct-ascent space launches from earth.

d) Following a 5-second vertical rise, and kickover if required by the final flight path angle, the spacecraft follows a constant pitch rate turn to main engine burnout.

e) Main engine burnout is followed by a liquid propellant vernier phase terminated by accelerometer command.

The launch vehicle was assumed to be a single stage vehicle with a specific impulse of 300 seconds. This I_{sp} is representative of solid propellants which will be available in the near future or of a storable liquid propellant. A liftoff thrust-to-earth weight ratio of 4 was chosen. This value is sufficiently large to avoid excessive gravity losses, while not imposing a maximum acceleration of more than 11 earth g's. The constant pitch rate profile provides flexibility in being able to attain any burnout flight path angle required by the transit trajectory, including a launch into a lunar parking orbit. Lunar powered flight information is given in Reference [6] for other I_{sp}'s, thrust-to-weight ratios, and pitch profiles. Figure 2-4 shows the time history of the principal powered flight variables for P-4. Pitch rates of 1.045 deg/sec (P-3) and 2.018 deg/sec (P-4) were used to produce the proper flight path angle at thrust termination. As in earth-to-moon flights, the energy at injection is critical rather than particular values of velocity and altitude. Thus, in simulating the powered flight profiles for P-3 and P-4, cutoff was chosen to produce an injection energy equivalent to the r_o and V_o values given in Table 2-1. The resulting lunar injection altitudes were 183,800 feet for P-3 and 145,500 feet for P-4.

The injection errors at the end of powered flight are composed of errors produced during guidance plus errors due to the uncertainty in the knowledge of the absolute location of the launch site and in establishing the initial launch reference directions. These latter errors were assumed to be:

$$\sigma_{Lat} = \sigma_{Long} = 0.05 \text{ deg}, \quad \sigma_{Altitude} = 1000 \text{ ft}$$

$$\sigma_{\text{plane of trajectory (launch azimuth error)}} = 0.25 \text{ deg}$$

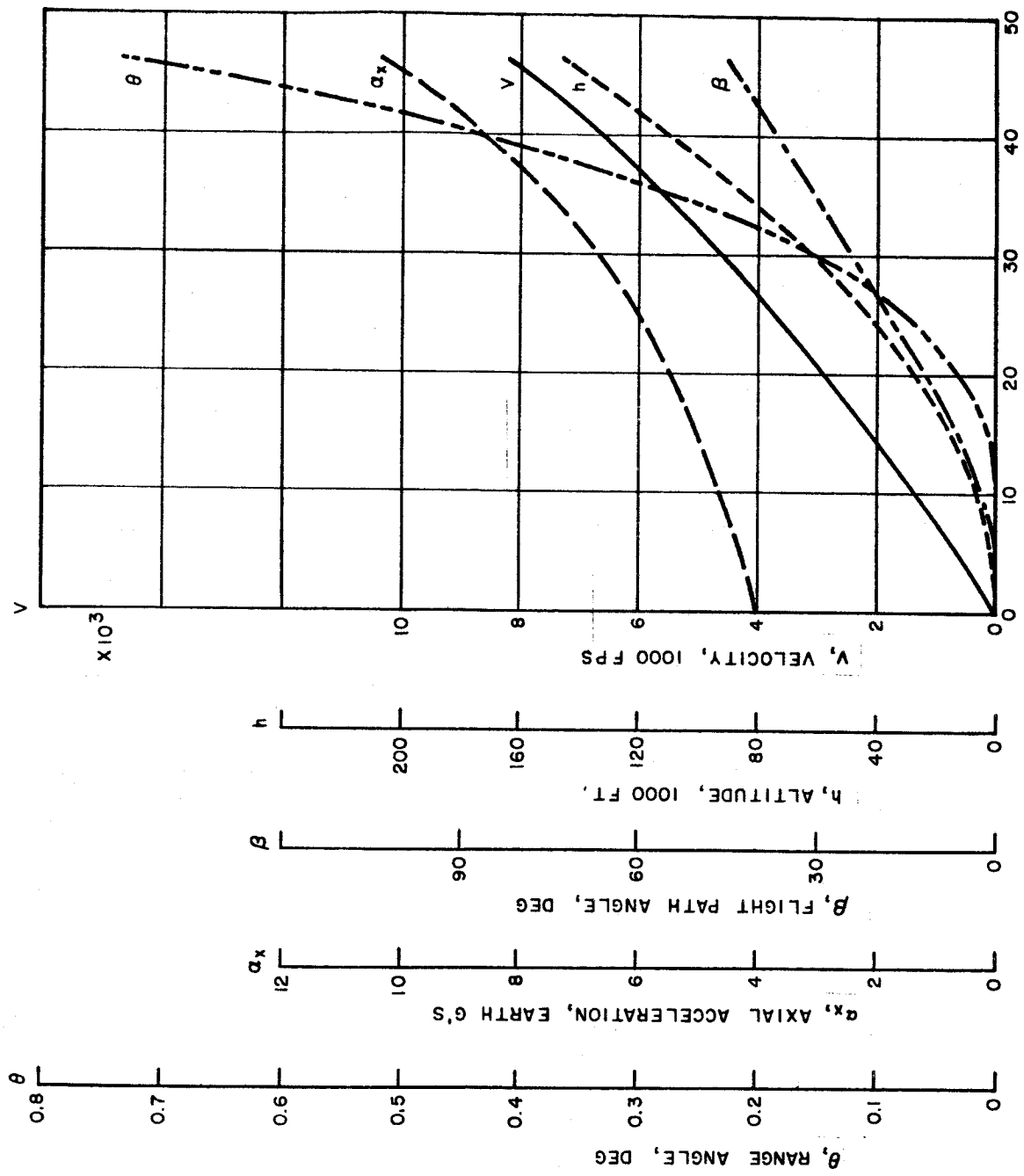

Figure 2-4. Powered Flight Profile for Trajectory P-4

A covariance matrix of injection errors resulting from the above sources and from a complete simulation of the autopilot or inertial guidance system was obtained for each trajectory using the methods outlined in Reference [6] . We shall discuss the error analysis of the two launch guidance methods in turn.

a. Autopilot Control

The following error sources were considered for the powered flight under autopilot control with integrating axial accelerometer cutoff in addition to the launch site and reference errors:

Liftoff weight, W_o	(percent)
Thrust, T	(percent)
Specific Impulse, I_{sp}	(percent)
Pitch rate, $\dot{\epsilon}$	(deg/sec)
Accelerometer scale	(percent)
Accelerometer bias	(earth g's)

Table 2-2 presents the following error analysis information for trajectories P-3 and P-4 under autopilot control:

1) Assumed values of the standard deviation of all independent error sources.

2) The standard deviation in re-entry latitude, longitude, and angle resulting from each of these independent source errors acting separately (i.e., source to re-entry "miss coefficients" scaled by a 1σ source error).

3) Variances and covariances of re-entry variables resulting from each source.

4) The re-entry variances and covariances for the total launch system. Since the source errors are independent, the total variances (and covariances) are simply the sums of the variances (and covariances) contributed by each source.

Table 2-2. Uncorrected Re-entry Error as a Function of Source Errors, Autopilot Controlled powered Flight

TRAJECTORY P-3, AUTO PILOT

No.	Source	σ	σ Long deg	σ Lat deg	σ_β deg	σ^2 Long deg^2	σ^2 Lat deg^2	σ_β^2 deg^2	Cov(Long, Lat) deg^2	Cov(Long, β) deg^2	Cov(Lat, β) deg^2
1	μ_o	0.05 deg	2.639	0.181	1.244	6.9639	0.03280	1.5485	-0.4780	-3.284	-0.2254
2	λ_o	0.05 deg	8.597	1.199	3.939	73.9075	1.43833	15.5174	-10.3104	-33.865	0.1538
3	A_o	0.25 deg	8.738	0.641	4.112	76.3475	0.41103	16.9083	-5.6019	-35.929	2.6362
4	W_o	0.5 %	30.383	4.108	13.664	923.1225	16.87763	186.7135	-124.8205	-415.163	56.1363
5	T	1.0%	61.368	8.298	27.600	3766.032	68.85882	761.7616	-509.2392	-1693.759	229.0284
6	I_{sp}	0.316%	5.327	0.711	2.373	28.3720	0.50502	5.6296	-3.7853	-12.638	1.6861
7	$\dot{\epsilon}$	0.1%	5.028	0.681	2.263	25.2786	0.46338	5.1228	-3.4221	-11.380	1.5405
8	r_o	10^3 ft.	0.416	0.075	0.231	0.1729	0.00562	0.0534	-0.0312	-0.096	0.0173
9	Accel. Scale	5×10^{-3}%	0.679	0.109	0.345	0.4615	0.01184	0.1193	-0.0739	-0.235	0.0376
10	Accel. Bias	3×10^{-5} ge	0.064	0.010	0.032	0.0041	0.00010	0.0011	-0.0007	-0.002	0.0003
				TOTAL MISS		$(70.005)^2$	$(9.437)^2$	$(31.518)^2$	-657.7629	-2206.350	296.0325

TRAJECTORY P4, AUTO PILOT

No.	Source	σ	σ Long deg	σ Lat deg	σ_β deg	σ^2 Long deg^2	σ^2 Lat deg^2	σ_β^2 deg^2	Cov(Long, Lat) deg^2	Cov(Long, β) deg^2	Cov(Lat, β) deg^2
1	μ_o	0.05 deg	0.539	0.024	0.349	0.2901	0.05740	0.12146	-0.12904	-0.18770	0.0835
2	λ_o	0.05 deg	2.525	0.694	0.926	6.3776	0.48125	0.84315	-1.75191	-2.31890	0.6370
3	A_o	0.25 deg	13.067	4.831	6.812	170.7494	23.33438	46.40562	-63.12188	-89.01563	32.9066
4	W_o	0.5%	2.930	3.273	4.039	8.5844	10.71523	16.31548	9.59080	11.83460	13.2221
5	T	1.0%	5.886	6.617	8.165	34.6398	43.78001	66.67337	38.94265	48.05779	54.0274
6	I_{sp}	0.316%	1.340	1.443	1.836	1.7968	2.08366	3.36966	-1.93494	-2.46063	2.6498
7	$\dot{\epsilon}$	0.1 %	0.057	0.734	0.918	0.0032	0.53906	0.84318	0.04164	0.05207	0.6742
8	r_o	10^3 ft	1.313	0.643	0.833	1.7246	0.41385	0.69360	-0.84483	-1.09373	0.5358
9	Accel. Scale	5×10^{-3}%	0.958	0.426	0.553	0.9185	0.18149	0.30618	-0.40829	-0.53031	0.2357
10	Accel. Bias	3×10^{-5} ge	0.093	0.041	0.054	0.0086	0.00171	0.00288	-0.00383	-0.00498	0.0022
				TOTAL MISS		$(15.003)^2$	$(9.033)^2$	$(11.644)^2$	-19.61935	-35.66716	104.9743

71

The information is grouped in the table as shown schematically:

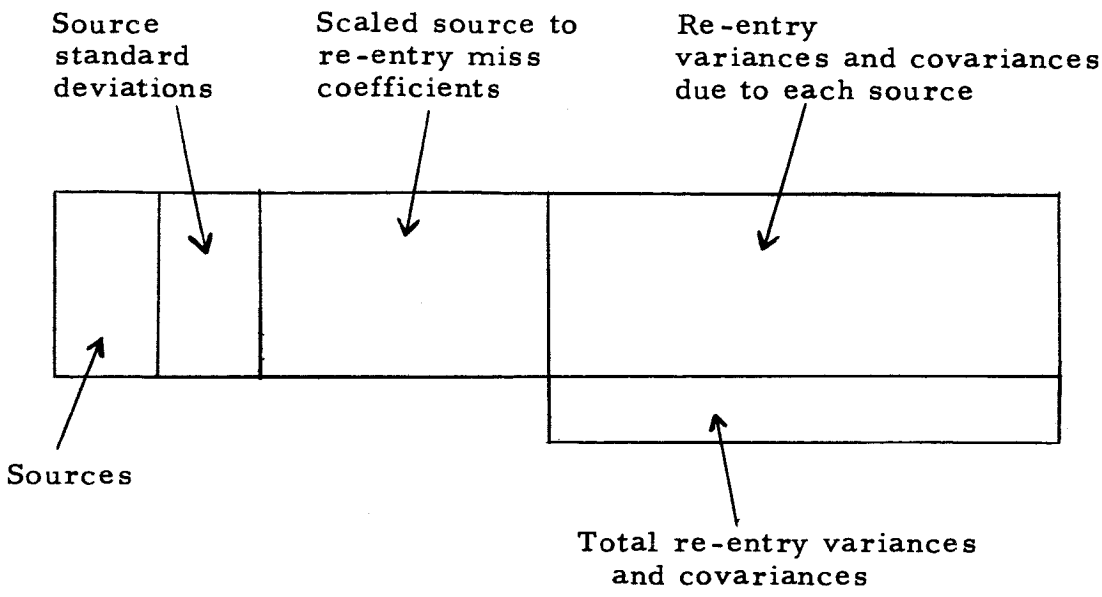

From this table the relative contribution of each error source to the final miss at re-entry can be seen. In addition the effect of a change in the magnitude of any source error can be readily estimated by scaling the variances and covariances due to the source by the square of the new source standard deviation. Table 2-3 lists the miss coefficients relating injection errors to re-entry errors for P-3 and P-4, used in producing Table 2-2.

b. Inertial Guidance

The inertial guidance errors were computed in the following way. Open loop powered flight profiles for trajectories P-3 and P-4 were entered into an STL inertial guidance error analysis program. From the profiles, the contributions to the injection covariance matrix of 45 independent error sources were computed. The resulting injection covariance matrix for the complete system was then combined with the contributions of the launch site and reference direction error and the miss coefficients of Table 2-3 (using the method described in Reference [1]) to produce a re-entry covariance matrix. The magnitudes of the source errors used are typical of a present state-of-the-art inertial guidance system. The final re-entry covariance matrices for P-3 and P-4 under inertial guidance are shown in Table 2-4.

Table 2-3. Injection Miss Coefficients

Re-entry Variation \ Injection Variation	Δr_o (ft)	$\Delta \lambda_o$ (deg)	$\Delta \mu_o$ (deg)	ΔV_o (fps)	$\Delta \beta_o$ (deg)	ΔA_o (deg)
Trajectory P-3 (50 hr)						
$\Delta\beta_i$(deg)	$0.272(10^{-3})$	80.5	-26.5	0.60	104	17.1
$\Delta Long_i$(deg)	$-0.462(10^{-3})$	-175.0	55.1	-1.10	-226	-35.7
ΔLat_i(deg)	$0.081(10^{-3})$	24.4	-4.0	0.18	31	2.7
Δt_f(min)	$-0.447(10^{-3})$	-24.7	17.2	-0.84	-32	-10.7
$\Delta b_2(10^6$ ft)*	$-38.0(10^{-6})$	-12.4	2.33	-0.086	-15.9	-1.58
$\Delta b_3(10^6$ ft)*	$6.9(10^{-6})$	-0.35	6.29	0.012	-0.70	-3.81
Trajectory P-4 (90 hr)						
$\Delta\beta_i$(deg)	$0.575(10^{-3})$	24.2	-4.69	0.960	39.3	23.3
$\Delta Long_i$(deg)	$-0.131(10^{-2})$	-50.5	11.1	-2.18	-82.0	-51.9
ΔLat_i(deg)	$0.642(10^{-3})$	13.9	-5.03	1.04	22.8	19.2
Δt_f(min)	$-0.192(10^{-2})$	44.2	19.6	-2.91	68.0	-28.2
$\Delta b_2(10^6$ ft)	$-137(10^{-6})$	-2.75	0.374	-0.221	-4.45	-2.24
$\Delta b_3(10^6$ ft)	$-8.03(10^{-6})$	-0.691	1.66	-0.014	-1.29	-4.52

*b_2 and b_3 are components of geocentric impact parameter.

c. Conclusions

From Tables 2-2 and 2-4 the following conclusions may be drawn:

1) For the error source magnitudes used, the final inertial guidance re-entry errors are much too large for manned re-entry without a midcourse correction.

2) In turn, the autopilot re-entry errors are from ~1.7 times (90 hours) to ~6 times as large as the IG re-entry errors.

3) For the autopilot cases,

   at 50 hr by far the largest re-entry error contributions are thrust, T, and liftoff weight, W_o, errors.

   at 90 hr the major contributors are errors in A_o, T, and W_o with the T and W_o error terms having much less effect than at 50 hr flight time.

4) The launch site and reference error sources μ_o, λ_o, A_o, r_o are common to both autopilot and IG cases. Thus even if the inertial guidance system performed with no error, these sources would limit the final accuracy to the following, unless improved:

$$\sigma_{Long} = 9^o, \ \sigma_{Lat} = 1.36^o, \ \sigma_{\beta} = 5.7^o, \ (50 \text{ hr})$$

Table 2-4. Uncorrected Miss Covariance Matrices

P3 - Powered Flight Inertially Guided

	Re-entry Long $(\text{deg})^2$	Re-entry Lat $(\text{deg})^2$	Re-entry Angle $(\text{deg})^2$
Re-entry Long	$(12.40)^2$	-16.1993	-71.4795
Re-entry Lat		$(1.37)^2$	7.5002
Re-entry Angle	Symmetric		$(5.76)^2$

P4 - Powered Flight Inertially Guided

Re-entry Long	$(13.41)^2$	-66.1285	-92.7996
Re-entry Lat		$(4.94)^2$	34.3354
Re-entry Angle	Symmetric		$(6.95)^2$

Comparing these with the final IG errors from Table 2-4 of

$$\sigma_{Long} = 12.4^{o},\ \sigma_{Lat} = 1.37^{o},\ \sigma_{\beta} = 5.8^{o},\ (50\ hr)$$

it is seen that almost all of the final re-entry error in the IG case is due to launch site uncertainty and reference direction errors.

4. Midcourse Guidance

a. The Basic Process

With a fully attitude controlled spacecraft, it is possible to correct three components of miss at a target, corresponding to three velocity components, each time a correction is made. In both of the midcourse corrections of the standard mission, three quantities -- re-entry latitude, longitude, and angle -- will be controlled. The following sequence of operations comprise the midcourse correction process:

1) Following lunar injection, the spacecraft is tracked by the three stations of the DSIF network. The data is relayed to the control computer where the spacecraft orbit is determined by a standard least squares tracking program. One output of the program is the covariance matrix of estimated re-entry conditions. When sufficient tracking data has been obtained to reduce the orbit determination uncertainty to a small value in comparison with the re-entry uncertainties based on the a priori injection guidance error covariance matrix, a first midcourse correction is computed. Two models of DSIF accuracy were used, as explained later. A data rate of one observation set (R, E, A) per minute was employed. No range data was included.

2) Approximately 8 to 12 hours after injection a midcourse correction is computed and transmitted to the spacecraft. On command, the spacecraft principal axis (rocket thrust axis) is turned to the computed direction with an angular accuracy of 2 mils (1σ) assumed in the basic comfiguration. On command, the computed velocity is added using the spacecraft vernier engines. The velocity increment is assumed to be controlled by an accelerometer cutoff to an accuracy of 0.4 (10^{-4}) times magnitude of correction. A cold gas propulsion system is used immediately following the hot gas correction as a vernier on the velocity increment. The thrust cutoff is assumed to be 0.01 fps (1σ). Following the correction, the spacecraft axis is returned to the cruise orientation.

3) The spacecraft is again tracked until the orbit determination errors are small in comparison with an a priori estimate of the re-entry condition including the statistics of the first midcourse execution errors.

4) 20 to 50 hours after the first midcourse correction, a second midcourse correction is made to remove a part of the previous tracking and midcourse execution errors.

5) Tracking of the spacecraft continues throughout the flight in preparation for the re-entry phase (not treated in this report), but no further midcourse correction is required.

b. Fuel Requirements for a Single Midcourse Correction

Two factors govern the choice of times t_1 and t_2 at which corrections are to be made:

1) Sufficient time must have elapsed before the first correction in order that the orbital elements may be determined with reasonable accuracy by tracking.

2) Consideration must be given to fuel requirements, whose statistics are a function of t_1 and t_2.

On a particular mission it may be desirable to apply values (weights) to accuracy and to required fuel, and to optimize a linear combination of these. We have not attempted to do this here.

The growth of orbit determination accuracy with the length of time the spacecraft has been tracked is illustrated in Ref. [3]. As a further guide to the choice of the first midcourse correction time t_1, it is of interest to consider the velocity increment required for a single midcourse correction as a function of the time of correction.

When the time t_1 at which the first midcourse correction is to be made is sufficiently late so that tracking errors are small compared with injection errors, then the probability distribution of the velocity corrections is essentially independent of tracking errors. We have studied fuel requirements of the first correction on this basis.* For a given

*A more accurate analysis based on a Monte Carlo simulation is presented later in this section.

trajectory, the uncorrected miss in latitude, longitude, and re-entry angle is characterized statistically by a 3 x 3 covariance matrix $\sum_1$. Let B be the 3 x 3 matrix which relates the midcourse correction velocity vector components $\begin{bmatrix} V_x \\ V_y \\ V_z \end{bmatrix}$ to variations in latitude, longitude, and re-entry angle. Then, $\sum_v = B^{-1} \sum_1 (B^{-1})^T$ is the covariance matrix of the correction vector $\begin{bmatrix} V_x \\ V_y \\ V_z \end{bmatrix}$. Figure 2-5 presents graphs of the 1σ values of the x, y, z components of the corrections versus time of execution for trajectories P-3 and P-4. From Figure 2-5 it may be seen that the midcourse velocity requirement does not vary strongly if the correction is made anywhere in the interval from 15 to 40 percent of t_f.

c. Method of Analysis

The tracking and midcourse correction sequence described above has been simulated by a Monte Carlo method to determine the probability distribution of errors after each correction and of the velocity increment required for each correction. The technique which was developed is applicable to an arbitrary number of midcourse corrections. Figure 2-6 is a block diagram of the gross features of an n-midcourse correction simulation. Let us consider the first block of this diagram, corresponding to the first midcourse correction. The inputs to this block are:

1) λ_1, μ_1, β_1, the actual (uncorrected) miss in re-entry coordinates before the first midcourse correction. This miss arises from lunar powered flight burnout errors. In general, λ_k, μ_k, β_k is the actual miss after the (k-1) st correction.

2) $\sum_1$, the 3 x 3 covariance matrix of λ_1, μ_1, β_1. $\sum_1$ is the covariance matrix of the uncorrected miss and comes from the powered flight analysis.

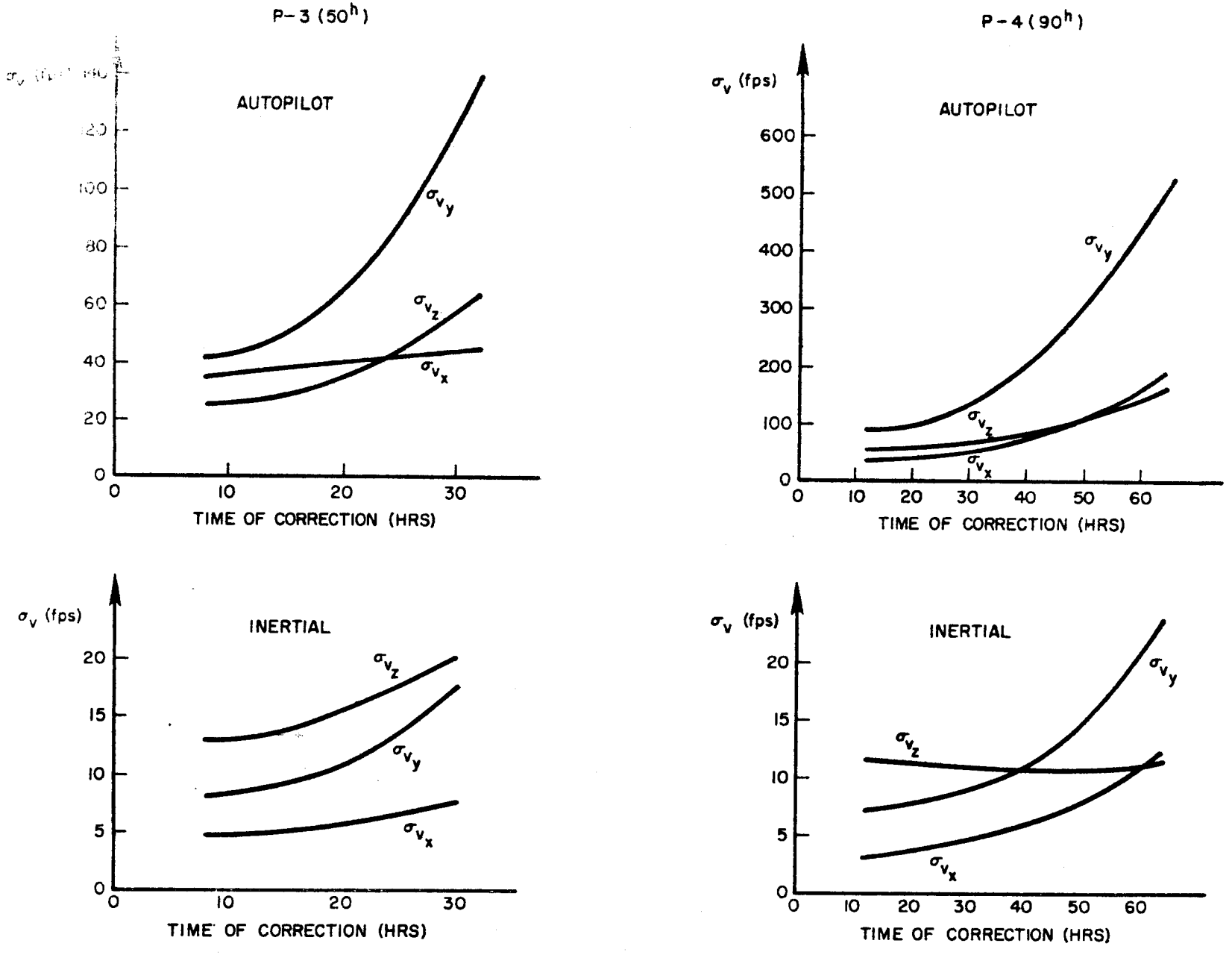

Figure 2-5. Single Correction Midcourse Velocity Requirements versus Time of Correction (Standard Mission)

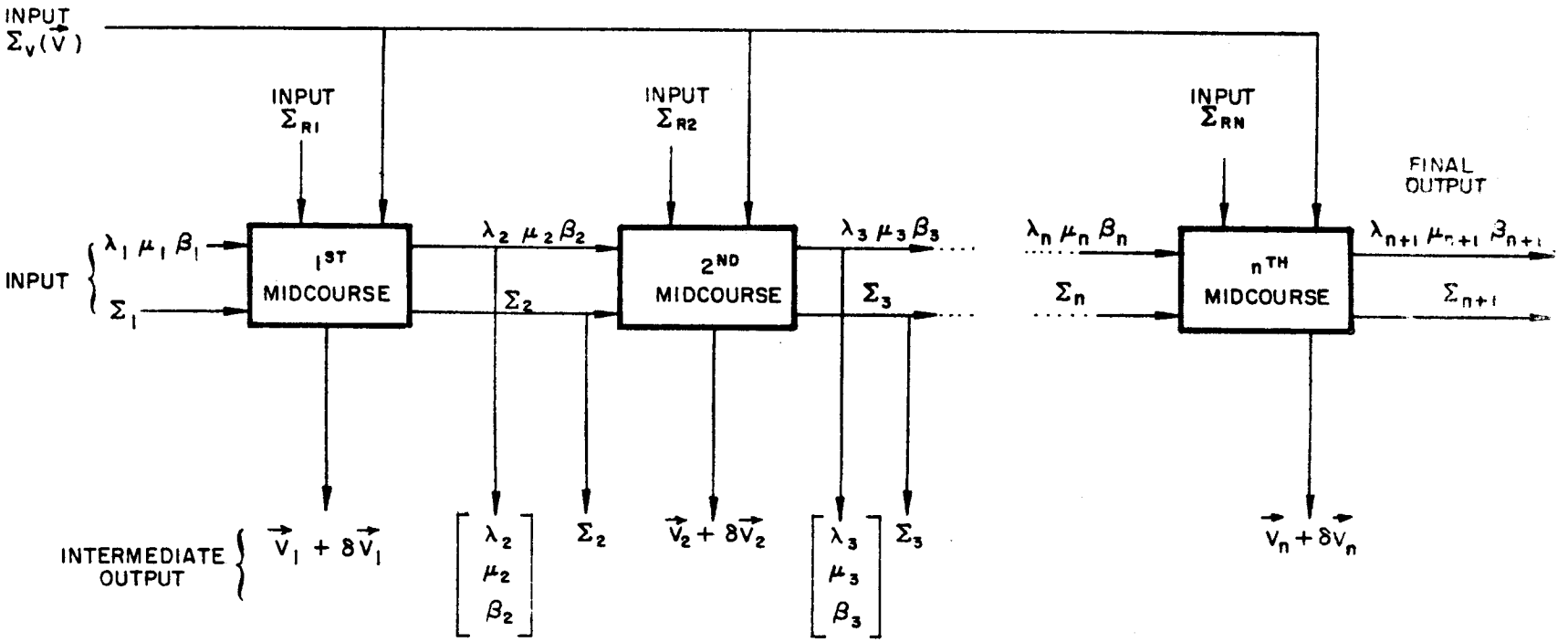

KEY: $\lambda_k, \mu_k, \beta_k$ = actual long., lat., flight path angle before k^{th} correction

Σ_k = 3 x 3 covariance matrix of λ_k, μ_k, β_k

$\vec{V}_k + \delta\vec{V}_k$ = velocity correction which is actually executed at the k^{th} midcourse, $\vec{V}_k$ being the commanded correction

$\Sigma_v(\vec{V})$ = covariance matrix of execution errors as a function of commanded correction

Figure 2-6. Block Diagram of Monte Carlo Simulation of n Midcourse Corrections

3) $\sum_v(\vec{v})$, the 3 x 3 covariance matrix of execution errors as a function of the commanded correction vector $\vec{v}$. $\sum_v(v)$ is discussed below.

4) $\sum_{R1}$, the 3 x 3 covariance matrix of λ, μ, β based (solely) on DSIF radar tracking from t_o, injection time, to t_1, the time of the first midcourse correction.

The outputs of the first block are $\vec{v}_1 + \delta\vec{v}_1$, λ_2, μ_2, β_2 and $\sum_2$. $\vec{v}_1 + \delta\vec{v}_i$ is later combined with $\vec{v}_2 + \delta\vec{v}_2$, etc. to determine the fuel requirements. $\sum_2$ is a 3 x 3 covariance matrix of the resultant accuracy if no other corrections were made. λ_2, μ_2, β_2 and $\sum_2$, together with $\sum_v(v)$ and $\sum_{R2}$, are the inputs to the next block. Note that $\sum_{R2}$ comes from DSIF tracking from t_1 to t_2.

A fundamental part of the Monte Carlo scheme is the STL Random Vector Generator (RVG) program which generates N Gaussian random variables having a prescribed N x N covariance matrix. N may be as large as 50. For example, if we input $\sum_1$ to this program,

$$\sum_1 \longrightarrow \boxed{\text{RVG}} \longrightarrow \lambda_1, \mu_1, \beta_1$$

the program will generate three Gaussian random variables λ_1, μ_1, β_1, having $\sum_1$ as their covariance matrix.

Let us now consider in detail the operation of the first block (first correction) in Figure 2-6:

1) $\left(\sum_1^{-1} + \sum_{R1}^{-1}\right)^{-1} = \sum_1' =$ 3 x 3 covariance matrix of best estimate of re-entry coordinates before correcting.

2) $\sum_1' \longrightarrow \boxed{\text{RVG}} \longrightarrow \begin{matrix}\delta\lambda_1 \\ \delta\mu_1 \\ \delta\beta_1\end{matrix}$;

these will constitute the portion of miss after the correction due to errors in orbit determination.

3) $$-B_1^{-1}\begin{bmatrix}\lambda_1 + \delta\lambda_1\\ \mu_1 + \delta\mu_1\\ \beta_1 + \delta\beta_1\end{bmatrix} = \vec{V}_1 = \text{commanded correction}$$

4) $\sum_v(\vec{V}_1)$ = 3 x 3 covariance matrix of execution errors (discussed below).

5) $\sum_v(v_1) \longrightarrow$ [RVG] $\longrightarrow \delta\vec{V}_1$ = errors in execution of commanded correction (Note: $\vec{V}_1 + \delta\vec{V}_1$ is the actual correction which is executed).

6) $$\begin{bmatrix}\lambda_2\\ \mu_2\\ \beta_2\end{bmatrix} = \begin{bmatrix}\delta\lambda_1\\ \delta\mu_1\\ \delta\beta_1\end{bmatrix} + B_1\,\delta\vec{V}_1 = \text{actual remaining}$$
miss after 1st correction

7) $\sum_2 = \sum_1' + B_1 \sum_V(\vec{v}_1) B_1^T$ = covariance

matrix of $\begin{bmatrix}\lambda_2\\ \mu_2\\ \beta_2\end{bmatrix}$.

The outputs $\begin{bmatrix}\lambda_2\\ \mu_2\\ \beta_2\end{bmatrix}$ and $\sum_2$ now serve as inputs to block 2.

This process can clearly be repeated as many times as desired to simulate an arbitrary number of midcourse corrections.

In the Monte Carlo simulation, a required input is the covariance matrix of execution errors, $\sum_v(\vec{V})$. To study execution errors, it is convenient to transform to spherical coordinates of the commanded correction, V, θ, ϕ, as shown in the accompanying diagram:

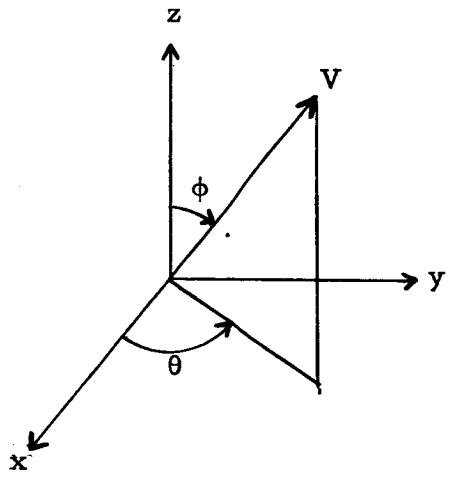

Then the expressions for velocity errors in terms of basic error sources are

$$\delta V = k_b + k_p V \quad ,$$

$$\delta V_\theta = V \sin \phi \, \delta\theta \quad ,$$

$$\delta V_\phi = V \delta\phi \quad ,$$

where k_b is velocity error due to engine cutoff control, k_p is a proportional accelerometer error, and $\delta\theta$ and $\delta\phi$ are angular orientation errors. We assume k_b, k_b, $\delta\theta$ and $\delta\phi$ are independent gaussian errors with known standard deviations. Provision is made, however, for these errors to be correlated from one correction to the next. Provision is also made to permit the standard deviations of these errors to be different for each midcourse correction.

Since the covariance matrix $\sum_v(\vec{V})$ is expressed in terms of rectangular coordinates, it is necessary to introduce a rotation, U,

relating variations in spherical coordinates to variations in rectangular coordinates:

$$\begin{bmatrix} \delta V_x \\ \delta V_y \\ \delta V_z \end{bmatrix} = U \begin{bmatrix} \delta V \\ \delta V_\theta \\ \delta V_\phi \end{bmatrix},$$

where

$$U = \begin{bmatrix} \sin\phi\cos\theta & -\sin\theta & \cos\phi\cos\theta \\ \sin\phi\sin\theta & \cos\theta & \cos\phi\sin\theta \\ \cos\phi & 0 & -\sin\phi \end{bmatrix}$$

The final form of $\sum_v(\overrightarrow{V})$ is therefore

$$\sum_v(\overrightarrow{V}) = \begin{bmatrix} V_x \\ V_y \\ V_z \end{bmatrix} \begin{bmatrix} V_x & V_y & V_z \end{bmatrix}$$

$$= V^2 U \begin{bmatrix} \overline{k_p^2} & & \\ & \overline{\delta\theta^2}\sin^2\phi & \\ & & \overline{\delta\phi^2} \end{bmatrix} U^T + U \begin{bmatrix} k_b^2 & & \\ & 0 & \\ & & 0 \end{bmatrix} U^T.$$

Thus $\sum_v(\overrightarrow{V})$ may be evaluated numerically as soon as V, θ, ϕ for the commanded correction are specified.

d. Simulation Results

Each complete cycle of the Monte Carlo program corresponds to a typical simulation of a moon-to-earth return. By cycling the program several thousand times, a random sample of outputs is obtained, from which cumulative probability distributions of midcourse velocity requirements and re-entry errors may be obtained.

Table 2-5 lists the results of a Monte Carlo simulation of the midcourse guidance and tracking phase of trajectories P-3 and P-4 using a sample size of 2000 runs. The DSIF and execution errors listed earlier were assumed (for convenience, these errors and the re-entry miss before midcourse correction are also listed in Table 2-5). Both autopilot control and inertial launch guidance are compared.

Table 2-6 is of interest because it shows the change in re-entry error and midcourse velocity requirement for four perturbations of the system configuration:

1) A factor of 10 degradation in velocity execution accuracy

2) A factor of 5 degradation in angular orientation accuracy at midcourse

3) Tracking data rate of 1 observation set each 10 minutes

4) Tracking data rate of 6 observation sets each minute (standard DSIF rate).

The entries labeled "standard" correspond to the tracking and execution errors listed in Table 2-5 and a DSIF data rate of one observation set per minute.

From Table 2-6, it became apparent that final accuracy was "tracking limited," in that the final accuracy attained was essentially the accuracy with which the orbit could be re-established by tracking from the first to the second midcourse maneuver. Within wide limits, execution errors were negligible. This fact made it imperative to take a second look at the DSIF accuracy model used in the simulations. In cooperation with JPL, a new DSIF model was decided upon: $\sigma_{\dot{R}} = 0.5$ ft/sec, $\sigma_A = \sigma_E = 0.2^o$, uncorrelated, at a data rate of one set of observations per minute. The new model degrades the accuracy assigned to angular measurements to take into account the fact that the true angular observations are actually correlated (see Part IV). The degradation factor depends on the assumed data rate and is lower for lower data rates.

Table 2-5. Standard Mission: Midcourse Velocity Requirement and Final Accuracy

- System Characteristics

1.	Launch site:	Near earth-moon line ($\sim 7^{\circ}$W, 5°N). Re-entry: 30°N Latitude
2.	Powered flight guidance:	Present state-of-the-art inertial guidance system, or autopilot with accelerometer cutoff.
3.	Tracking:	DSIF, 3 stations, $\sigma_{angles} = 0.04^{\circ}$, $\sigma_{\dot{R}} = 0.5$ fps, no range data included, data rate = 1 point/minute
4.	Execution errors:	Orientation angles 2 mils (1σ) Accelerometer constant $0.4(10^{-4})$ (1σ) Thrust cutoff 0.01 fps (1σ)

- 50 Hr Flight (P-3), Inertial Guidance

	Lat (deg)	Long (deg)	β_{re} (deg)	ΔV (fps)
Uncorrected miss (1σ)	1.37	12.4	5.75	
After 1st midcourse at 8^h(68 percent*)	0.23	1.3	0.58	16.1
After 2nd midcourse at 32^h(68 percent*)	0.014	0.10	0.04	7.3
			($V_T = 22.8$)	
Autopilot				
Uncorrected miss (1σ)	9.44	70.0	31.5	
After 1st midcourse at 8^h(68 percent)	0.23	1.3	0.58	49.8
After 2nd midcourse at 32^h(68 percent)	0.014	0.10	0.04	7.3
			($V_T = 55.4$)	

- 90 Hr Flight (P-4), Inertial Guidance

Uncorrected miss (1σ)	4.94	13.4	6.95	
After 1st midcourse at 12^h(68 percent)	0.48	1.5	0.67	14.0
After 2nd midcourse at 64^h(68 percent)	0.021	0.068	0.029	3.5
			($V_T = 16.5$)	
Autopilot				
Uncorrected miss (1σ)	9.03	15.0	11.6	
After 1st midcourse at 12^h(68 percent)	0.50	1.5	0.68	112
After 2nd midcourse at 64^h(68 percent)	0.022	0.067	0.031	3.5
			($V_T = 115$)	

*Monte Carlo Simulation, 2000 runs.

Table 2-6. Effect of Changes in Midcourse Execution Accuracy and Tracking Data Rate

- System Configuration

  90 hr flight (P-4), all characteristics as listed in Table 2-1

- Inertial Guidance

	Lat (deg)	Long (deg)	β_{re} (deg)	ΔV (fps)
After 1st midcourse at 12^h(68 percent*)				
Standard configuration	0.48	1.45	0.67	14.0
Velocity execution degraded (x10)	0.50	1.50	0.70	14.0
Angle execution degraded (10 mils)	0.50	1.50	0.67	14.0
Tracking rate 1/10 min	1.50	4.70	2.10	14.5
Tracking rate 6/min	0.20	0.60	0.27	14.0
After 2nd midcourse at 64^h(68 percent)				
Standard configuration	0.021	0.068	0.029	3.5
Velocity execution degraded (x10)	0.026	0.080	0.037	3.5
Angle execution degraded (10 mils)	0.024	0.075	0.034	3.5
Tracking rate 1/10 min	0.069	0.220	0.097	11.1
Tracking rate 6/min	0.009	0.029	0.013	1.4

- Autopilot

After 1st midcourse at 12^h(68 percent)				
Standard configuration	0.50	1.5	0.68	112
Velocity execution degraded (x10)	0.50	1.5	0.70	112
Angle execution degraded (10 mils)	0.70	2.2	0.95	112
Tracking rate 1/10 min	1.6	4.7	2.2	112
Tracking rate 6/min	0.23	0.7	0.33	112
After 2nd midcourse at 64^h(68 percent)				
Standard configuration	0.022	0.067	0.031	3.5
Velocity execution degraded (x10)	0.026	0.085	0.038	3.5
Angle execution degraded (10 mils)	0.024	0.076	0.035	4.3
Tracking rate 1/10 min	0.069	0.220	0.097	11.0
Tracking rate 6/min	0.009	0.029	0.013	1.5

*Monte Carlo, 2000 runs

New simulations were then performed using the new DSIF model. Since it has already been established that final accuracy was tracking limited, it was of primary interest to simulate the tracking from first to second midcourse maneuver. The results are presented in Table 2-7 for Trajectory P-4, corresponding to the second midcourse correction being made at 64 hours (as before) and also at 80 hours.

Table 2-7. Standard Mission

Tracking Interval (hours from injection)	σ_{Long} (deg)	σ_{Lat} (deg)	σ_{β} (deg)
12-64	0.21	0.067	0.096
12-80	0.053	0.016	0.023

Final accuracy for P-4 using new DSIF model ($\sigma_{\dot{R}}$ = 0.5 fps, $\sigma_A = \sigma_E = 0.2^o$, one set of observations per minute), corresponding to making the second midcourse correction at 64 hours and 80 hours, respectively.

The accuracies quoted in Table 2-7 are somewhat pessimistic, since no a priori information was used in the tracking. If a priori information were included, one could expect the results at 64 hours to be reduced by at least 50 percent. The results at 80 hours, however, will not be very sensitive to a priori data.

We have already seen in Table 2-6 that the fuel requirement (ΔV) for the first midcourse maneuver depends only on injection errors and is insensitive to tracking accuracy or execution errors, within wide limits. Thus, the fuel requirement for the first midcourse maneuver, given by Table 2-5, is not altered by using the new DSIF model. The fuel requirement for the second midcourse maneuver, however, depends on how well the first maneuver is performed, which in turn depends on DSIF accuracy. Thus for P-4, the fuel requirement for the second midcourse made at 64 hours will be approximately 11 fps (68 percent level) when the new DSIF model is used. When the second midcourse is made at 80 hours for P-4, the fuel requirement will be somewhat higher due to the loss of sensitivity. We have not performed the exact simulation to obtain this value.

We shall summarize this section by drawing the following considerations:

1) The system simulated, when used with two midcourse corrections, provides adequate accuracy for manned re-entry. Typical re-entry dispersions are (inertial launch guidance, 90 hour flight, 2nd midcourse at 64 hours):

σ_{Lat} = 0.07 degree (4 n mi)

σ_{Long} = 0.2 degree (10 n mi)

$\sigma_{\beta_{re}}$ = 0.1 degree

(These values may be reduced by a factor of 4 by making the second correction at 80 hours. For comparison, a typical manned capsule with an L/D = 0.5 should allow reaching a landing site anywhere within a re-entry footprint 800 n mi in width and extending from a point 1500 n mi from the sub-re-entry point to a point 3500 n mi from re-entry. A re-entry flight path angle tolerance of 3 degrees - full corridor width - can be permitted).

2) Compared with an allowable 3 degree corridor width ($\pm$1.5 degree): neither guidance system (or t_f) will suffice uncorrected. Both systems and t_f's are very accurate after two corrections ($\sim$0.1 degree 1σ).

3) Following execution of the first midcourse correction, there is essentially no difference in re-entry accuracy between the autopilot and inertial systems for a given flight time.

4) The autopilot controlled flights require 2 to 5 times as much midcourse fuel (velocity increment) as the inertially guided flights. The total velocity increments required are (68 percent):

50 hours IG	38 fps	90 hours IG	25 fps
50 hours autopilot	72 fps	90 hours autopilot	123 fps

5) Employing two midcourse corrections, degradations of a factor of 10 in velocity execution accuracy or a factor of 5 in angular orientation accuracy cause negligible change in re-entry accuracy.

It should be reemphasized that the mission analysis carried out here has neglected the effects of physical constant and station location errors which will degrade the performance displayed here somewhat. However, the use of the full DSIF data rate and of ground based range data and possibly moon-based doppler could all serve to improve the tracking safety margin.

C. Minimal Mission

The minimal mission discussed in this chapter has many features in common with the standard mission of Section B. Therefore, although computational results are given for all phases, in order to avoid undue repetition, only those features which are unique to this mission will be stressed.

1. Mission Description

The moon-earth mission analyzed in this chapter is a "minimal" mission in that it meets the following conditions:

a) Attitude is controlled by spin-stabilization

b) Lunar powered flight lasts until fuel depletion, or as an alternative an accelerometer cutoff may be used.

c) Restrictions on re-entry are loose in that accelerations and heating rates outside manned re-entry tolerances are permitted. Only longitude and latitude of re-entry are controlled by midcourse corrections.

At launch, the vehicle is pointed in the proper direction and spun up, either slightly before or slightly after it is released by the launching mechanism. Maintaining this fixed attitude, the vehicle burns either to fuel depletion or to accelerometer cutoff, depending on the details of the system employed. Two spin-stabilized midcourse corrections to modify re-entry longitude and latitude are scheduled at pre-selected times t_1 and t_2, where t_1 is typically 10 hours after launch and t_2 is typically 20 to 30 hours after t_1. The free flight of the spacecraft is tracked by the DSIF from lunar burnout until t_1, at which time an orbit determination by least squares fit is performed. Both midcourse velocity corrections are computed on the basis of this tracking prior to t_1. The remaining free flight portions of the trajectory are then tracked by DSIF for two purposes:

a) This additional information may be used to slightly modify the magnitude and timing of the second correction.

b) The tracking is used in the prediction of the actual re-entry.

2. Transit Trajectory

In the generation of moon-to-earth free flight trajectories for the minimal mission, the longitude of the lunar launch point was chosen to be near the vertical landing area of a spacecraft on a 66-hour earth-moon flight ($\lambda \sim -50$ degrees, $\mu \sim 0$ degree). Several trajectories originating in this area were generated, and three of these were selected for detailed analysis. These trajectories (S-1, S-3, and S-5) correspond approximately to the following flight time re-entry combinations:

S-1 t_f = 50 hours β_{re} = 170 degrees (i.e., 80 degrees from the horizontal)

S-3 t_f = 90 hours β_{re} = 110 degrees (i.e., 20 degrees from the horizontal)

S-5 t_f = 90 hours β_{re} = 170 degrees (i.e., 80 degrees from the horizontal)

All three return to approximately 30^{o}N latitude at re-entry. Table 2-8 lists the complete burnout and re-entry conditions for the trajectories.

Miss coefficients (i.e., variations in re-entry conditions withrespect to variations in burnout conditions) are given in Table 2-9 for S-1, S-3 and S-5. Figures 2-7 and 2-8 show projections of the S-5 trajectory on the x-y and x-z planes. In this equatorial coordinate system, the x-axis is toward the vernal equinox while the z-axis points North in a right handed system. The near-restilinear character of the steep re-entry trajectory is apparent in these figures.

3. Powered Flight and Injection Guidance

Launch from the moon's surface is to be effected using a single stage spin-stabilized vehicle. As in the standard mission, I_{sp} = 300 and liftoff thrust-to-earth weight is four. Using these parameters, it is possible to fit constant attitude powered flight profiles to the burnout conditions of S-1, S-3 and S-5.

The above three constant attitude powered flight profiles are quite similar, so that for the error analysis, a single nominal profile was used to generate the Λ_2 covariance matrix of in-plane burnout errors. (Previous studies of similar lunar powered flight profiles [1] have shown that this is a

Table 2-8. Burnout and Re-entry Conditions for Trajectories S-1, S-3, S-5

Burnout:

Trajectory	r (ft)	λ (deg)	μ (deg)	V (fps)	β (deg)	A (deg)
S-1	5733000.	-45.009	4.022	9494.47	65.674	90.932
S-3	5733000.	-45.0803	5.19	8710.07	78.49	77.486
S-5	5733000.	-45.013	3.867	8445.96	80.862	92.755

Burnout time

S-1	191.790 minutes after 0^h GMT,	Feb. 5, 1963	(maximum lunar declination)
S-3	774.214	Feb. 20,1963	(minimum lunar declination)
S-5	689.387	Feb. 5, 1963	

Re-entry Conditions:

Trajectory	Long (deg)	Lat (deg)	β_{re} (deg)	t_f (min)	Altitude (ft)
S-1	-93.216	31.290	163.226	3014	400,000
S-3	-60.359	32.266	109.301	5219	400,000
S-5	-82.914	28.707	164.658	5363	400,000

Table 2-9. Re-entry Miss Coefficients

	Δt_f, min	$\Delta\beta_{re}$, deg	ΔLat_{re}, deg	$\Delta Long_{re}$, deg
Trajectory S-1				
Δr_o = 50,000 ft	- 21.3	+ 0.386	+ 0.003	+ 4.495
$\Delta\lambda_o$ = 1 deg	+ 20.5	+ 5.695	+ 3.199	-19.937
$\Delta\mu_o$ = 1 deg	- 0.3	- 0.459	+ 1.236	+ 0.735
Δv_o = 50 fps	- 35.1	+ 1.893	+ 0.451	+ 4.556
$\Delta\beta_o$ = 1 deg	+ 28.8	+ 7.901	+ 2.515	-27.766
ΔA_o = 1 deg	+ 0.3	+ 1.504	-15.100	- 3.247
Trajectory S-3*				
Δr_o = 5,000 ft	- 4	- 1.57	- 0.29	- 2.72
$\Delta\lambda_o$ = 1 deg	+ 82.88	- 3.56	- 1.23	-29.33
$\Delta\mu_o$ = 1 deg	+ 5.51	+ 2.28	- 1.9	+ 3.94
Δv_o = 50 fps	- 53.5	-17.40	+ 2.94	-17.66
$\Delta\beta_o$ = 1 deg	+126.7	- 3.4	- 2.47	-39.93
ΔA_o = 1 deg	- 26.8	+ 6.00	- 4.94	+20.3
Trajectory S-5				
Δr_o = 50,000 ft	- 83.4	+ 5.068	+ 1.340	+ 9.088
$\Delta\lambda_o$ = 1 deg	+ 68.8	+ 1.241	+ 1.204	-20.227
$\Delta\mu_o$ = 1 deg	- 3.5	+ 0.694	- 5.289	- 0.331
Δv_o = 50 fps	-118.4	+ 8.046	+ 1.852	+ 9.998
$\Delta\beta_o$ = 1 deg	+116.3	+ 2.109	+ 1.424	-34.158
ΔA_o = 1 deg	+ 2.2	+ 0.886	- 8.617	- 2.457

*Note that Δr = 5,000 on trajectory S-3, but Δr = 50,000 on all other trajectories.

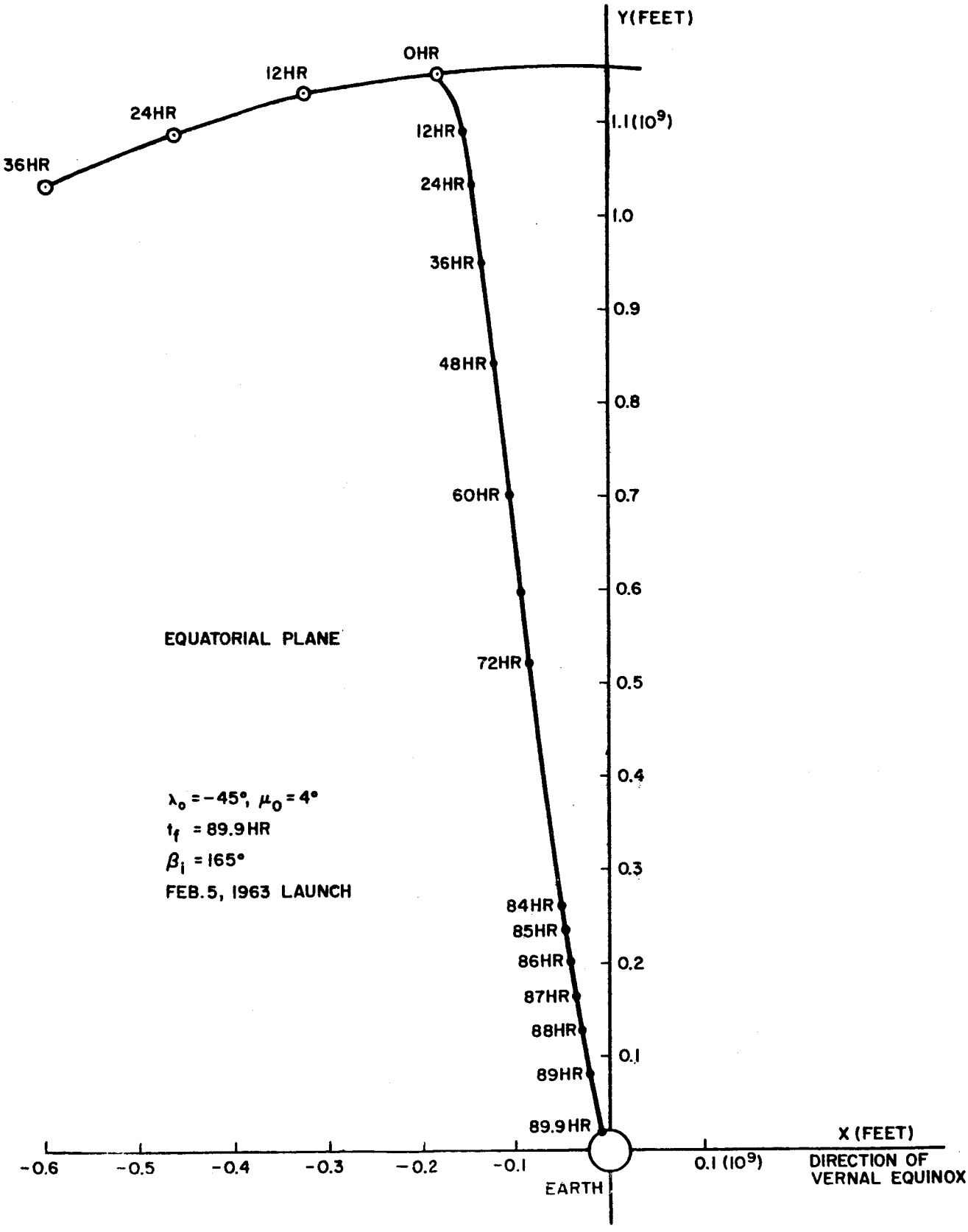

Figure 2-7. Trajectory S-5. Equatorial Plane View

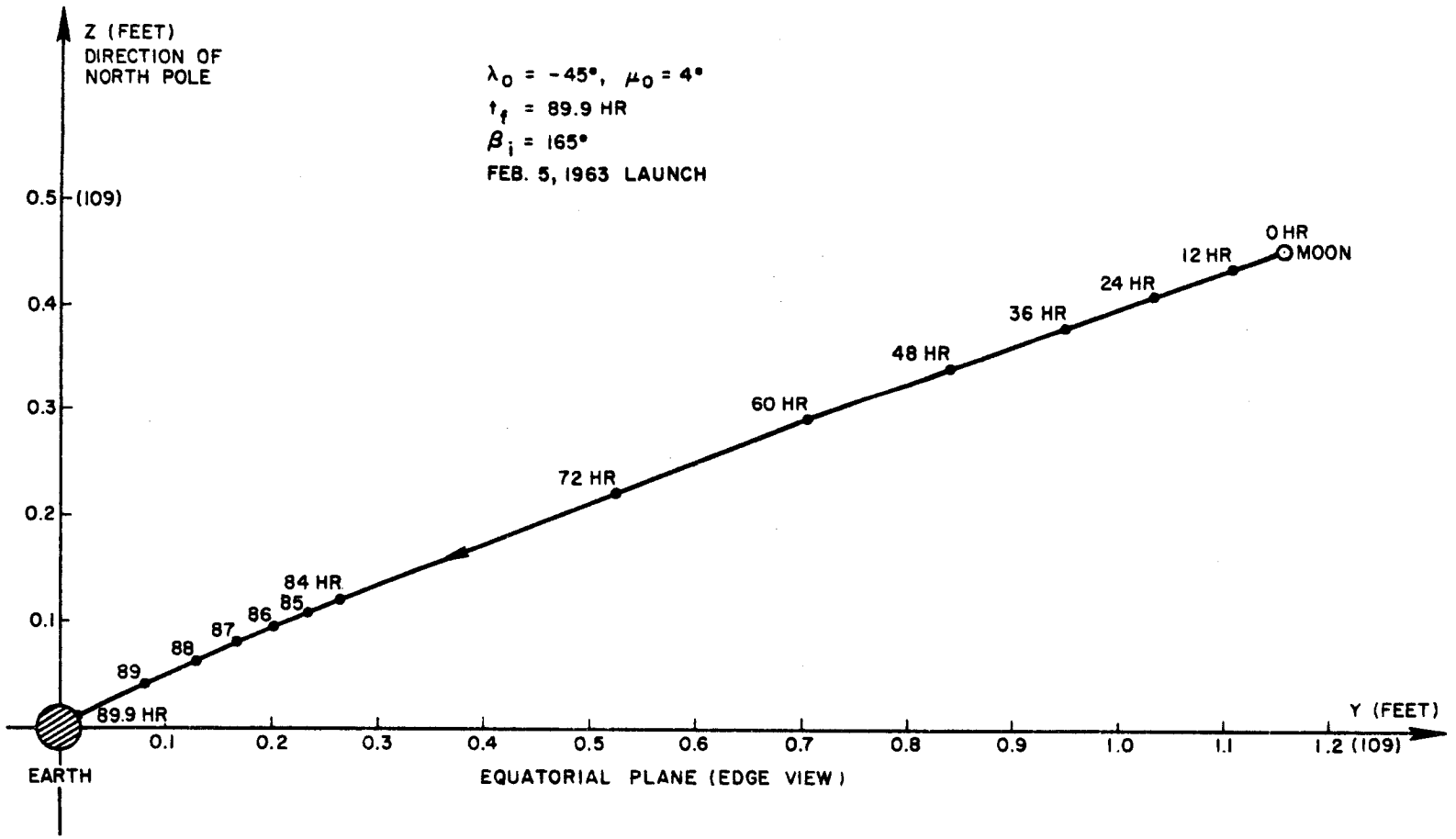

Figure 2-8. Trajectory S-5. Y-Z Plane View

valid approximation). The burnout conditions for this nominal profile are listed below:

V_o = 8473 fps, h_o = 25,000 ft, β_o = 80.0 deg (10 degree elevation above horizontal)

Energy = 5.68 (10^6) ft^2/sec^2, powered flight arc = 1.6 degrees.

Since this is a rather flat trajectory, it suggests that consideration should be given in any actual mission to the terrain clearance problem. If terrain clearance should become a problem, a more lofted powered flight correcponding to a faster flight time or to a more easterly launch site would be required.

The basic powered flight error sources for cutoff on fuel depletion versus cutoff on command from an integrating axial accelerometer are listed below:

Fuel Depletion		Axial Accelerometer	
Dry weight, w_d	(%)	Liftoff weight, w_o	(%)
Propellant weight, w_p	(%)	Thrust, T	(%)
Thrust, T	(%)	I_{sp}	(%)
I_{sp}	(%)	Launch angle, β_{Lo}	(deg)
Launch angle, β_{Lo}	(deg)	Accelerometer scale	(%)
		Accelerometer bias	(0.01 g)

In addition to these error sources, the miss due to not knowing the exact position and orientation on the moon of the launch mechanism was considered. Uncertainties in position and orientation were considered to have the same values as in the standard mission, i.e.:

$$\sigma_{lat} = \sigma_{long} = 0.05^o, \quad \sigma_{alt} = 1000 \text{ ft}$$

1σ uncertainty in orientation of trajectory plane (launch azimuth error) = 0.25 degree.

Table 2-10 shows the 1σ values assigned to each basic error source, together with the standard deviation, variance and covariance of the resultant

Table 2-10. Re-entry Error Due to Each Independent Powered Flight Error Source. Trajectory S-1 (50 hr, $\beta_i = 170^o$)

TRAJECTORY S-1, FUEL DEPLETION

No.	Source	σ	σ Long deg	σ Lat deg	σ_β deg	σ^2 Long deg^2	σ^2 Lat deg^2	σ^2_β deg^2	Cov(Long, Lat) deg^2	Cov(Long, β) deg^2	Cov(Lat, β) deg^2
1	μ_o	0.05 deg	0.032	0.041	0.021	0.00104	0.00165	0.00043	0.00131	0.00067	-0.00085
2	λ_o	0.05 deg	0.998	0.160	0.285	0.99371	0.02558	0.08108	-0.15945	-0.28385	0.04555
3	A_o	0.25 deg	0.812	3.784	0.378	0.65920	14.32208	0.14273	3.07264	-0.30673	-0.14272
4	W_d	0.5 %	2.719	0.240	1.001	7.39206	0.5779	1.00123	0.65360	2.72050	0.24054
5	W_p	0.1 %	0.521	0.059	0.212	0.27156	0.00289	0.04508	0.02800	0.11065	0.01409
6	T	1.0 %	0.343	0.047	0.079	0.11737	0.00222	0.00617	-0.01614	-0.02690	0.00370
7	I_{sp}	0.316 %	2.507	0.246	0.985	6.28347	0.06055	0.96842	0.61681	2.46679	0.24215
8	β_{LO}	0.25 deg	6.885	0.642	2.016	47.40838	0.41255	4.06412	-4.42247	-13.88068	1.29485
9	r_o	10^3 ft	0.009	0.000	0.008	0.00008	0.00000	0.00004	0.00000	0.00007	0.00000
				TOTAL MISS		$(7.945)^2$	$(3.858)^2$	$(2.512)^2$	-0.22570	-9.20085	0.40763

TRAJECTORY S-1, ACCELEROMETER CUTOFF

No.	Source	σ	σ Long deg	σ Lat deg	σ_β deg	σ^2 Long deg^2	σ^2 Lat deg^2	$\sigma^2_{\beta_2}$ deg^2	Cov(Long, Lat) deg^2	Cov(Long, β) deg^2	Cov(Lat, β) deg^2
1	μ_o	0.05 deg	0.032	0.041	0.021	0.00104	0.00165	0.00043	0.00131	-0.00067	-0.00085
2	λ_o	0.05 deg	0.998	0.160	0.285	0.99371	0.02558	0.08108	-0.15945	-0.28390	-0.04555
3	A_o	0.25	0.812	3.784	0.378	0.65920	14.32208	0.14273	3.07264	-0.30673	-0.14272
4	W_o	0.5 %	0.173	0.023	0.039	0.03002	0.00055	0.00149	-0.00405	-0.00668	0.00090
5	T	1.0 %	0.348	0.047	0.076	0.12134	0.00217	0.00583	-0.01624	-0.02659	0.00356
6	I_{sp}	0.316 %	0.034	0.006	0.007	0.00114	0.00004	0.00005	-0.00020	-0.00024	0.00004
7	β_{LO}	0.25 deg	6.827	0.633	1.999	46.60563	0.40076	3.99748	-4.32177	-13.64936	1.26571
8	r_o	10^3 ft	0.009	0.000	0.008	0.00008	0.00000	0.00004	0.00000	0.00007	0.00000
9	Accel. Scale	0.5×10^{-2}%	0.003	0.004	0.002	0.00001	0.00002	0.00000	0.00001	0.00000	0.00000
10	Accel.	0.3×10^{-4} g's	0.006	0.010	0.017	0.00358	0.00609	0.00029	-0.00057	-0.00102	0.00016
				TOTAL MISS		$(6.958)^2$	$(3.841)^2$	$(2.057)^2$	-1.42761	-14.27344	0.11475

miss at re-entry due to each error source for S-1. Since the source errors are independent, the miss variances and covariances from the sources may be summed to yield the total variance and covariance of the miss in longitude, latitude and angle of re-entry. This analysis was performed for S-1, S-3, S-5, and both fuel depletion and accelerometer cutoff cases.

The total variances and covariances described above correspond to the uncorrected miss at re-entry. The uncertainties in longitude and latitude may be characterized by 1σ (40 percent) ellipses in longitude-latitude. Table 2-11 lists the semi-major axis, the semi-minor axis and the angle α from the longitude axis to the major axis for each ellipse.

Table 2-11. Parameters of 40 Percent (1σ) Uncorrected Miss Ellipses

Trajectory	Semi-major Axis (deg)	Semi-minor Axis (deg)	α Angle (deg)	σ_β (deg)
S-1 Fuel depletion	7.95	3.86	0.27	2.51
S-1 Accelerometer cutoff	6.96	3.83	2.42	2.06
S-3 Fuel depletion	17.97	1.99	5.17	13.65
S-3 Accelerometer cutoff	11.56	1.34	0.20	1.92
S-5 Fuel depletion	11.81	2.47	-4.16	6.29
S-5 Accelerometer cutoff	8.53	2.16	1.62	0.66

It is seen that no marked decrease in re-entry σ_{long} is obtained by using an accelerometer cutoff. This can be explained by referring to Table 2-10, where this component of miss may be traced back as arising mainly from liftoff angle error $\delta\beta_{Lo}$. This error source is unaffected by the type of velocity cutoff. Similarly, σ_{lat} is not appreciably reduced by using accelerometer cutoff. (In S-1 and S-5, this component of miss may be traced back as due principally to azimuthal misalignment, which is unaffected by the type of velocity cutoff.) One concludes, therefore, that with the assumed uncertainties in launch position and orientation, accelerometer cutoff is only

weakly effective in reducing re-entry misses. However, if the initial pointing and spin-up errors (A_o and β_{Lo}) could be reduced, then accelerometer cutoff would be of great value in further reducing the miss.

4. Midcourse Guidance

a. Basic Method

The underlying principal of spin-stabilized midcourse guidance is that velocity impulses applied along the spin axis at different times produce different effects at the target. This is illustrated schematically below, where the effects of 1 fps velocity impulses along the spin axis at two times, t_1 and t_2, are plotted as vectors in longitude and latitude of re-entry. In this diagram, any vector miss in the longitude-latitude plane can be expressed as a linear combination of the t_1 and t_2 vectors, and can therefore be cancelled by velocity increments of the proper magnitude and polarity applied along the spin axis at times t_1 and t_2.

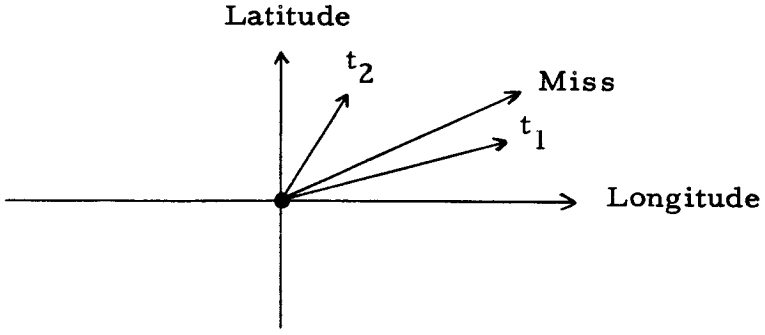

For trajectory S-1, the effects of velocity increments applied along the spin axis are plotted in Figure 2-9 as vectors in the longitude-latitude plane with the time of the impulse as a parameter. In general, it is desirable that these vectors sweep out a wide angle with time, in order that misses in arbitrary directions may be efficiently cancelled. It is also generally true that expected midcourse fuel requirements are reduced if the times t_1 and t_2 are selected in advance so that the most probable uncorrected miss vector (major axis of error allipse) lies between the t_1 and t_2 vectors. Otherwise, the correction at time t_2 will probably have to cancel, rather than reinforce, part of the t_1 correction in order to cancel the miss.

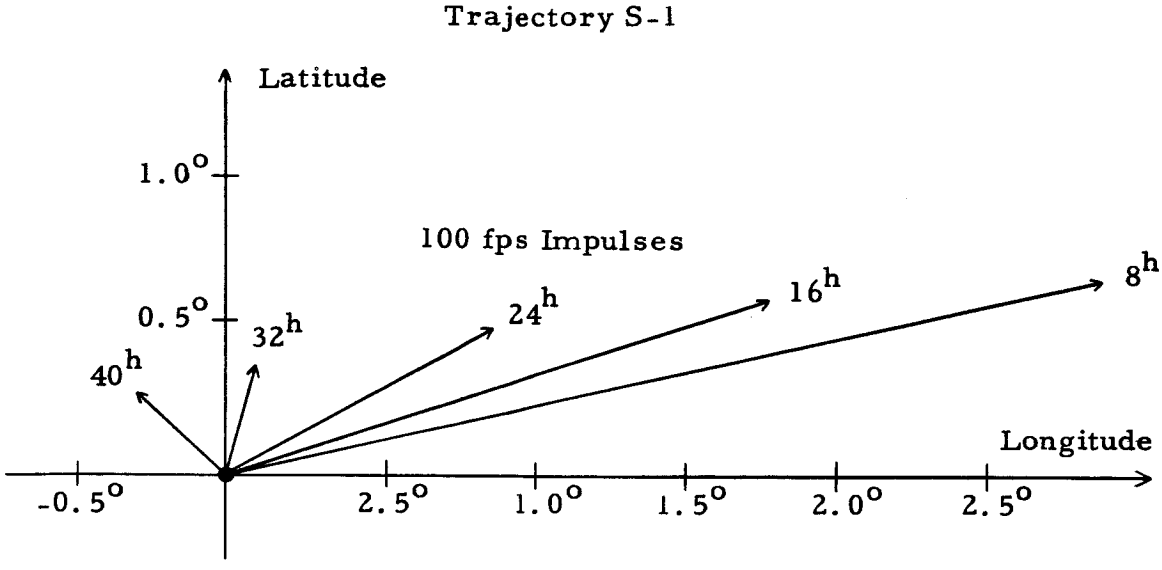

Figure 2-9. Effect on Re-entry Point of Velocity Impulses Applied Along the Spin Axis at Different Times.

b. Midcourse Fuel Requirements

Midcourse fuel requirements for the minimal mission can be accurately predicted from the statistics of the uncorrected miss, ignoring the weak interaction with uncertainties in orbit determination. The analysis is similar to computing the first correction for the standard mission and will not be reproduced here. The results are presented in Table 2-12 and Figure 2-10 for different combinations of correction times, t_1 and t_2, for S-1, S-3, S-5.

It can be seen from Figure 2-10 that, for the source errors assumed, the 50-hour trajectory (S-1) requires approximately three times the midcourse velocity increment required for 90-hour flights (S-3 and S-5).

c. Error Analysis and Final Accuracy

For a mission that used spin-stabilization midcourse corrections, there are two basic problems associated with the error analysis, First, a midcourse correction logic must be chosen. Second, the non-gaussian statistics resulting from the products of gaussian variables must be analyzed.

The simplest possible guidance logic is proposed here for the minimal mission:

Table 2-12. Midcourse Velocity Requirements for the Minimal Mission

Trajectory	Guidance	Time 1 (hr)	Time 2 (hr)	σ_{v_1} (fps)	σ_{v_2} (fps)	$\rho_{v_1 v_2}$
S-1	Fuel depletion	8	32	288	1170	-0.500
		16	40	370	1266	-0.086
		24	40	646	1339	-0.338
S-1	Accelerometer cutoff	8	32	254	1160	-0.511
		16	40	327	1241	0.003
		24	40	572	1275	-0.236
S-3	Fuel depletion	6	60	151	282	-0.995
		15	60	226	368	-0.995
		30	60	380	557	-1.000
		45	75	359	760	-0.998
S-3	Accelerometer cutoff	6	60	67	130	-0.978
		15	60	100	167	-0.990
		30	60	168	250	-0.994
		45	75	158	339	-0.991
S-5	Fuel depletion	12	64	179	207	0.997
		32	64	357	21	-0.703
S-5	Accelerometer cutoff	12	64	103	388	0.442
		32	64	206	352	0.128

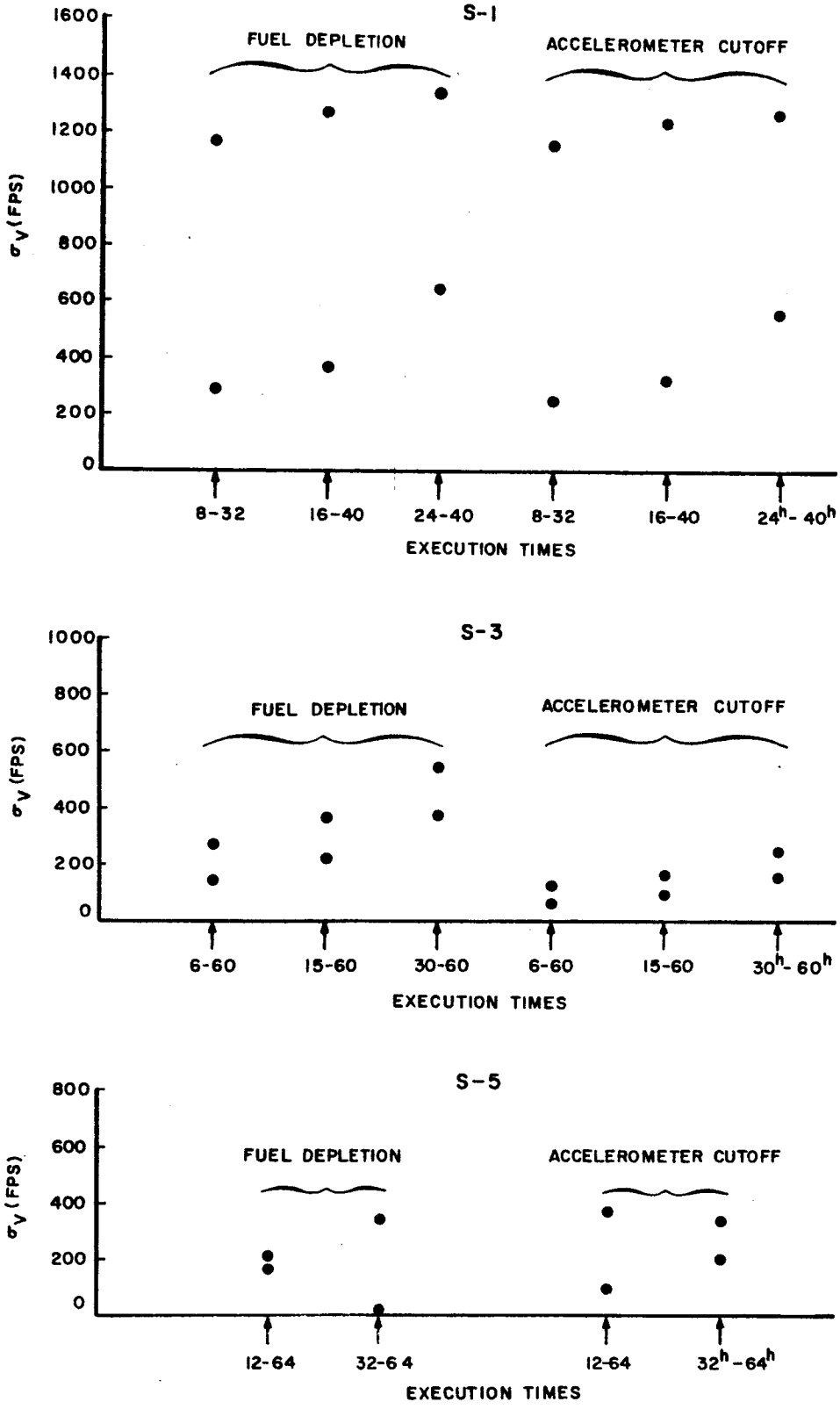

Figure 2-10. Midcourse Velocity Requirements for Various Correction Time Pairs. (Dots show 1σ values of the two corrections)

1) Select the two midcourse correction times (t_1 and t_2) in advance

2) Track from injection until just before t_1

3) Determine the apparent miss from the tracking data

4) Calculate the correction velocities, V_1 and V_2

5) Fire V_1 at t_1

6) Fire V_2 at t_2.

The following operations are performed for each Monte Carlo simulation of a flight:

1) Select the uncorrected miss and the spin axis error with the Random Vector Generator from their a priori distribution. (These are selected simultaneously since they are correlated.)

2) Select the tracking error, using the tracking covariance matrix.

3) Calculate the apparent miss, which is the sum of the actual miss and the tracking error.

4) Calculate the desired correction velocities from the apparent miss, using the sensitivities corresponding to nominal spin axis orientation.

5) Calculate the actual fired velocities by adding the randomly selected bias and scale-factor errors.

6) Calculate the effects of firing the actual velocities with the actual spin axis orientation.

7) Add the correction effects to the uncorrected miss to determine the final miss.

The Monte Carlo simulation is quite fast. If all of the runs for this report (12) were submitted to the STL 7090 computer in one batch, the total running time would be less than 3.5 minutes.

Table 2-13 shows the results of 1000 Monte Carlo samples for each of several sets of errors for trajectories S-1 and S-5. The uncorrected miss covariance matrix for fuel depletion was used in each case since the

Table 2-13. Final Accuracies for Minimal Mission Utilizing Two Spin Stabilized Midcourse Corrections. Results are 99% Values Out of 1000 Monte Carlo Runs, Nominal and Perturbed Error Sources

	Resultant Re-entry Miss (99% values)	
	Long (deg)	Lat (deg)
Trajectory S-1, Nominal Errors (Corrections at 16 and 40 hours)	2.26	1.55
Tracking Error XO. 1	1.62	1.48
Velocity Bias XO. 1	2.28	1.54
Velocity Scale Factor XO. 1	2.26	1.53
Spin Axis Orientation XO. 1	1.75	0.82
All Errors XO. 1	0.21	0.16
Trajectory S-5, Nominal Errors (Corrections at 32 and 64 hours)	1.74	1.15
Tracking Error XO. 1	1.69	1.09
Velocity Bias XO. 1	1.74	1.14
Velocity Scale Factor XO. 1	1.56	1.13
Spin Axis Orientation XO. 1 (Uncorrelated)	1.00	0.58
All Errors XO. 1	0.16	0.11

improvement in uncorrected miss obtained with accelerometer cutoff is slight. For each trajectory, runs were made with the nominal errors, with each error reduced by a factor of ten, and with all errors reduced by a factor of ten simultaneously.

The nominal execution errors (1σ) used are:

Velocity bias	2 fps
Velocity scale factor	0.02

The spin axis orientation error used corresponds to independent errors of 0.5 degree (1σ) in azimuth and elevation at launch. Since the initial miss is also a function of launch azimuth and elevation, it is correlated with the error in spin axis orientation. This correlation is included in the Monte Carlo Program.

The standard tracking error used is the result of tracking to the time of the first correction at one point per ten minutes with the DSIF on the assumption of 0.5 fps and 0.2 degree (1σ) errors.

From the results it can be seen that the tracking and spin axis orientation errors are dominant for the S-1 trajectory and that the velocity scale factor and the spin axis orientation are dominant for the S-5 trajectory. For both trajectories, however, improving the knowledge of the spin axis gives the largest reduction in final miss.

Since the spin axis orientation error is important in both trajectories, the accuracy with which it can be measured with tracking data was calculated. In the calculation it was assumed that the direction of the velocity with respect to the moon at burnout is along the spin axis. This is a reasonable assumption since the powered flight is very short.

The accuracy with which the three components of burnout velocity can be measured was determined with tracking data up to the time of the first correction. These accuracies were then converted to accuracies in the angles θ and ϕ used in the simulation. (The angles θ and ϕ are the usual spherical coordinates of the velocity vector relative to the inertial x, y, z reference.) The following are the results:

Trajectory	A Priori 1σ Errors (milliradians)		Tracking (only) 1σ Errors (milliradians)	
	θ	φ	θ	φ
S-1	4.69	3.99	0.398	16.8
S-5	4.62	4.27	0.840	19.0

The tracking data allows a considerable improvement in the knowledge of θ, but tracking accuracy is not as good as the a priori knowledge of ϕ. However, if the data rate were increased (e.g., to 1 point per 10 seconds), improvement in the knowledge of ϕ could also be obtained.

The result of reducing all the errors by a factor of 10 simultaneously is essentially a reduction of the final miss by a factor of 10. This is to be expected since the final miss is the sum of the tracking error, the velocity bias error, and errors proportional to the correction velocities. For the trajectories studied, the magnitude of the required correction velocities are essentially the same for the normal and the reduced tracking error. As a result, the miss proportional to velocity is reduced almost exactly in the same ratio as the other terms. If the tracking error were comparable to the initial miss, on the other hand, the proportional miss would be reduced by a greater factor.

D. Orbit Determination for Return Mission

This section deals with aspects of orbit determination which are peculiar to the moon-earth mission, as opposed to the general discussion contained in Part IV. For the lunar return missions, it is assumed that orbit determination is effected by tracking the free flight portions of the trajectory with the three DSIF stations, and then applying least squares procedures to estimate the six orbital elements at a chosen epoch. The radar elements used were range rate ($\dot{R}$), azimuth (A) and elevation (E).

The primary purpose of tracking the spacecraft is to establish the various free flight trajectory portions with sufficient accuracy to enable the midcourse corrections to be computed. This is an essential function for both the standard and the minimal missions, since we have already seen that the uncorrected misses are too large to be acceptable. Thus, one of the objectives

of orbit determination analysis is to simulate this real-time function. A secondary objective is to determine in advance the favorable times at which to make the midcourse maneuvers. This is done by simulation methods, also, and must take into account fuel requirements as well as final accuracy requirements. Lastly, orbit determination analysis must be concerned with making these simulations as realistic as possible. This involves using noise models which are as realistic as possible and take into account "hidden" errors such as correlations and biases in the observation.

1. Standard Mission

As mentioned earlier, some of the initial tracking simulations were done using an "old" model for DSIF noise in which $\sigma_{\dot{R}} = 0.5$ fps, $\sigma_A = \sigma_E = 0.04^o$, with all observations being uncorrelated. These results were used in Monte Carlo simulations of the standard mission, and are described below.

On the standard mission, the time of the first midcourse correction was set somewhat arbitrarily at 12 hours. This choice was based primarily on fuel rather than accuracy requirements. (Table 2-7 has shown that even with the old (optimistic) DSIF noise model, tracking errors dominate the uncertainty in re-entry just after the first midcourse.) Thus the critical tracking period, to determine final accuracy, was from 12 hours after injection to the time of the second midcourse maneuver. Table 2-14 shows re-entry uncertainty due to tracking in this interval, as a function of the time of the second midcourse correction for trajectory P-4. This table includes the effect of a priori data at 12 hours and is based on the old DSIF model.

In Table 2-14, a priori information was handled in an approximate way as follows: Let Λ_1 be the 6 x 6 covariance matrix of 0^h - 12^h tracking, evaluated at 12 hours. Let Λ_E,

$$\Lambda_E = \left[\begin{array}{c|c} 0 & 0 \\ \hline 0 & \sum_V \end{array}\right]$$

be the 6 x 6 covariance matrix of execution errors, where $\sum_V$ is the 3 x 3 covariance matrix of execution velocity errors evaluated for a correction of

magnitude "2σ" in the x, y, z directions. Then $\Lambda_1 + \Lambda_E$ was used as the 6 x 6 a priori tracking covariance matrix. If Λ_2 denotes the 6 x 6 covariance matrix for tracking from 12 hours to the second midcourse, evaluated at 12 hours, then $\tilde{\Lambda}_2$,

$$\tilde{\Lambda}_2 = \left[\Lambda_2^{-1} + (\Lambda_1 + \Lambda_E)^{-1}\right]^{-1}$$

is the covariance matrix representing tracking from 12 hours to the second midcourse correction, including a priori data. To compare Λ_2 and $\tilde{\Lambda}_2$ it is convenient to update these matrices to re-entry time and look at the corresponding uncertainties in re-entry conditions. This is done in Table 2-15.

Table 2-14. Standard Mission, Trajectory P-4. Re-entry uncertainty resulting from 12^h to second midcourse correction. $\sigma_{\dot{R}} = 0.5$ fps $\sigma_A = \sigma_E = 0.04^o$, one set of observations per minute. A priori information included, correlations and biases neglected (old DSIF model)

Tracking Interval (hours from lunar B.O.)	σ Longitude (deg)	σ Latitude (deg)	σ Re-entry angle (deg)
12 - 32	0.45	0.14	0.21
12 - 48	0.15	0.047	0.067
12 - 64	0.065	0.021	0.030
12 - 80	0.034	0.010	0.015

Table 2-15. Standard Mission, Trajectory P-4. Re-entry uncertainty resulting from using or not using a priori data in tracking from 12^h to second midcourse correction. $\sigma_{\dot{R}} = 0.5$ fps, $\sigma_A = \sigma_E = 0.04^o$, one set of observations per minute (old DSIF model)

Tracking Interval (hours from lunar B.O.)	With A Priori Data			Without A Priori Data		
	σ_{long}	σ_{lat}	σ_β	σ_{long}	σ_{lat}	σ_β
12 - 64	0.065	0.021	0.030	0.140	0.045	0.063
12 - 80	0.034	0.010	0.015	0.041	0.013	0.018

In this table, it is seen that when the second midcourse correction is made at 64 hours or earlier, final uncertainty can be significantly reduced by using a priori data. On the other hand, at 80 hours a priori information does not strongly affect the final uncertainty.

The Monte Carlo runs using the old DSIF model indicated that even after the second midcourse maneuver the final accuracy was still tracking limited. This led to a re-examination of the DSIF noise model to insure that the basic assumptions were as realistic as possible. The result was a new, more conservative model for angular noise which included correlations and biases:

A or E Noise Component	RMS Value	Time Constant
Random	0.01 deg	10 sec
Random	0.01 deg	5 hours
Bias	0.005 deg	∞

For a nominal data rate of one set of observations per minute, it can be shown that the random components of noise in the above model produce an effect which is no worse than that produced by uncorrelated noise having RMS value 0.2 deg (see example 3 of Part IV). Thus, by simulating the tracking operation with $\sigma_{\dot{R}} = 0.5$ fps, $\sigma_A = \sigma_E = 0.2^o$, uncorrelated, at one observation set per minute (which we shall call the new DSIF noise model), we can study the effects of the random components of noise. (For different data rates, the degradation factor on angles is different.) Biases will be considered later.

Table 2-16 shows a comparison of the old and new DSIF noise models for tracking from first to second midcourse correction, Trajectory P-4. Also included is the result of using no angular data at all ($\sigma_A = \sigma_E = \infty$), from which one can see that almost all the information is contained in the $\dot{R}$ data. No a priori data was used in this table. Including a priori data would reduce the uncertainty for 12^h - 64^h tracking by approximately 50 percent, but would probably not affect the 12^h - 80^h tracking significantly.

The deleterious effects of unsuspected biases in angular measurements can be studied by the methods described in Part IV. Table 2-17 contains the

Table 2-16. Standard Mission, Trajectory P-4. Effects on re-entry uncertainty of degraded angular accuracy, keeping $\dot{R}$ accuracy fixed. No a priori. Data rate one set of observations per minute

Tracking Interval (hours from lunar B.O.)	Old DSIF $\sigma_{\dot{R}} = 0.5$ fps, $\sigma_A = \sigma_E = 0.04^\circ$			New DSIF $\sigma_{\dot{R}} = 0.5$ fps, $\sigma_A = \sigma_E = 0.2^\circ$			$\dot{R}$ Only $\sigma_{\dot{R}} = 0.5$ fps, $\sigma_A = \sigma_E = \infty$		
	σ_{long} (deg)	σ_{lat} (deg)	σ_β (deg)	σ_{long} (deg)	σ_{lat} (deg)	σ_β (deg)	σ_{long} (deg)	σ_{lat} (deg)	σ_β (deg)
12 - 64	0.140	0.045	0.063	0.21	0.067	0.096	0.23	0.073	0.10
12 - 80	0.041	0.013	0.018	0.053	0.016	0.023	0.057	0.017	0.025

results of such an analysis for the old and the new DSIF models. This table shows the effects of "unsuspected" biases in A and E measurements for each tracking station of RMS (a priori) value 0.01 degree. It is seen that the old DSIF model is quite sensitive to angular biases, since it weights angular data more heavily. In fact, comparison with Table 2-15 shows that it is better not to include angular data at all than to weight it according to an RMS value of 0.04 degree when the RMS bias is 0.01 degree. One sees that angular biases do not affect the new DSIF model significantly, since angular accuracies have been considerably degraded.

Table 2-17. Standard Mission, Trajectory P-4. Effects of unsuspected biases on re-entry uncertainty. In least squares fit, data is weighted according to the RMS of its uncorrelated component. Data rate is one set of observations per minute

Tracking Interval (hours from lunar B.O.)	Tracking Noise			Re-entry Uncertainty		
	Uncorrelated		Bias			
	σ_R (fps)	σ_A, σ_E (deg)	σ_A, σ_E (deg)	σ_{long} (deg)	σ_{lat} (deg)	σ_β (deg)
12 - 64	0.5	0.04	0.01	0.27	0.084	0.12
12 - 80	0.5	0.04	0.01	0.071	0.020	0.031
12 - 80	0.5	0.2	0.01	0.055	0.017	0.024

2. Minimal Mission

For the minimal mission, the critical tracking period was, of course, the period from lunar burnout to the time of the first midcourse correction. (Subsequent tracking was not utilized in the simple guidance logic for this mission, although this logic could be modified to include later tracking if it were considered desirable or necessary.) Both the old and the new DSIF noise models were used in the tracking simulations. Since the latter model is of chief interest, we have summarized the results in Table 2-18. This table does not include any a priori information. In the Monte Carlo simulations, a priori information is entered separately and combined with tracking information in the computer.

Table 2-18. Minimal Mission Tracking Results for σ_R = 0.5 fps, $\sigma_A = \sigma_E = 0.2^o$, one set of observations per 10 minutes

Trajectory	Tracking Interval (hours from lunar B.O.)	Re-entry Uncertainty		
		σ_{long} (deg)	σ_{lat} (deg)	Correlation Coefficient ρ
S-1	0 - 16	0.63	0.30	0.3
S-5	0 - 12	0.49	1.17	0.67
S-5	0 - 32	0.15	0.22	0.38

III. CIRCUMLUNAR TRAJECTORIES

This Part describes the study plan for research currently being performed in the field of lunar trajectories, and some preliminary results and considerations which are available.

A. Free-Return Circumlunar

1. Introduction

We shall discuss first a preliminary analysis of free-return circumlunar trajectories which led to a better understanding of the overall properties of such trajectories and subsequently to the Analytic Circumlunar Program. The model on which this analysis and the Circumlunar Program is based was described and used in Part I in connection with moon-to-earth trajectories. It consists of enclosing the moon in a sphere within which only the moon's gravity is considered and outside of which only the earth's gravitational field is in effect. With such a model, a circumlunar trajectory consists of a conic in the moon phase (within the sphere) and two conics in the earth phase, as shown in Figure 3-1. These conics are such that positions and velocities match at the phase boundary. The apparent discontinuity in the velocity in Figure 3-1 is due to the fact that both earth-frame and moon-frame conics have been shown in a single figure; since the moon is revolving about the earth a velocity translation is required at the junction.

We shall treat three dimensional circumlunar trajectories, restricted to single revolution trajectories. That is, they will begin near the earth, enter the sphere of action in some manner, and then exit and return to the earth. The moon-phase conic will be hyperbolic, except in very rare cases, whereas each leg of the earth-phase conics may be independently elliptic, hyperbolic, or parabolic.

2. General Analysis

Consider now some of the general properties of circumlunar trajectories. As indicated in Figure 3-1, there are two "corridors" connected with the moon's sphere of influence, i. e., an entrance corridor lying in the western hemisphere of the moon and an exit corridor lying in the eastern hemisphere. These corridors exist with respect to a moon-centered coordinate

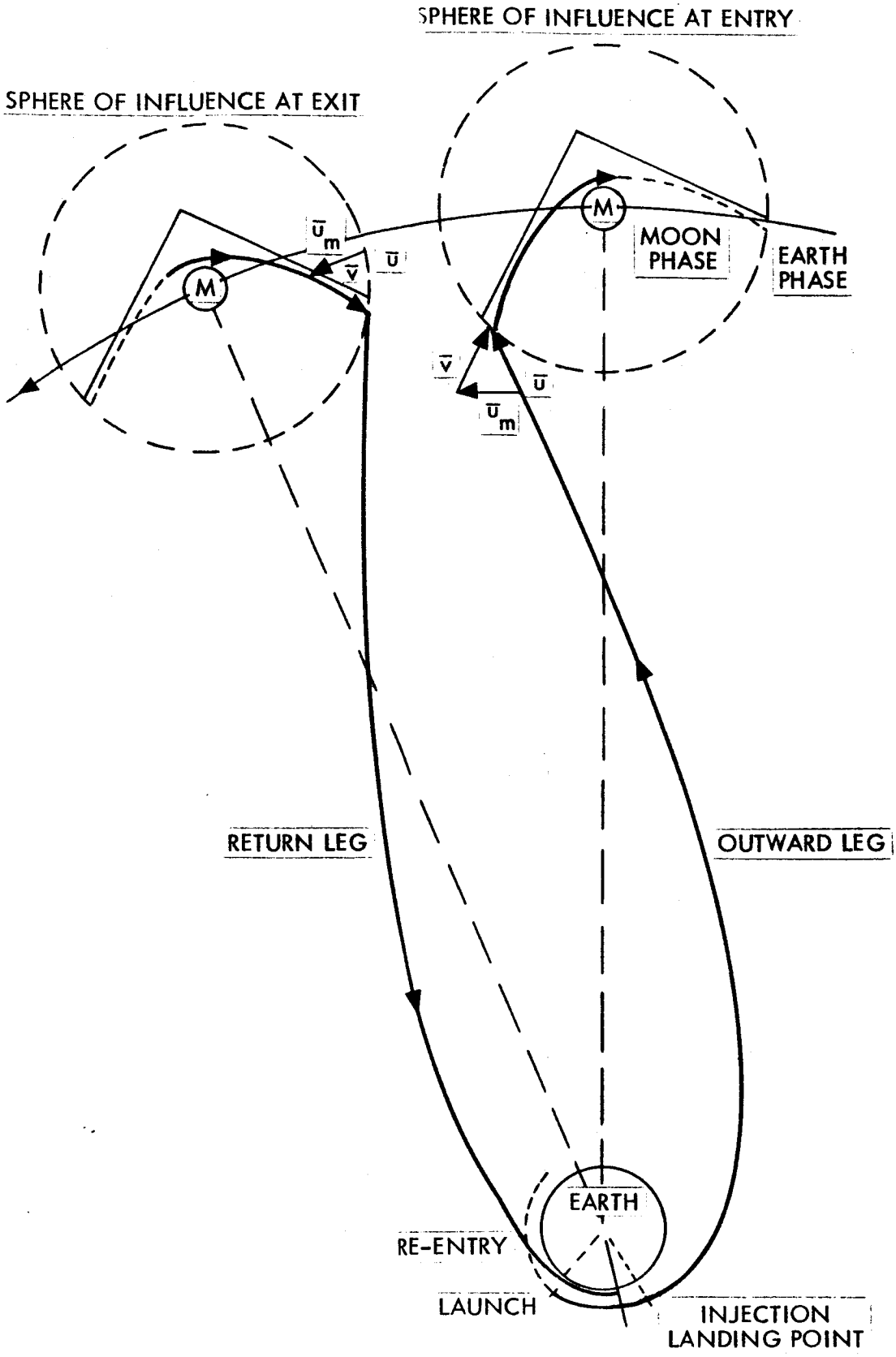

Figure 3-1. Schematic of Circumlunar Flight

system. It is realized that circumlunar trajectories other than the type shown in this figure exist, such as one going considerably beyond the moon [32], but only that class of trajectories which produce the closest approach to the moon will be considered here.

Figure 3-2 shows the configuration of these corridors on the moon's sphere of influence as seen by an observer on the moon. The horizontal plane is taken as the moon's orbit plane. If the complete class of trajectories launched from the earth from a fixed altitude and impacting the moon were considered for a fixed time of flight (or equivalently a fixed energy) then all trajectories launched by direct ascent with flight path angle β_L will have a fixed in-plane conic section. The only degrees of freedom which this conic may have is then the orientation of its plane and all possible orientations may be produced by essentially rotating the conic section about the line connecting the center of the earth and the $\beta_L = 0$ point on the sphere of influence. The result will be the generation of the constant β_L contours shown in Figures 3-2a. That is, the trajectory will have its velocity vector pointing from this contour to the center of the moon when it reaches the sphere of influence. For the class of trajectories which produce circumlunar results, i.e., returning to the earth's atmosphere, these constant β_L contours will be displaced slightly to compensate for non-impact. Also, it is clear that launching from a parking orbit will represent the limiting flight path launch azimuth contour of $\beta_L = 90$ degrees. It is interesting to observe that the set of all possible parking orbit launched trajectories will form the envelope of all direct ascent trajectories.

Returning to the assumption that the earth-phase energy on the outward leg is fixed, then the magnitude of the vehicle's earth-phase velocity $\bar{u}$ at the sphere will remain constant whereas its direction will vary within a few degrees of the earth-moon line. The moon-phase entry velocity $\bar{v}$ will depend on the vector addition, $\bar{v} = \bar{u} - \bar{u}_m$, where $\bar{u}_m$ is the moon's orbital velocity. Referring to the velocity vector diagram in Figure 3-2a, it is seen that $\bar{v}$ can take on various magnitudes, increasing as its direction moves further from that of the earth-moon line. The lowest velocity (or energy) $\bar{v}$ occurs when the earth-phase velocity is directed to the left of the earth-moon line, which will be the case for eastward launches.

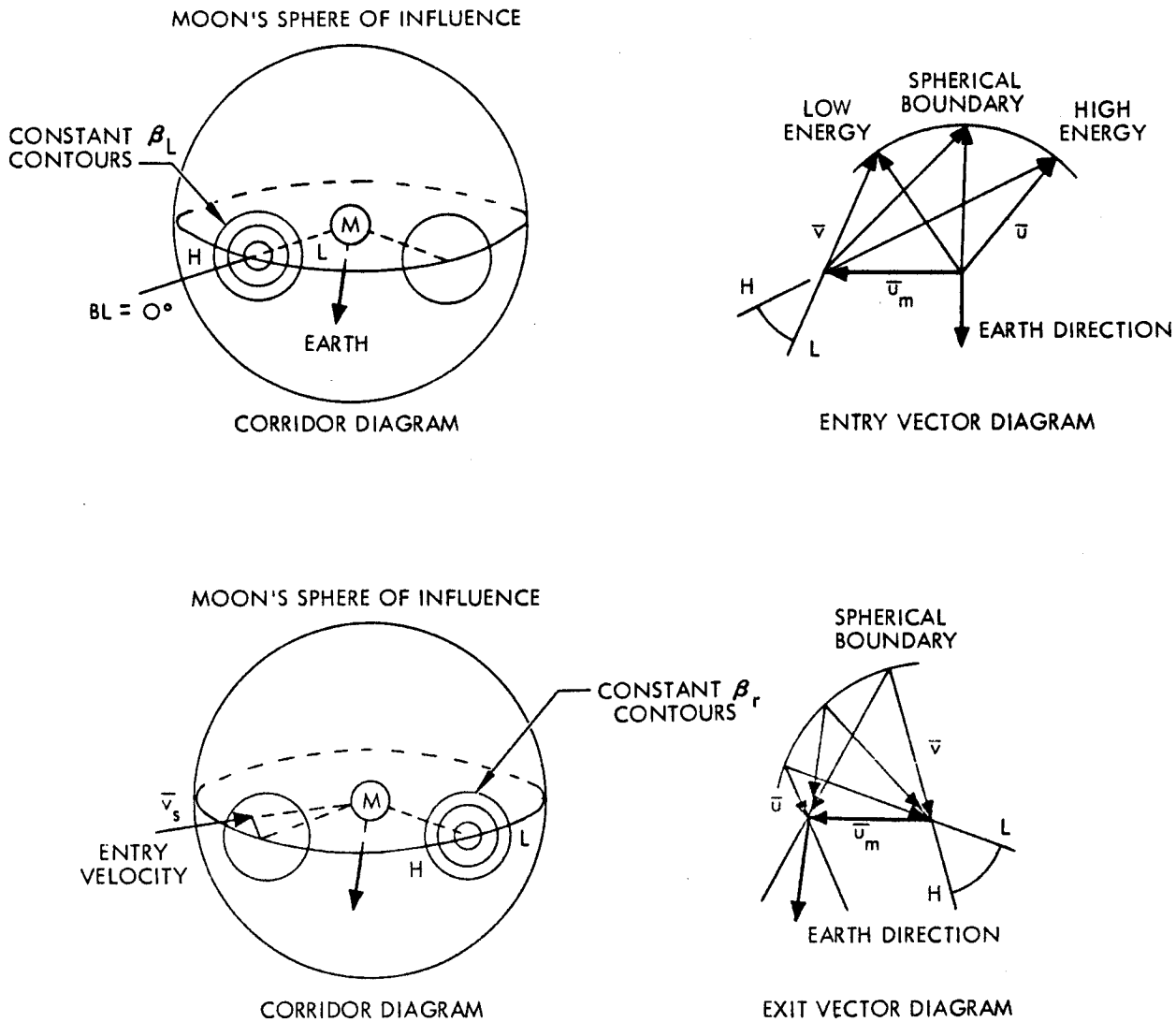

Figure 3-2. Entry and Exit Corridors at the Moon's Sphere of Influence for Circumlunar Trajectories

The analysis of the exit corridors of circumlunar trajectories is very similar to that of the entry corridors which were just discussed. Here, however, to prevent the discussion from becoming too involved, it is necessary to restrict the outward leg to a "single" launch trajectory. This is shown in Figure 3-2b. By a single launch trajectory it is meant that the magnitude and inertial direction of the velocity at entry into the sphere is fixed whereas the entry point may vary. This is acceptable since small perturbations of the launch conditions will have considerable affect on the entry position but very little affect on the magnitude and orientation of the entry velocity. Choice of position of entry into the sphere allows two degrees of freedom which may be looked upon as freedom of impact in the impact parameter plane; that is, in a plane perpendicular to the hyperbolic entry asymptote. Once this impact point has been chosen, the complete circumlunar trajectory will be determined. Also, for a particular point in the impact parameter plane, the trajectory may or may not return and impact the earth. In any case, there will be a certain region in the impact parameter plane representing earth impact return trajectories. Because of a one-to-one correspondence of the points in the impact parameter plane to points at exit on the moon's sphere of influence, a similar region exists at the sphere. This is shown in Figure 3-2b. Here, contours similar to those of the entry corridor are shown. Specifically, these are constant earth re-entry flight path angle contours, and again $B_r = 90^o$ represents the grazing or limiting case.

Analysis of the exit vector diagram is similar to that of the entry vector diagram. One significant difference is that since the entry velocity vector has been chosen to be fixed, then the moon phase entry velocity will be fixed since $\overline{v} = \overline{u} - \overline{u}_m$. Thus, by conservation of energy, the magnitude of the moon-phase exit velocity will be equal to its entry velocity and therefore constant. This is indicated in the exit vector diagram by the spherical boundary on the $\overline{v}$ vector. By observation, it is clear that the earth-phase exit velocity will vary in magnitude. Note that the high energy return trajectories are closer to the earth-moon line indicating that these will have a tendency to approach the earth in a counterclockwise manner, whereas the low energy return will approach the earth in a clockwise manner. In any case the return trajectory may approach the earth in a plane having any inclination with the

moon's orbit plane leading to the conclusion, similar to that for launch trajectories, that the grazing return trajectories form the envelope of all possible return trajectories.

Further, it is clear that the re-entry or impact conditions for circumlunar trajectories will be very sensitive with respect to the initial or injection conditions. Since this is the case, once a circumlunar trajectory has been found which impacts the earth anywhere on return, only slight perturbations in the initial conditions are required to map out the contours shown in Figure 3-2b. Also, from the discussion above, it will be possible to satisfy only two re-entry conditions by means of these small perturbations; say, the inclination of the return trajectory plane and the re-entry angle. If a third condition is to be satisfied, such as re-entry longitude, a major change in the launch trajectory is required. This observation is utilized in the construction of the circumlunar search program discussed in the next section.

3. Input Parameters

It is desirable when solving for circumlunar trajectories to satisfy certain initial conditions and certain terminal conditions. In this manner, utilizing an iteration scheme similar to that used in the Analytic Lunar Return Program, it is possible to solve the split end-point problem.

The quantities which will be considered to be inputs into the Analytic Circumlunar Program are the following:

a) the day of launch
b) the launch azimuth
c) the powered flight angle from launch to burnout
d) the flight path angle at injection
e) the parking orbit altitude
f) the time of flight to the moon
g) the re-entry flight path angle
h) the re-entry altitude
i) the re-entry maneuver downrange angle
j) the maneuver time to touchdown
k) the latitude of the landing site
l) the longitude of the landing site.

4. Program Logic

The first six quantities above are required to solve for the outward leg of the earth-phase trajectory. This portion of the program calculates the time of launch, time of coast (the outward leg is injected from a parking orbit), conic elements, and the position, velocity and time of any point on the outward leg. The first aiming point for this portion of the trajectory is the center of a massless moon. The successive aiming points, calculated from the second iteration on, will be the entry point at the moon's sphere of influence (with the mass of the moon considered).

The next five input parameters together with the moon-phase exit velocity from the sphere of influence, which will be equal to the moon-phase entry velocity, may be used to solve for the earth-phase return leg of the trajectory. As indicated in the Program Logic Chart (Figure 3-3), the solution of this phase requires an iteration procedure. The reason for this is that although the magnitude of moon-phase exit velocity is known, its direction is not known resulting in an unknown earth-phase energy. A first guess, such as assuming that the energy is equal to that of the outward leg, is made and successive iterations performed until the calculated earth-phase velocity at the exit point is consistent with the required moon-phase velocity.

After calculating the return phase conic, the exit velocity vector may be calculated. This velocity vector may be found with respect to the moon by subtracting off vectorially the velocity of the moon with respect to the earth at the time of exit. An ephemeris tape is utilized to obtain the position and velocity of the moon at any time.

The two velocity vectors, at entrance and exit of the sphere, completely determine the moon-phase conic; the plane being determined by the cross-product of the two vectors, and the conic elements, a and e, being determined by the dot product and the magnitude of the vectors. From the conic elements, the entry and exit positions at the sphere may be found. At this point, the calculated positions are compared with those found from the earth-phase conics. If they lie within specified tolerances, then the search is complete. If not, the program replaces old positions and times at the sphere by the new values just calculated and returns to the launch phase calculation to

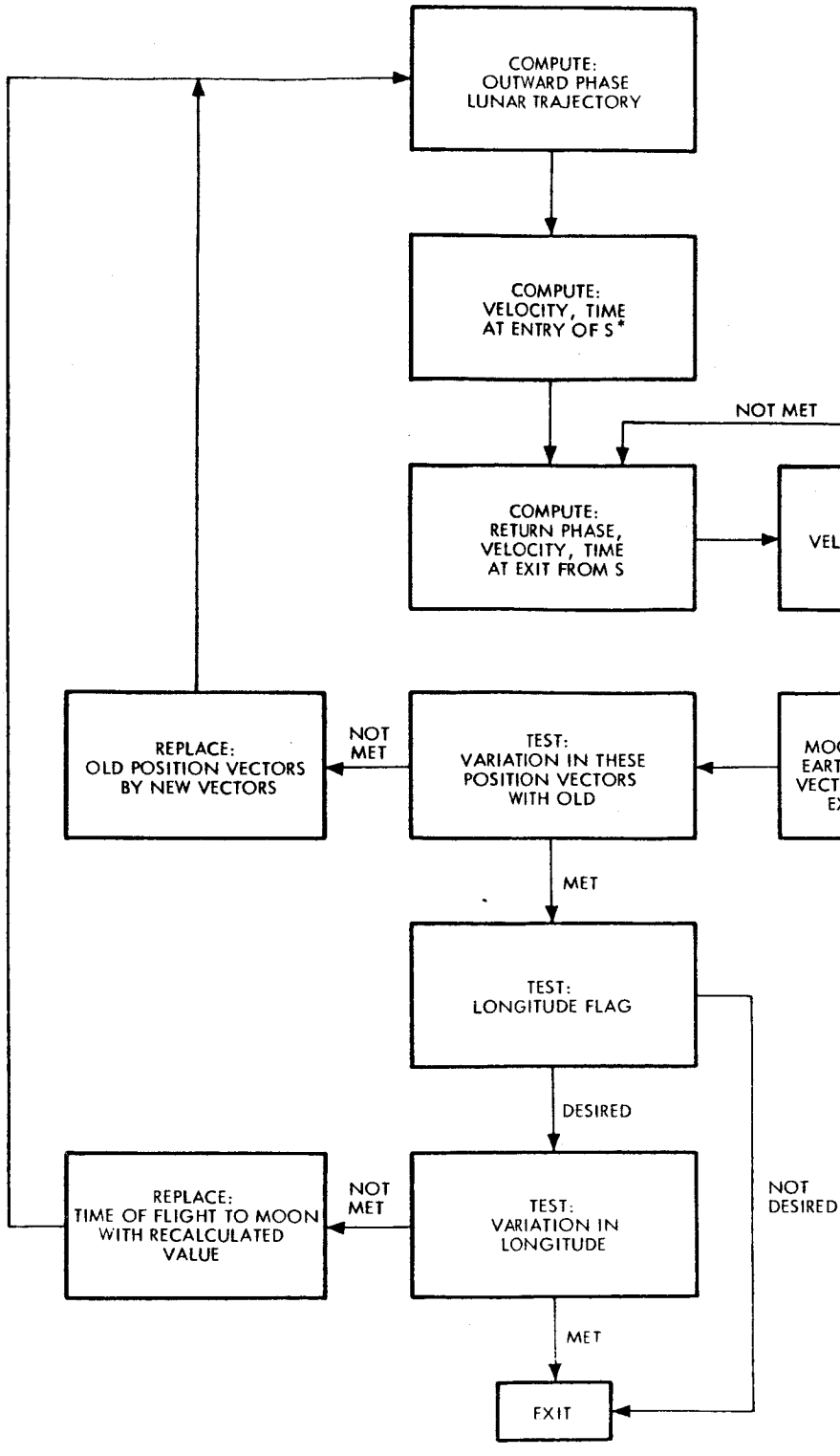

*S = MOON'S SPHERE OF INFLUENCE

Figure 3-3. General Logic Block Diagram

repeat the entire process. After several loops presumably tolerances will be met and the search completed. This process is indicated in Figure 3-3. Thus far, no use has yet been made of the landing site longitude. The reason for this was indicated in the last section where it was shown that for a specified trajectory to the moon only two terminal conditions may be satisfied. To satisfy the additional constraint on landing site longitude, the total time of circumlunar flight may be altered. This will give the earth a chance to have the correct orientation with respect to the moon at re-entry to obtain the desired landing longitude. The total time of flight is altered by changing the input time of flight to the moon in the launch phase. Once this is done, the entire circumlunar search process is repeated until, finally, the landing site longitude tolerance is met.

5. Applications

The possible uses of the Analytic Circumlunar Program will be similar to those of the Analytic Lunar Return Program, i. e.,

a. To perform general parametric studies such as relating the distance of closest approach to the earth-phase energy, relating the orientations of the conics in various phases, and calculating launch and re-entry restriction curves.

b. To obtain launch conditions which may be used as a first approximation in the exact program to search for exact trajectories. Empirical correction schemes such as that used in the ALR Program may be added to better solve the end-point problem.

c. To calculate sensitivity coefficients of terminal conditions with respect to injection or midcourse conditions. It has yet to be shown, probably by direct comparison with exact results, that the coefficients yielded by the Analytic Circumlunar Program will be of sufficient accuracy to be useful.

B. Non-Free-Return Circumlunar Trajectories

1. Introduction

The term "non-free-return" circumlunar trajectories applies to those circumlunar trajectories which require the spacecraft to supply a

velocity change in the vicinity of the moon. The following missions, for example, would require a non-free-return trajectory:

a. The spacecraft is to pass around the moon at an inclination to the lunar equator, i, (say, to pass over a specified point on the lunar surface) and with a specified distance of closest approach, h. In general a velocity impulse, ΔV, will be required at, say, closest appraoch in order that the trajectory will return to a specified earth landing site with a specified re-entry angle. ΔV will be a function of i and h (as well as date, etc.) and those i - h combinations corresponding to $\Delta V = 0$ will be the free-return circumlunar trajectories discussed in the last section.

b. The spacecraft is to enter a circular orbit about the moon such that it passes over a specified point and at a specified altitude. After a few revolutions, the spacecraft is to be injected into a return trajectory. *

c. This mission would be similar to (b) except that a landing from a circular orbit and then launch into a circular orbit is added before injection into a return trajectory.

It is clear from these sample missions that non-free circumlunar trajectories may involve any combination of injection into or out of a circular orbit (or elliptic orbit), direct landing or direct launch, coming within a specified pericynthion distance, and passing over a specified lunar site. This section will be concerned with the means by which the existing Analytic Circumlunar and the Analytic Lunar Return Programs may be modified to encompass missions of this type.

2. Modification of the Analytic Circumlunar Program

Presently, the two requirements on the ACP in the vicinity of the moon are the calculation of the moon centered hyperbola given the entry and exit velocity vectors at the moon's sphere of influence, and the calculation of a direct impact trajectory, if desired. For the mission first mentioned above, it is necessary to calculate the moon centered hyperbola whose

*It is assumed in all of these missions that the spacecraft is to return to a specified landing site on earth with specified re-entry conditions, as in the ALR program.

pericynthion distance is specified and which contains a fixed selenographic vector. The equations for this case are fairly simple since the hyperbolic plane must contain this vector and the entry velocity vector. The major axis can be obtained from the vehicle's moon centered energy and the eccentricity from the pericynthion distance.

If the spacecraft is to perform a direct landing on the moon, the problem is a little more difficult. In this case, although the selenographic landing site vector would be known, the eccentricity of the hyperbola could not be found unless another parameter, such as the flight path angle at the sphere of influence, were known. Since the solution of the outward leg involves search iterations, it is a simple matter to approximate this parameter (it is always less than 2 degrees) and let additional iterations improve upon this value.

For injecting into a circular orbit whose radial distance and selenographic inclination are specified, a similar situation exists. As soon as the hyperbolic asymptote is known (selenographic coordinates), the problem is explicitly solvable. The orientation of the asymptote, however, depends upon an unknown parameter which, as above, may be found by successive iterations.

One can, of course, think of more complex missions than those discussed here, such as injecting into elliptic orbits under given constraints. For modification of the Analytic Circumlunar Program to include such cases, individual analyses would be required.

3. Modification of the Analytic Lunar Return Program

The return phase of the non-free circumlunar trajectory is essentially independent of the outgoing phase. Certainly this will be the case if a lunar landing is a trajectory requirement. In this case, no changes in the ALR Program are required since the program will presently search for a return trajectory launched from the surface of the moon.

Next, launch from a circular lunar orbit which passes over a given lunar site requires only a simple modification to the ALRP if the time of injection from the orbit is not specified. The change is similar to that discussed above for the outward phase. A launch may then be made from a given launch site into a circular orbit followed by injection from the orbit, with the time of launch and injection being calculated by the program.

If the spacecraft is already in a specified orbit such as in missions (a) and (b) above, then the return trajectory, with the inputs required in the ALR Program, is overspecified and some trajectory parameter must be released. The parameter which is the least harmful and the most effective is the time of flight of the return phase. The method that may be used in searching for a "fixed injection time" trajectory is to first assume a total flight time. Then, after a first iteration, a more accurate flight time may be calculated which is consistent with the fixed time of injection.

This, however, is not the only problem when launching from a specified lunar orbit. A critical problem is where in the given orbit one should inject to return to the earth. It is clear that the most efficient way to return is to inject from a point on the orbit such that the injection velocity vector is along the orbital velocity vector. This, however, places a very tight restriction on the return trajectory. This can be understood more clearly if one remembers that the velocity at the moon's sphere of influence is determined by the earth landing conditions, and that this velocity must be contained by the selenocentric hyperbolic plane. However, if this plane is restricted to that of the orbit plane, then the chances are that the exit velocity from the sphere is not contained in the orbit plane. A lunar polar orbit for example will contain the return velocity vector only twice during a lunar month.

The approach recommended here to cover launch from a specified lunar orbit is to allow launching out of the orbit plane and then to solve for that point on the orbit which minimizes the return injection velocity. In this case, the only modification required of the ALR Program is to launch from a fixed selenographic point at a fixed time. If necessary the program may also be modified to empirically search for the minimum injection velocity.

IV. ORBIT DETERMINATION THEORY

A. Background

The basic way in which statistical regression analysis enters into orbit determination may be formulated as follows: A set of noisy, redundant observations of a spacecraft (radar, optical, etc.) denoted by an n-vector z is given. From the laws of mechanics and from geometrical considerations, the true vector value μ of the observations is expressible as a known function of a finite set of parameters denoted by the p-vector γ: $\mu = \mu(\gamma)$. In the simplest case, γ denotes six components of spacecraft position and velocity at a specified epoch t_o. In general, however, the set γ may include other non-orbital parameters such as physical constants, biases in observations, tracking station location coordinates, etc., subject to $p < n$. The nonlinear regression equation is then

$$z = \mu(\gamma) + w \tag{4.1}$$

where w denotes an n-vector of noise on the true values of the observations. Given z, the functional form of μ, and the statistical properties of w, the problem is to estimate γ.

In practice, Eq. (4.1) is linearized by expanding μ about an initial guess g_o. Letting $\Delta\gamma = \gamma - g_o$ and $\Delta z = z - \mu(g_o)$ (the components of Δz are called "residuals"), and letting θ denote the $n \times p$ matrix of partial derivations of μ with respect to γ,

$$\theta = \left(\frac{\delta\mu}{\delta\gamma}\right)\Bigg|_{\gamma = g_o},$$

the linearized regression equation is

$$\Delta z = \theta\,\Delta\gamma + w. \tag{4.2}$$

The nonlinear equation (4.1) is then solved by iteratively solving the linear equation (4.2). Since we shall be chiefly concerned in this chapter with the

solution of the linear equation (4.2), and not with the problem of convergence, we shall frequently drop the Δ's in (4.2) in the future and simply write

$$z = \theta \gamma + w \tag{4.3}$$

There are three well-known statistical techniques for the estimation of γ in (4.3). These are described below. In the discussions to follow, the noise w will be assumed unbiased (except when otherwise noted) with non-singular $n \times n$ covariance matrix R. The diagonal elements of R form the (diagonal) $n \times n$ matrix M^2 of variances; M denotes the (positive) square root of M^2.

(i) Least Squares. The least squares (LS) estimate of γ in (4.3) is

$$\boxed{g_{LS} = (\theta' M^2 \theta)^{-1} \theta' M^2 z} \tag{4.4}$$

Thus it is necessary to know M, within a constant factor, to compute g_{LS}. This estimate has the properties that it is linear, unbiased, and it minimizes the sum of squares of residuals weighted according to M^2; i.e., $F(g) = (z - \theta g)' M^2 (z - \theta g)$ is a minimum for $g = g_{LS}$. The covariance matrix of g_{LS} is

$$\boxed{G_{LS} = (\theta' M^2 \theta)^{-1} \theta' M^2 R M^2 \theta (\theta' M^2 \theta)^{-1}} \tag{4.5}$$

(ii) Minimum Variance. The estimate

$$\boxed{g_{MV} = (\theta' R^{-1} \theta)^{-1} \theta' R^{-1} z} \tag{4.6}$$

has the property that of all linear unbiased estimates, g_{MV} has minimum covariance matrix. (I.e., if g is any other linear unbiased estimate of γ with covariance matrix G, then $G_{MV} \leq G$ in the sense that $G - G_{MV}$ is non-negative definite.) Thus g_{MV} is called the minimum variance (or sometimes the Markov) estimate of γ. Note that it is necessary to know R, within a constant factor, to compute g_{MV}. The covariance matrix of g_{MV} is

$$\boxed{G_{MV} = (\theta' R^{-1} \theta)^{-1}} \tag{4.7}$$

(iii) Weighted Least Squares. As a generalization of g_{LS}, we shall also consider estimates of the form

$$\boxed{g_{WLS} = (\theta' W \theta)^{-1} \theta' W z} \tag{4.8}$$

where W is a diagonal, non-negative $n \times n$ "weighting" matrix. This estimate, which is linear and unbiased, has the property that it minimizes $(z - \theta g)' W (z - \theta g)$. It is thus called a weighted least squares (WLS) estimate. The covariance matrix of g_{WLS} is

$$\boxed{G_{WLS} = (\theta' W \theta)^{-1} \theta' W R W \theta (\theta' W \theta)^{-1}} \tag{4.9}$$

We shall discuss later some criteria for selecting the matrix W.

There is still a fourth estimation technique, maximum likelihood, which merits comment here. The maximum likelihood (ML) estimate of γ is defined as that value of g which, when substituted for γ in the sample probability density (or "likelihood") function, maximizes this function for the sample in question. Thus g_{ML} is in general a complicated, nonlinear function of the sample. It is a theorem of statistics that $g_{ML} = g_{MV}$ when the noise is gaussian. To the author's knowledge, ML is never used in orbit determination except when accompanied by the assumption that the noise is gaussian, in which case ML reduces to MV. For these reasons, the authors' feel justified in neglecting ML, with the understanding that when the noise is gaussian ML and MV may be used interchangeably.

B. Correlated Observations

One of the SSAS objectives was to study the estimation techniques just described in order to arrive at a final technique considered most suitable for the handling of correlated observations in orbit determination. That study and its conclusions will be described here.

Consider first the comparison of LS and MV. The role of WLS will be considered later. Note first that the LS estimate is the same as the MV estimate when the noise is uncorrelated (i.e., $R = M^{-2}$), as is obvious from (4.4) and (4.6). However, we are concerned here with the situation when the

noise is correlated. In that event, there are four important theorems regarding the relative performance of LS and MV.

Before proceeding to these theorems, it is necessary to introduce the concept of the spectrum of the noise correlation matrix. The noise correlation matrix is simply the normalized covariance matrix, $\rho = MRM$. Since R is by hypothesis non-singular, this matrix will possess n positive eigenvalues $\lambda_1, \ldots, \lambda_n$ and n (orthonormal) eigenvectors $\psi_1, \ldots, \psi_n$ such that

$$\rho \psi_i = \lambda_i \psi_i , \quad i = 1, \ldots, n ,$$

and

$$\psi_i \psi_j = \delta_{ij} , \quad i, j = 1, \ldots, n.$$

When the noise is stationary, so that $\rho_{ij} = \rho_{i-j}$, the spectrum of the correlation matrix has an interesting interpretation: if the sampling frequency is kept uniform and constant while the length of the sample is allowed to increase, then the noise eigenvectors approach the ordinary trigonometric functions asymptotically, and the asymptotic eigenvalues are are proportional to the Fourier transform of the correlation function, i.e., the spectral density of the noise process. Since for most noise processes which one expects in orbit determination, the spectral density has its maximum at zero frequency, this has the important implication that one can expect the maximum eigenvalues to be associated with the "low frequency" eigenvectors.

We shall next introduce the notation $G_{UC} = (\theta' M^2 \theta)^{-1}$. Thus G_{UC} would be the covariance matrix of the LS (or MV) estimate of γ if the noise were uncorrelated (i.e., $R = M^{-2}$). This matrix, it might be added, is commonly computed whenever an LS determination is performed.

The following three theorems regarding the comparison of LS and MV are derived in Reference [5].

Theorem 1. $G_{MV} = G_{LS}$ if and only if the space spanned by the p n-vectors which are the columns of $M\theta$ coincides with the space spanned by exactly p eigenvectors of ρ, then both G_{LS} and G_{MV} are similar to a diagonal matrix whose elements are the corresponding p eigenvalues of ρ.

Theorem 2. If λ_{max} and λ_{min} denote the maximum and minimum eigenvalues of ρ, then

$$\lambda_{min} G_{UC} \leq G_{MV} \leq G_{LS} \leq \lambda_{min} G_{UC} \tag{4.10}$$

Theorem 3. $$G_{LS} \leq \frac{1}{4}(\lambda_{max} + \lambda_{min})(\frac{1}{\lambda}_{max} + \frac{1}{\lambda}_{min}) G_{MV} \tag{4.11}$$

A fourth theorem, due to Grenander and Rosenblatt [33], states conditions on the regression vectors (actually, on the columns of $M\theta$) such that when the noise w is stationary, G_{LS} and G_{MV} will be asymptotically equal as the length of the sample is increased. The reader is referred to the cited reference for the exact mathematical formulation. The implications of their theorem are that G_{LS} and G_{MV} will be asymptotically equal whenever the regression vectors are polynomials, trigonometric functions or a mixture of these. Because these are just the kinds of regression vectors which one encounters in orbit determination, the theorem indicates that when long portions of data for which the noise is stationary are analyzed by LS method, one can expect the resulting estimates to be near optimum.

Let us now see how these theorems may be applied to practical orbit determination work. One of the characteristics of tracking data is that it usually occurs in several "data types," according to the quantity which is measured (Doppler, angles, etc.) and according to the tracking station from which it originates. We shall suppose here that equation (4.3) decomposes into k regression equations,

$$z_i = \theta_i \gamma + w_i, \qquad i = 1, \ldots, k \tag{4.12}$$

each of which is a vector regression equation in the same vector regression parameter γ corresponding to one of k mutually uncorrelated data types. Let θ_i, R_i, M_i, etc., be defined for each data type as in Section A. Then for each data type one can, in principle,* construct the LS estimate g_i,

*For some data types, $\theta_i' M_i^2 \theta_i$ may be poorly conditioned or even singular, making g_i impossible to obtain explicitly. This is not important to the argument as long as $\sum_1^k \theta_i' M_i^2 \theta_i$ is non-singular. Looking at the individual g_i is a conceptual, rather than a real, operation.

$$g_i = (\theta_i' M_i^2 \theta_i)^{-1} \theta_i' M_i^2 w_i \tag{4.13}$$

having covariance matrix G_i,

$$\begin{aligned} G_i &= (\theta_i' M_i^2 \theta_i)^{-1} \theta_i' M_i^2 R M_i^2 \theta_i (\theta_i' M_i^2 \theta_i)^{-1} \\ &\leq \lambda_i (\theta_i' M_i^2 \theta_i)^{-1} \end{aligned} \tag{4.14}$$

where λ_i is the maximum eigenvalue (or an upper bound on the maximum eigenvalue) of the noise correlation matrix $\rho_i = M_i R_i M_i$ going with the i^{th} data type. (The inequality in (4.14) is an application of Theorem 2.)

Two questions arise regarding the g_i : (a) how good are the individual estimates and (b) how may they best be combined into a single estimate of γ? We shall examine these questions below.

(a) To decide how good the individual estimates are, we shall compare g_i with the optimal MV estimate g_{MV_i},

$$g_{MV_i} = (\theta_i' R_i^{-1} \theta_i)^{-1} \theta_i' R_i^{-1} w_i \tag{4.15}$$

having covariance matrix G_{MV_i},

$$G_{MV_i} = (\theta_i' R_i^{-1} \theta_i)^{-1} \tag{4.16}$$

In most orbit determination situations, one can expect the regression vectors (i.e., the columns of $M\theta$) to resemble low frequency and/or secular functions. Thus, the regression vectors will ordinarily be expressible as linear combinations of the lower frequency eigenvectors, primarily, with only small contributions from high frequency eigenvectors occurring. We have also seen that the low frequency eigenvectors are generally associated with the maximum noise eigenvalues. Thus, application of Theorems 1, 3 and 4 suggest that G_i and G_{MV_i} will be nearly equal and will, in turn, be closely approximated by $\lambda_i (\theta_i' M_i^2 \theta_i)^{-1}$. (It should be emphasized that these are tendencies which, in exceptional cases, will not be true. Conditions which do hold rigorously in all cases are given by Theorems 1, 2 and 3.)

(b) Given g_i and G_i, $i = 1, \ldots, k$, the optimal way to combine the g_i into a single estimate would be to weight each g_i according to G_i^{-1}. However, this procedure has the following disadvantages: (a) it is numerically complicated and (b) it requires a detailed knowledge of each R_i. We therefore propose as a compromise solution that each g_i be weighted according to $\theta_i' M_i^2 \theta_i / \lambda_i$. This procedure has the advantage in that (a) it is numerically simple; (b) $\lambda_i (\theta_i' M_i^2 \theta_i)^{-1}$ can be expected to be a rather good approximation to G_i, as we have just seen; and (c) since $G_i \leq \lambda_i (\theta_i' M_i^2 \theta_i)^{-1}$, in all cases, the weighting is conservative since it does not tend to overly weight highly correlated data.

The fact which makes the above solution numerically simple is that it corresponds precisely to using a WLS estimate based on <u>all</u> of the observations,

$$g_{WLS} = (\theta' W \theta)^{-1} \theta' W w \tag{4.8}$$

in which the diagonal weighting matrix W is given by

$$W = \begin{bmatrix} M_1^2/\lambda_1 & & \\ & \ddots & \\ & & M_k^2/\lambda_k \end{bmatrix} \tag{4.17}$$

The formula for the covariance matrix G_{WLS} of g_{WLS} is given by equation (4.9). More interesting, perhaps, is the inequality

$$\boxed{G_{WLS} \leq (\theta' W \theta)^{-1} \leq \lambda_i (\theta_i' M_i^2 \theta_i)^{-1}, \quad i = 1, \ldots, k} \tag{4.18}$$

Here, $(\theta' W \theta)^{-1}$ constitutes an easily computed upper bound on G_{WLS} which satisfies the condition that it is less than or equal to the upper bound on the covariance matrix of each g_i. The reader is referred to Example 1 and 2 at the end of this Chapter for application of the principles developed in this Section.

By contrast with the above estimate, the conventional LS estimate of γ based on <u>all</u> of the data is,

$$
\begin{aligned}
g_{LS} &= (\theta' M^2 \theta)^{-1} \theta' M^2 w \\
&= \Big(\sum_1^k \theta_i' M_i^2 \theta_i\Big)^{-1} \sum_1^k \theta_i' M_i^2 w_i \\
&= \Big(\sum_1^k \theta_i' M_i^2 \theta_i\Big)^{-1} \sum_1^k \theta_i' M_i^2 \theta_i g_i
\end{aligned}
\tag{4.19}
$$

Thus, g_{LS} may be regarded as a linear combination of the g_i in which g_i is weighted according to $\theta_i' M_i^2 \theta_i$. The weakness in this estimation procedure comes from the fact that although g_i may be a "good" estimate based on the i^{th} data, $\theta_i' M_i^2 \theta_i$ can be a very poor approximation to the inverse of the covariance matrix of g_i. In fact, if the data type is highly correlated, $\theta_i' M_i^2 \theta_i$ may be an order of magnitude larger than G_i^{-1} (for example, when λ_i is of order 10^2 or 10^3, as can easily occur. See Example 2 at the end of this Chapter.) This can lead to overly weighting a highly correlated data type in such a way as to degrade the accuracy of g_{LS} compared with not using that particular data type at all. The WLS estimate previously described carefully avoids this pitfall.

Closely associated with the problem of how to handle correlated data is the problem of how frequently to take observation when it is known that the observations are correlated in time. This aspect has been studied by Hoel [34] and others. We do not have any new and fundamental contributions to make at this time except to re-iterate two well-known principles: (a) Regardless of the particular nature of the noise, it is generally advisable and profitable to include a sufficient number of observations so that, in the absence of noise correlations, the structures of the various regression vectors would be well-followed. A clue as to when this occurs is to observe when the matrix $(1/n)\ \theta' W \theta$, as a function of the number of observations n, approaches a stable (asymptotic) matrix. (b) Adding more observations beyond this point will be of value only if noise "cancellation" occurs (e.g., when the noise is "white"). When the noise is correlated, it is usually not profitable to further increase the frequency of observation beyond the point where observations adjacent in time are 50 percent correlated (positively, with no intervening minima in the noise correlation function between the origin and the sampling interval).

C. Special Topics

Having concluded that a weighted least squares type of estimation was most suitable for handling correlated data, we attempted next to apply this technique to some of the special problems which are peculiar to orbit determination. Specifically, we studied (1) handling a priori data, (2) separating parameters into classes according to whether or not they are to be estimated, (3) tracking through midcourse maneuvers, and (4) modification of the computational techniques for onboard use. The results of these studies are reported in Reference [6] and are summarized here.

When the WLS technique is to be used, it is a great convenience to introduce the concept of "equivalent-or-worse" uncorrelated noise. The basis of this idea is as follows: If R denotes the true $n \times n$ covariance matrix of the observational noise w in equation (4.3), then the WLS weighting matrix which we have chosen is, in effect, the "largest" $n \times n$ diagonal matrix satisfying $R \leq W^{-1}$. This fact results in the inequality

$$G_{WLS} = (\theta' W \theta)^{-1} \theta' W R W \theta (\theta' W \theta)^{-1} \leq (\theta' W \theta)^{-1} \qquad (4.20)$$

Therefore, if we replace the true noise w with (hypothetical) uncorrelated noise w^* having covariance matrix W^{-1}, any conclusions we may draw concerning the accuracy of our statistical estimates will be "conservative." In the following discussions, we shall treat the noise as if it were uncorrelated, having covariance matrix equal to the reciprocal of the diagonal weighting matrix W, with the understanding that noise which was originally correlated has already been replaced (conceptually) with equivalent or worse uncorrelated noise. It might be added that this idea is also useful when simulating the effects of correlated noise in space mission analysis. In that event, the correlated noise is replaced in fact, rather than in theory, by uncorrelated noise. (See Example 2.)

1. A Priori Data

Let the initial guess g_o for γ in (4.1) have a priori "information" matrix S. S is a $p \times p$ matrix of weights applicable to the a priori value g_o which is such that when its inverse exists, it is the a priori covariance matrix

of g_o. However, there is no requirement that S be non-singular, and S may have rows and columns of zeros corresponding to components of g_o for which no a priori variances are available. Then the combined estimate of γ, based both on a priori information and on observational data, is given by

$$\boxed{g_1 = g_o + (\theta' W \theta + S)^{-1} \theta' W \Delta z} \tag{4.21}$$

and has covariance matrix

$$\boxed{G = (\theta' W \theta + S)^{-1}} \tag{4.22}$$

In case several iterations of the WLS procedure are required to solve the non-linear equation (4.1), then equations for successive estimates become slightly more complicated:

$$\boxed{g_n = g_{n-1} + (\theta'_{n-1} W \theta_{n-1} + S)^{-1} \theta'_{n-1} W \Delta z_{n-1} + (\theta'_{n-1} W \theta_{n-1} + S)^{-1} S (g_o - g_{n-1})} \tag{4.23}$$

where Δz_{n-1} and θ_{n-1} denote residuals and partial deviatives evaluated for $\gamma = g_{n-1}$, the result of the previous iteration. The final covariance matrix is, of course, given by (4.22) with θ evaluated at the final estimate of γ.

2. Separation of Parameters

Sometimes the components of the vector parameter γ will naturally fall into two classes, denoted by the sub-vectors γ_1 and γ_2. For example, γ_1 may denote orbital parameters while γ_2 denotes physical constants, tracking station coordinates, or other non-orbital parameters which affect μ. Suppose now that we intend to estimate only γ_1, either because we are unaware of uncertainties in γ_2 or else because we feel there is insufficient information contained in the observational data to warrant the simultaneous estimation of γ_1 and γ_2. It is important to be able to estimate statistically the effects of using an incorrect value for γ_2.

We shall rewrite the regression equation (4.1) as

$$z = \mu(\gamma_1, \gamma_2) + w \tag{4.24}$$

which linearizes to

$$\Delta z = \theta_1(\gamma_1 - g_{10}) + \theta_2(\gamma_2 - g_{20}) + w \tag{4.25}$$

g_{10} and g_{20} being the initial guesses for γ_1 and γ_2. When we solve only for γ_1, the WLS estimate for γ_1 is

$$g_{11} = g_{10} + (\theta_1' W \theta_1 + S_{11})^{-1} \theta_1' W \Delta z \tag{4.26}$$

S_{11} being the a priori information matrix of g_{10}. To analyze the effect of the error $\gamma_2 - g_{20}$, it is useful to write (4.26) as

$$\begin{aligned} g_{11} = \gamma_1 + (\theta_1' W \theta_1 + S_{11})^{-1} \Big[& - S_{11}(\gamma_1 - g_{10}) \\ & + \theta_1' W \theta_2(\gamma_2 - g_{20}) + \theta_1' W w \Big] \end{aligned} \tag{4.27}$$

This formulation exhibits g_{11} as an unbiased estimate of γ_1 in which there are three sources of error: (1) the a priori estimate g_{10} of γ_1, (2) the incorrect estimate g_{20} for γ_2, and (3) the observational noise w. Assuming that g_{10} and g_{20} are uncorrelated,* the covariance matrix of g_{11} is

$$\boxed{G_{11} = (\theta_1' W \theta_1 + S_{11})^{-1} + (\theta_1' W \theta_1 + S_{11})^{-1} \theta_1' W \theta_2 \Lambda_2 \theta_2' W \theta_1 (\theta_1' W \theta_1 + S_{11})^{-1}} \tag{4.28}$$

where Λ_2 is the covariance matrix of uncertainty in g_{20}. The second term on the right in (4.28) thus shows statistically the effect of having used the incorrect value for γ_2. In Example 3 at the end of this section, the effects of "unsuspected" biases are derived using equation (4.28).

---

*In case g_{10} and g_{20} are correlated with a priori covariance matrix Λ,

$$\Lambda = \left[\begin{array}{c|c} \Lambda_{11} & \Lambda_{12} \\ \hline \Lambda_{21} & \Lambda_{22} \end{array}\right] = \text{covariance matrix of } \left[\begin{array}{c} g_{10} \\ \hline g_{20} \end{array}\right],$$

then, the formula for G_{11} becomes

$$\begin{aligned} G_{11} = (\theta_1' W \theta_1 + \Lambda_{11}^{-1})^{-1} + (\theta_1' W \theta_1 + \Lambda_{11}^{-1})^{-1} \Big\{ & \theta_1' W \theta_2 \Lambda_{22} \theta_2' W \theta_1 \\ & - \theta_1' W \theta_2 \Lambda_{21} \Lambda_{11}^{-1} - \Lambda_{11}^{-1} \Lambda_{12} \theta_2' W \theta_1 \Big\} (\theta_1' W \theta_1 + \Lambda_{11}^{-1})^{-1} \end{aligned}$$

For purposes of comparison, it is sometimes of interest to know how well one could have estimated γ_1 is one had simultaneously estimated both γ_1 and γ_2 from observational data. Using the notation

$$C = \left[\begin{array}{c|c} C_{11} & C_{12} \\ \hline C_{21} & C_{22} \end{array}\right] = \left[\begin{array}{c|c} \theta_1' W \theta_1 + S_{11} & \theta_1' W \theta_2 + S_{12} \\ \hline \theta_1' W \theta_1 + S_{21} & \theta_2' W \theta_2 + S_{22} \end{array}\right], \tag{4.29}$$

the inverse of C will be the covariance matrix of uncertainty in the estimation of both $\left[\begin{array}{c} \gamma_1 \\ \hline \gamma_2 \end{array}\right]$,

$$C^{-1} = \left[\begin{array}{c|c} C^{11} & C^{12} \\ \hline C^{21} & C^{22} \end{array}\right] \tag{4.30}$$

Thus C^{11} shows how well γ_1 is determined. The following formula for C^{11} is derived in [2]:

$$\boxed{C^{11} = (C_{11} - C_{12} C_{22}^{-1} C_{21})^{-1}} \tag{4.31}$$

which may be compared with G_{11}.

The following relation among the various covariance matrices for estimates of γ_1 will hold:

$$\boxed{(\theta_1' W \theta_1 + S_{11})^{-1} \leq C^{11} \leq G_{11} = (\theta_1' W \theta_1 + S_{11})^{-1} + \text{additional terms}} \tag{4.32}$$

3. Midcourse Maneuvers

Tracking "through" a midcourse maneuver involves the statistical combining of pre-midcourse tracking data, the maneuver itself, and post-midcourse tracking data to re-establish the orbit of the spacecraft. There are, of course, several ways in which this may be done. Typically, the procedure is as follows: From pre-midcourse tracking (plus any additional a priori information) one computes an estimate g_o and covariance matrix G_o applicable to spacecraft position and velocity at time t_o, just prior to the maneuver. At time t_o, one commands a maneuver Δg. If the maneuver is impulsive, i.e.,

of very short duration in time, then Δg consists of the three components of the velocity impulse. If the maneuver is of appreciable duration, the true maneuver can be represented by an equivalent impulsive change in all six coordinates of position and velocity.* In either event, $g_o + \Delta g$ becomes the new estimate of position and velocity at $t_o +$, just after the maneuver, and has covariance matrix $G_o + \Lambda(\Delta g)$, where $\Lambda(\Delta g)$ is the covariance matrix of uncertainty in the actual execution of the maneuver and, as indicated, is generally a function of Δg. Then $g_o + \Delta g$ and $G_o + \Lambda$ may be used as a priori information in subsequent free-flight tracking.

Consider now the matrix Λ. The following model of execution errors is, while not the most general, typical of maneuvers occurring on many space missions. Let the correction be impulsive so that the commanded maneuver is a vector velocity increment V in the (θ, ϕ) direction, as shown below:

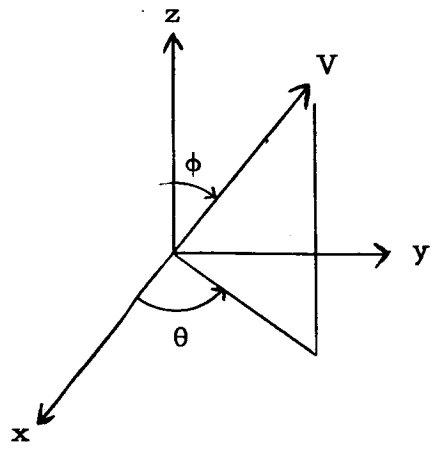

The expressions for errors in the execution of V are

$$\delta V = \epsilon_1 + \epsilon_2 |V|$$
$$\delta V_\theta = \epsilon_3 + \epsilon_4 |V|$$
$$\delta V_\phi = \epsilon_5 + \epsilon_6 |V|$$

*The problem of tracking during the actual maneuver is not treated here.

where $|V|$ is the magnitude of V and

ϵ_1 = speed error due to engine shutdown

ϵ_2 = proportional speed error due to accelerometer

ϵ_3 and ϵ_5 = lateral velocity errors due to autopilot

ϵ_4 and ϵ_6 = pointing errors due to angular misalignment

We assume that the ϵ_i are mutually uncorrelated with zero means and $E\epsilon_1^2 = k_1$, $E\epsilon_2^2 = k_2$, $E\epsilon_3^2 = E\epsilon_5^2 = k_3$, $E\epsilon_4^2 = E\epsilon_6^2 = k_4$. A rotation U will relate the above velocity errors to components in the rectangular reference system x, y, z:

$$\begin{bmatrix} \delta V_x \\ \delta V_y \\ \delta V_z \end{bmatrix} = U \begin{bmatrix} \delta V \\ \delta V_\theta \\ \delta V_\phi \end{bmatrix}$$

where

$$U = \begin{bmatrix} \sin\phi\cos\theta & -\sin\theta & \cos\phi\cos\theta \\ \sin\phi\sin\theta & \cos\theta & \cos\phi\sin\theta \\ \cos\phi & 0 & -\sin\phi \end{bmatrix}$$

Thus, the final 3 x 3 covariance matrix of execution errors, $\sum(V)$, is

$$\sum(V) = U \begin{bmatrix} k_1 & & \\ & k_2 & \\ & & k_3 \end{bmatrix} U' + V^2 \, U \begin{bmatrix} k_2 & & \\ & k_4 & \\ & & k_4 \end{bmatrix} U'$$

The 6 x 6 matrix Λ is

$$\Lambda = \left[\begin{array}{c|c} 0 & 0 \\ \hline 0 & \sum(V) \end{array}\right]$$

When the 3-vector V is specified numerically, as it is during real-time analysis of an actual mission (or in a Monte Carlo simulation of a mission*),

*The Monte Carlo simulation of space missions, including midcourse maneuvers, is described in Part II.

then Λ may be evaluated numerically. On the other hand, in the preflight analysis of a mission, Δg (or V) is not known in advance, but only its probability distribution is known, the distribution (or covariance matrix thereof) being derived from a priori knowledge of how close to nominal the trajectory is expected to be and the guidance logic which determines the maneuver. In that event, one averages Λ over the distribution of the commanded maneuver Δg (or V) to obtain $\bar{\Lambda}$. $G_o + \bar{\Lambda}$ is then used as the a priori covariance matrix of position and velocity in subsequent orbit determination analysis. Lass and Solloway [35] have derived a simple integration technique for evaluating $\bar{\Lambda}$. Since this technique is being incorporated into the Tracking Accuracy Prediction Program and will be described in later documents, it will not be discussed further here. We shall merely note that a conservative upper bound on $\bar{\Sigma}$ (and hence on $\bar{\Lambda}$) is given by

$$\boxed{\bar{\Sigma} \leq (\lambda + \bar{v}\bar{\mu})\, I_3} \qquad (4.34)$$

where $\lambda = \max(k_1, k_3)$ and $\mu = \max(k_2, k_4)$.

4. Updated Least Squares

This section describes an orbit determination technique which, because it does not require the storage of large quantities of observational data, is especially adapted to real time operation by an on-board computer. The essential features of this method have been proposed by Smith and Schmidt [36] who, because of the analogy between the estimation of orbits and the prediction of a time series by linear filtering, refer to this scheme as an "optimal filter" method. From our point of view, however, it is more natural to regard it as a least squares estimation procedure in which estimates of orbital parameters are continually updated and modified as new data arrives.

Consider the following estimation problem: an initial unbiased estimate g_o of spacecraft position and velocity at time t_o, together with an a priori 6 x 6 covariance matrix G_o of uncertainty in g_o, is provided. At each observation time t_k, $k = 1, 2, \ldots$, a q-vector of unbiased observations z_k is taken. We assume for the present that all observations are uncorrelated, and that the observations taken at time t_k are characterized by known (diagonal)

covariance matrix R_k, $k = 1, 2, \ldots$. Then at each observation time t_k, it is required to combine the old estimate of the orbit with the new data to form a new "best" estimate of position and velocity at t_k, and to determine the covariance matrix G_K of g_k. This concept is illustrated in Figure 4-1 in which γ_o, γ_1, γ_2, ... denote the true position and velocity vector at t_o, t_1, t_2, ...

In the solution to this problem, it is sufficient to describe the calculations performed just after the k^{th} set of observations is taken. Let X_k denote the result of integrating the equations of motion from t_{k-1} to t_k, using g_{k-1} as initial conditions. Then X_k serves as an initial estimate of γ_k for which the "a priori" covariance matrix, Λ_k, is G_{k-1} updated to time t_k:

$$\Lambda_k = \phi(k, k-1)\, G_{k-1}\, \phi'(k, k-1), \tag{4.35}$$

where $\phi(k, k-1)$ is a known 6 x 6 transition matrix satisfying

$$\Delta\gamma_k = \phi(k, k-1)\ \Delta\gamma_{k-1}\,. \tag{4.36}$$

The observations z_k satisfy the non-linear regression equation

$$z_k = \mu_k(\gamma_k) + w_k \tag{4.37}$$

where μ_k is a known function of the orbital parameters γ_k, and w_k is noise for which $E\, w_k\, w_k' = R_k$. We may now proceed exactly as in Section C-1. The linearized form of (4.37) is

$$\Delta z_k = \theta_k\, \Delta\gamma_k + w_k\,, \tag{4.38}$$

where $\Delta\gamma_k = \gamma_k - X_k$, $\Delta z_k = z_k - (X_k)$, and $\theta_k = (\partial\mu_k / \partial\gamma_k)$ is a q x p matrix of known coefficients. Setting $W_k = R_k^{-1}$, the new estimate of γ_k is

$$\boxed{g_k = X_k + G_k\, \theta_k'\, W_k\, \Delta z_k}\,, \tag{4.39}$$

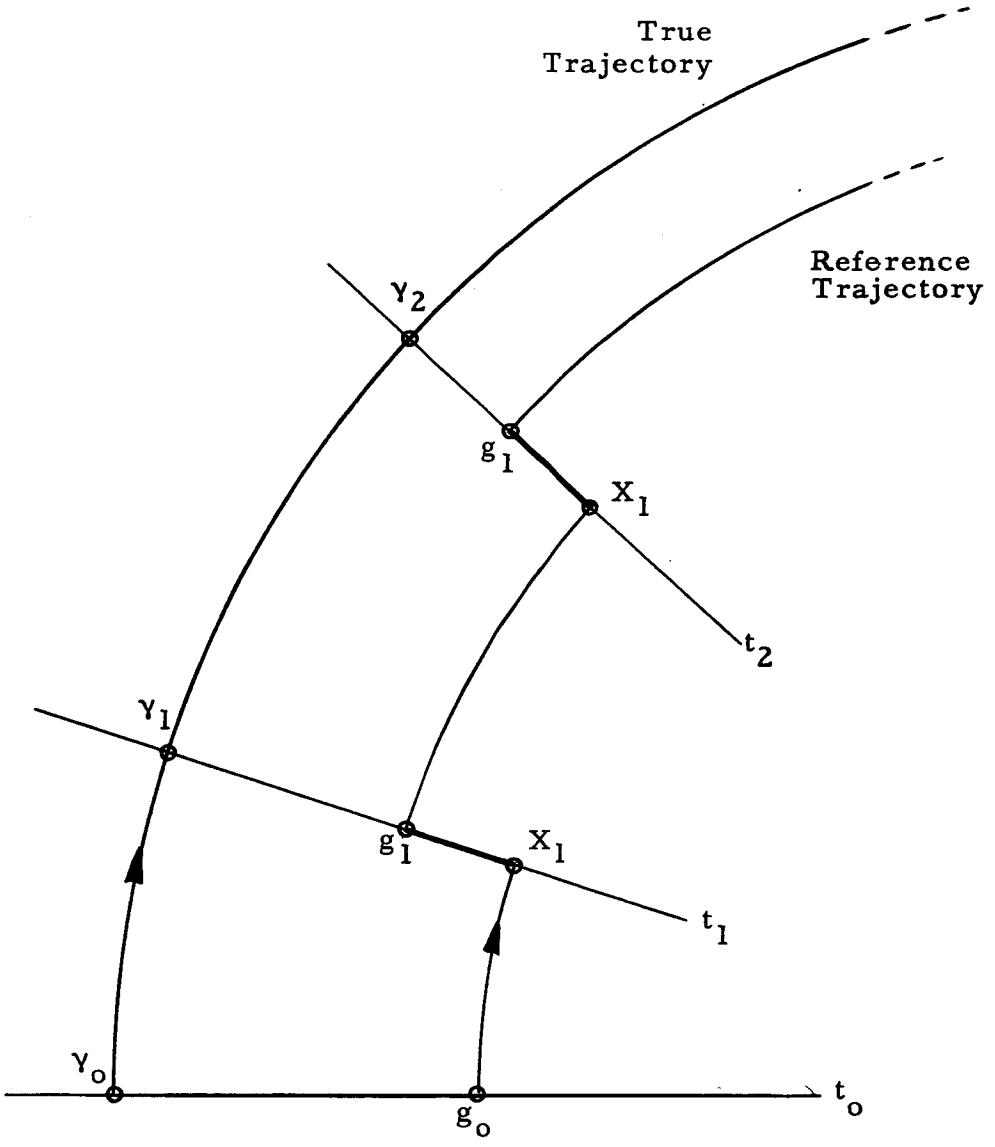

Figure 4-1. Updated Least Squares Orbit Determination. γ_o, γ_1,... denote the true position-velocity vectors at time t_o, t_1,... g_K is the "best" estimate at time t_K, while X_K is g_{K-1} updated to time t_K

where G_k is the covariance matrix of g_k ,

$$\boxed{G_k = (\theta_k' W_k \theta_k + \Lambda_k^{-1})^{-1}} \quad . \tag{4.40}$$

We have described above the basic orbit determination technique. This technique can be generalized and/or modified to fit different situations. Some such modifications are described below.

(i) Matrix Identity. An equivalent formulation of (4.40) is as follows:

$$\boxed{G_k = \Lambda_k - \Lambda_k \theta_k' (W_k^{-1} + \theta_k \Lambda_k \theta_k')^{-1} \theta_k \Lambda_k} . \tag{4.41}$$

When $q < 6$, this formula has the computational advantage that the matrix which must be inverted is of order $q \times q$, rather than 6×6 as in (4.40). This new formula follows from (4.40) as a result of the matrix identity derived in Reference [6].

(ii) Midcourse Maneuvers. The (real time) handling of midcourse maneuvers can be incorporated quite easily into the updated least squares routine. For example, if a maneuver occurs just prior to time t_k , then the commanded correction should be added to the estimate X_k, and the covariance matrix of execution errors should be added to Λ_k, to form a new a priori estimate and covariance matrix at t_k .

D. Examples

Example 1. Estimating Orbital Parameters

This example, extracted from Reference [5] , describes a simulation of the determination of the six orbital elements of an actual space trajectory. The purpose of this simulation was to develop techniques for analyzing space missions, rather than to demonstrate any conclusive results concerning a particular mission. Consequently, only short portions of a trajectory were tracked, and the noise models used are not necessarily characteristic of any

particular real system. What is demonstrated is how the following problems connected with space mission analysis may be systematically studied:

a) What is the effect of correlated noise on orbit determination?

b) How does LS compare with MV when applied to orbit determination?

c) How sharp is the upper bound on LS and MV covariance matrices given in Theorem 2 of Section B?

d) What is the result of varying the density and/or extent of observations when the tracking noise is correlated?

The details of the simulation are described below.

1. Trajectory

A 66-hour earth-moon trajectory injected from a parking orbit (similar to a RANGER or SURVEYOR trajectory) is used. Table 4-1 lists injection conditions for this trajectory. The trajectory is tracked from the Johannesburg DSIF station using $\dot{R}$, A, E data, with tracking commencing 30 minutes after injection. Two data samples A and B are simulated: Sample A consists of 21 sets of observations taken 20 seconds apart and covering 400 seconds; Sample B consists of 21 sets of observations taken 80 seconds apart and lasting 1600 seconds. Since three data types are employed ($\dot{R}$, A, E), each sample contains a total of 63 points. The STL General Tracking Program was used to compute for each sample the 63 x 6 matrix θ of regression coefficients:

$$\theta = \left(\frac{\partial \mu}{\partial \gamma}\right) .$$

2. Noise

The 63 x 63 diagonal matrix M^2 is composed of reciprocal variances of observations, with $\sigma_{\dot{R}} = 0.5$ fps, $\sigma_A = \sigma_E = 0.04$ degrees. $\dot{R}$, A, E data are assumed to be mutually uncorrelated, with each data type being auto-correlated in time according to the same 21 x 21 correlation matrix. Two correlation models I and II are described in Table 4-2a. The

actual correlation matrices take different forms for the different samples because of the different data rates. Thus, there are a total of four cases, IA, IIA, IB, IIB, corresponding to the two samples and two noise models. For each correlation matrix in Table 4-2a, the maximum eigenvalue is listed in Table 4-2b. The use of these eigenvalues is described below.

Table 4-1. Initial (Injection) Conditions for Earth-Moon Trajectory Employed in Orbit Determination Study

Right Ascension	0.20895299 E3
Declination (deg)	-0.86249977 E1
Flight Path Angle (deg)	0.88045999 E2
Azimuth (deg)	0.12201200 E3
Radius (ft)	0.21553734 E8
Velocity (fps)	0.34889200 E5

3. Results

For each of the two data samples and two noise correlation models, the following matrices were computed:

$$G_{UC} = (\theta' M^2 \theta)^{-1} ,$$

$$G_{LS} = (\theta' M^2 \theta)^{-1} \theta' M^2 R M^2 \theta (\theta' M^2 \theta)^{-1} ,$$

$$G_{MV} = (\theta' R^{-1} \theta)^{-1} .$$

By Theorem 2 of Section B,

$$\lambda_{min} G_{UC} \leq G_{MV} \leq G_{LS} \leq \lambda_{max} G_{UC} ,$$

where λ_{min} and λ_{max} are minimum and maximum eigenvalues of the noise correlation matrix. (For the noise models used here, λ_{min} and λ_{max} are

Table 4-2a. Two Noise Correlation Models

Model I	$\rho(t) = e^{-\left\|t\right\|/80}$		(t in sec)
Sample A	$\rho_{ij} = e^{-\left\|i-j\right\|/4}$		i, j = 1, ... , 21
Sample B	$\rho_{ij} = e^{-\left\|i-j\right\|}$		i, j = 1, ... , 21
Model II	$\rho(t) = \frac{1}{1+(t/80)^2}$		(t in sec)
Sample A	$\rho_{ij} = \frac{1}{1+\left(\frac{i-j}{4}\right)^2}$		i, j = 1, ... , 21
Sample B	$\rho_{ij} = \frac{1}{1+(i-j)^2}$		i, j = 1, ... , 21

Table 4-2b. Maximum and Minimum Eigenvalues of the Four Correlation Matrices

Correlation Matrix	λ Max	λ Min
IA	6.74	0.136
IB	8.74	0.11×10^{-3}
IIA	2.13	0.464
IIB	2.85	0.275

identical with the minimum and maximum eigenvalues of the sub-matrices in Table 4-2.) This implies that for any particular orbital element, the corresponding standard deviations satisfy the inequality

$$\sqrt{\lambda_{min}}\,\sigma_{UC} \leq \sigma_{MV} \leq \sigma_{LS} \leq \sqrt{\lambda_{max}}\,\sigma_{UC} \quad .$$

In Tables 4-3 and 4-4, the standard deviations of orbital elements corresponding to UC, LS and MV estimations are listed, together with $\sqrt{\lambda_{max}}\,\sigma_{UC}$, to enable LS and MV to be compared and to provide a check on how sharp the above upper bound is.

Although our examples are too limited to permit one to draw general conclusions, the following tendencies are apparent:

a) MV does not show a marked improvement over LS. In this connection, the relative performance of MV over LS is better for Model II noise than for Model I.

b) $\sqrt{\lambda_{max}}\,\sigma_{UC}$ is a useful upper bound on σ_{LS} and σ_{MV}, since it is not overly pessimistic. This is particularly true for the longer (in time) Sample B.

The fact that the points are more densely packed in Sample A does not contribute significantly to the accuracy of estimates based on that sample, since adjacent observations are highly correlated. Thus, one could have expected approximately the same accuracy of estimation from Sample A if only every fourth point were used.

Example 2. Weighting Correlated Data

Experience indicates that the angular measurements of azimuth, A, and elevation, E, made by the Goldstone DSIF station contain errors conforming roughly to the following model:*

$$E(\delta A) = E(\delta E) = 0,\ E(\delta A \times \delta E) = 0 \quad ,$$

$$E(\delta A(t') \times \delta A(t' + t)) = E(\delta E(t') \times \delta E(t' + t)) = R(t)$$

*This noise is in addition to a residual (uncorrected) bias of 0.005^{o}. We ignore the effects of this bias here. E(...) denotes the expected value.

Table 4-3. Comparison of LS, MV and Uncorrelated Case Standard Deviations of Uncertainty in Orbital Elements at Epoch (Injection) for Lunar Trajectory, Data Sample A

	σ_{LS}	σ_{MV}	σ_{UC}	$\sqrt{\lambda_{max}}\,\sigma_{UC}$
Right Ascension (deg)	0.35	0.31	0.18	0.46
Declination (deg)	0.30	0.27	0.15	0.40
Flight Path Angle (deg)	0.27	0.24	0.14	0.36
Azimuth (deg)	0.075	0.069	0.038	0.097
Radius (ft)	8.5×10^4	7.5×10^4	4.5×10^4	11×10^4
Velocity (fps)	81	72	42	110
NOISE MODEL I				
Right Ascension (deg)	0.37	0.30	0.18	0.52
Declination (deg)	0.33	0.26	0.15	0.45
Flight Path Angle (deg)	0.29	0.22	0.14	0.41
Azimuth (deg)	0.082	0.066	0.038	0.11
Radius (ft)	9.1×10^4	7.0×10^4	4.5×10^4	13×10^4
Velocity (fps)	86	66	42	130
NOISE MODEL II				

Table 4-4. Comparison of LS, MV and Uncorrelated Case Standard Deviations of Uncertainty in Orbital Elements at Epoch (Injection) for Lunar Trajectory, Data Sample B

	σ_{LS}	σ_{MV}	σ_{UC}	$\sqrt{\lambda_{max}}\,\sigma_{UC}$
Right Ascension (deg)	0.13	0.12	0.091	0.13
Declination (deg)	0.11	0.11	0.083	0.12
Flight Path Angle (deg)	0.091	0.089	0.067	0.098
Azimuth (deg)	0.037	0.036	0.027	0.039
Radius (ft)	3.3×10^4	3.3×10^4	2.5×10^4	3.6×10^4
Velocity (fps)	30	30	23	33
NOISE MODEL I				
Right Ascension (deg)	0.14	0.13	0.091	0.15
Declination (deg)	0.13	0.12	0.083	0.14
Flight Path Angle (deg)	0.098	0.095	0.067	0.11
Azimuth (deg)	0.040	0.040	0.027	0.045
Radius (ft)	3.6×10^4	3.5×10^4	2.5×10^4	4.1×10^4
Velocity (fps)	33	32	23	37
NOISE MODEL II				

where

$$R(t) = 10^{-4}\left[1 - \frac{|t|}{10}\right] + 10^{-4}\left[1 - \frac{|t|}{18,000}\right] (\text{deg}^2), \quad 0 \leq |t| \leq 10 \text{ sec}$$

$$= 10^{-4}\left[1 - \frac{|t|}{18,000}\right] (\text{deg}^2), \quad 10 \text{ sec} \leq |t| \leq 18,000 \text{ sec}$$

$$= 0, \quad 18,000 \text{ sec} \leq |t| .$$

The autocovariance function $R(t)$ is illustrated in Figure 4-2. The RMS value of the noise is $\sigma = \sqrt{R(0)} = 0.014^{\circ}$.

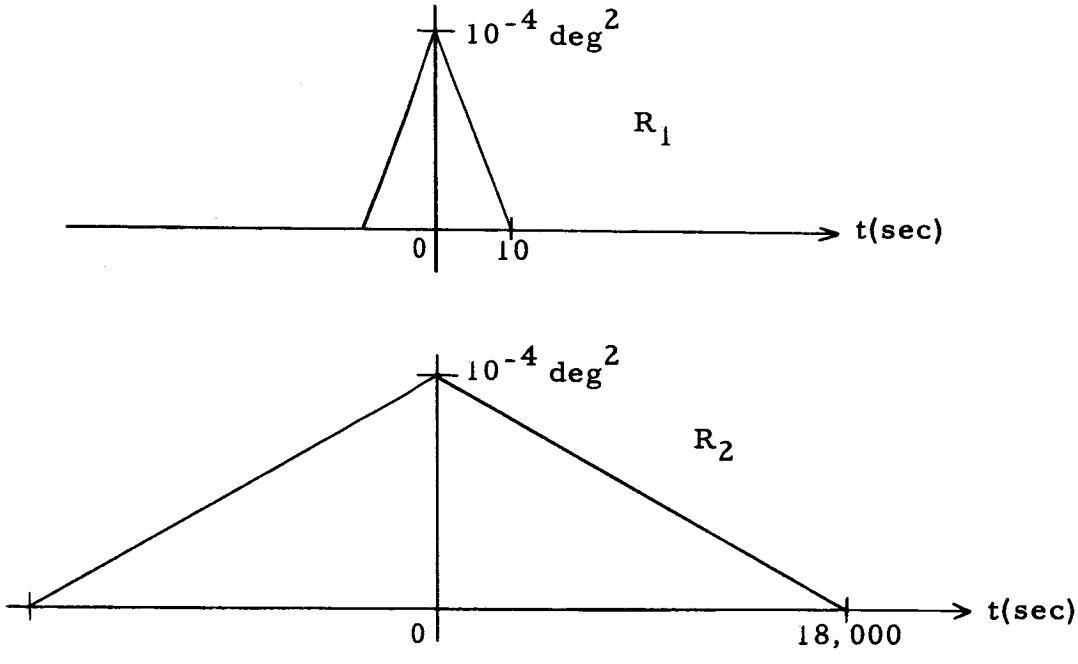

Figure 4-2. Autocovariance Function $R = R_1 + R_2$ for Noise on Goldstone Angular Tracking Data.

We wish to determine the weight to be applied to this angular data to include the effects of correlations, according to Section B. The weight is most easily expressed in terms of an "equivalent or worse σ," $\tilde{\sigma}$, which is the product of the true $\sigma = 0.014^{\circ}$ and the square root of the maximum eigenvalue of the noise covariance matrix: $\tilde{\sigma} = \sigma\sqrt{\lambda_{max}}$.

The value of $\tilde{\sigma}$ will depend on the sampling interval Δt. First, let $\Delta t = 1$ sec Equation (37) of [5] gives an upper bound on λ_{max}:

$$\lambda_{max} \leq \sum_{-\infty}^{\infty} \left|\rho_k\right| \doteq \frac{1}{\sigma^2} \int R(t)\, dt \doteq 9,000$$

thus $\tilde{\sigma} = (0.014^\circ)\,(9,000)^{1/2} = 1.35^\circ$. Table 4-5 summarizes $\tilde{\sigma}$ as a function of Δt, with λ_{max} being determined by the above formula. For a data rate of one-per-minute ($\Delta t = 60$ sec), $\tilde{\sigma} = 0.174^\circ$. An even more conservative value of $\tilde{\sigma} = 0.2^\circ$ was used for the "new DSIF model" in Part II.

Δt (sec)	σ (deg)
$\Delta t < 1$	$1.35\,(\Delta t)^{-1/2}$
1	1.35
10	0.43
60	0.174
600	0.055
18,000	0.014
$\Delta t > 18,000$	0.014

Example 3. Effects of Unsuspected Biases

This example involves the simulated tracking of a 90-hour moon-earth trajectory, using the three DSIF Stations (Goldstone, Johannesburg and Woomera). $\dot{R}$, A and E data are taken at a rate of one set of observations per minute from 12 to 80 hours after injection. Since a controlled re-entry into the earth's atmosphere was one of the objectives of the mission, the ability to predict and control the re-entry flight path angle β, which was nominally 96 degrees, was a measure of the "success" of the mission and is so used here. The following results for different simulations were obtained:

a) The data was assumed uncorrelated with $\sigma_{\dot{R}} = 0.5$ fps and $\sigma_A = \sigma_E = 0.04^\circ$. Using conventional LS orbit determination, it was found that the uncertainty in the predicted flight path angle was $\sigma_\beta = 0.018^\circ$.

b) The effect of unsuspected angular biases was studied by applying Equation (4.28) using 0.01 degree as the 1 - σ uncertainty in the angular bias

at each tracking station. When the data was weighed as before, $\sigma_{\dot{R}} = 0.5$ fps, $\sigma_A = \sigma_E = 0.04^o$, the resulting total uncertainty in β, due to both random and bias errors, was $\sigma_\beta = 0.031^o$. Thus, by weighing the angular observations according to their RMS values, the effect of biases in angular measurements is nearly to double the uncertainty in the predicted value of β.

c) Angular data was discarded and the LS fit was made on $\dot{R}$ data, only, with $\sigma_{\dot{R}} = 0.5$ fps. The resultant uncertainty in β was $\sigma_\beta = 0.025^o$.

Here, then, we have an example in which the inclusion of "bad" (i.e., improperly weighted) angular data led to a poorer orbit determination than if that data had been omitted entirely. It is an interesting problem to determine the proper, or optimum, weighting of the angular data (including angular biases) which would minimize the resultant value of σ_β. Experimenting with different weights indicated that the proper weighting was slightly less than 0.2 degree, leading to $\sigma_\beta \doteq 0.022$ degree.

V. TRACKING ACCURACY PREDICTION PROGRAM

A. Introduction

In the design of space flight trajectories and hardware it is necessary to determine the answers to questions of the following nature:

> In a nominal operation, how accurately will the spacecraft trajectory or certain terminal variables be determined from tracking, as a function of time throughout the flight?
>
> What is the sensitivity of this nominal accuracy to the number and location of tracking stations, the quantities measured, observation noise models, data biases, etc.?
>
> What is the effect of uncertainties in physical constants and station locations on the nominal accuracy?
>
> What is the effect of a midcourse correction on the orbit determination accuracy?

The Tracking Accuracy Prediction Program (TAPP) has been designed specifically for the statistical analysis of such preflight orbit determination problems, as distinct from the operational processing of data to determine a particular orbit once a flight has occurred. In developing the program, emphasis has been placed on computational speed, capability of handling a wide range of problems, and ease of future program modification. To these ends, the following features have been included: For speed, trajectory computation is based on a three-dimensional, multi-center, patched conic model so that no integration is required.* In addition, the ephemerides of celestial bodies are computed from formulas rather than by table look-up, and frequent tracking observations are interpolated from a basic mesh of time steps.

The orbit computational scheme is completely general in that it can deal with all types of conics with essentially no alterations in the formulas. No difficulties are encountered in such troublesome cases as parabolic, near parabolic, circular, and zero inclination orbits. This flexibility is made possible by the use of the Cartesian coordinates at a fixed epoch as the orbital elements

*Extensive comparison at STL of the results of such models and the results of "exact" integrating programs has shown good agreement for both lunar and interplanetary flights.

along with Herrick's unified parameters (Reference [37]) for finding the spacecraft position velocity vector on the orbit.

A variety of observation types may be simulated, including range, range rate, hour angle, declination, elevation, and azimuth from earth-based stations; planetary diameters and star-planet sightings from the spacecraft; and range and range rate from a lunar-based station. Rise and set times are computed, allowing the user to specify the observations to be taken by convenient "rules" and placing the burden of generating the observation times on the program. A number of noise models and station locations are prestored in the program and may be specified by a code number. Other models and station locations may, of course, be entered as input quantities. The effects of uncertainties in station locations, physical constants, and biases may be studied. Up to 25 orbital elements and non-orbital parameters may be solved for, and the effect of executing a midcourse maneuver may be simulated. A choice of five printout formats is provided covering trajectory variables, midcourse quantities, and tracking matrices, and varying in the amount and type of detail printed out.

TAPP Mod I was designed for the tracking analysis of flights containing a single midcourse correction. An extended version (TAPP Mod II) is under development which will allow simulation of n midcourse and terminal guidance corrections. This latter program employs a Monte Carlo method of analysis and is intended for combined tracking-guidance "mission analysis," including studies of midcourse fuel requirements, relative efficiencies of guidance logics, and the study of adaptive correction systems.

B. General Program Description

In the computation of orbits, it is assumed that an orbit is determined as a function of time from the equations of motion if the combined initial position and velocity vector, x_o, is given at one instant, t_o. In practice x_o is never known exactly but can be estimated from observations made along the orbit. Such observations are subject to random noise which introduces fluctuations into the calculated values of x_o.

The object of the present program is the evaluation of orbit determination accuracy on the basis of a given noise model and the details of observations

along the orbit. For our purpose, the accuracy criterion is the covariance matrix of a set of variables which are known functions of x_o. Usually these variables are taken to be the impact parameter vector with respect to a target planet or in the case of elliptic motion, the spacecraft position vector at a fixed time.

In order to find the covariance matrix referred to above, the method of least squares is used to estimate the initial position and velocity vector, x_o, from the observations. The covariance matrix for x_o is obtained from the weighted least squares matrices. The covariance matrix for functions of x_o can then be obtained by a linear transformation. (That is, except for effects of physical constants which will be discussed later.)

Briefly, the tasks required for finding the covariance matrix of impact errors are outlined in block diagram form in Figure 5-1.

In addition to the primary purpose of tracking accuracy evaluation, the program may sometimes be used to compute from x_o,

1) The approximate spacecraft trajectory and a set of auxiliary quantities such as the elements of the earth-escape hyperbola, various geometrical quantities associated with the sun-phase transfer orbit, and the vector impact parameter at the target planet.

2) The spacecraft rise and set times from a number of stations over a time span of interest

3) Target sensitivity coefficients for midcourse maneuvers at prescribed points in the orbit

4) The program may also be used to simulate midcourse maneuver errors from a given set of systems performance parameters and prescribed tracking data.

The functions of the major program blocks are described in the following paragraphs.

1. Orbit and Ephemeris Computation

The trajectory of a spacecraft is usually found by solving the equations of motion including all pertinent force terms. To enhance the speed of orbit computation, deviations from Kepler motion are neglected so that all trajectories are combinations of conics. For cases in which there is a sequence of

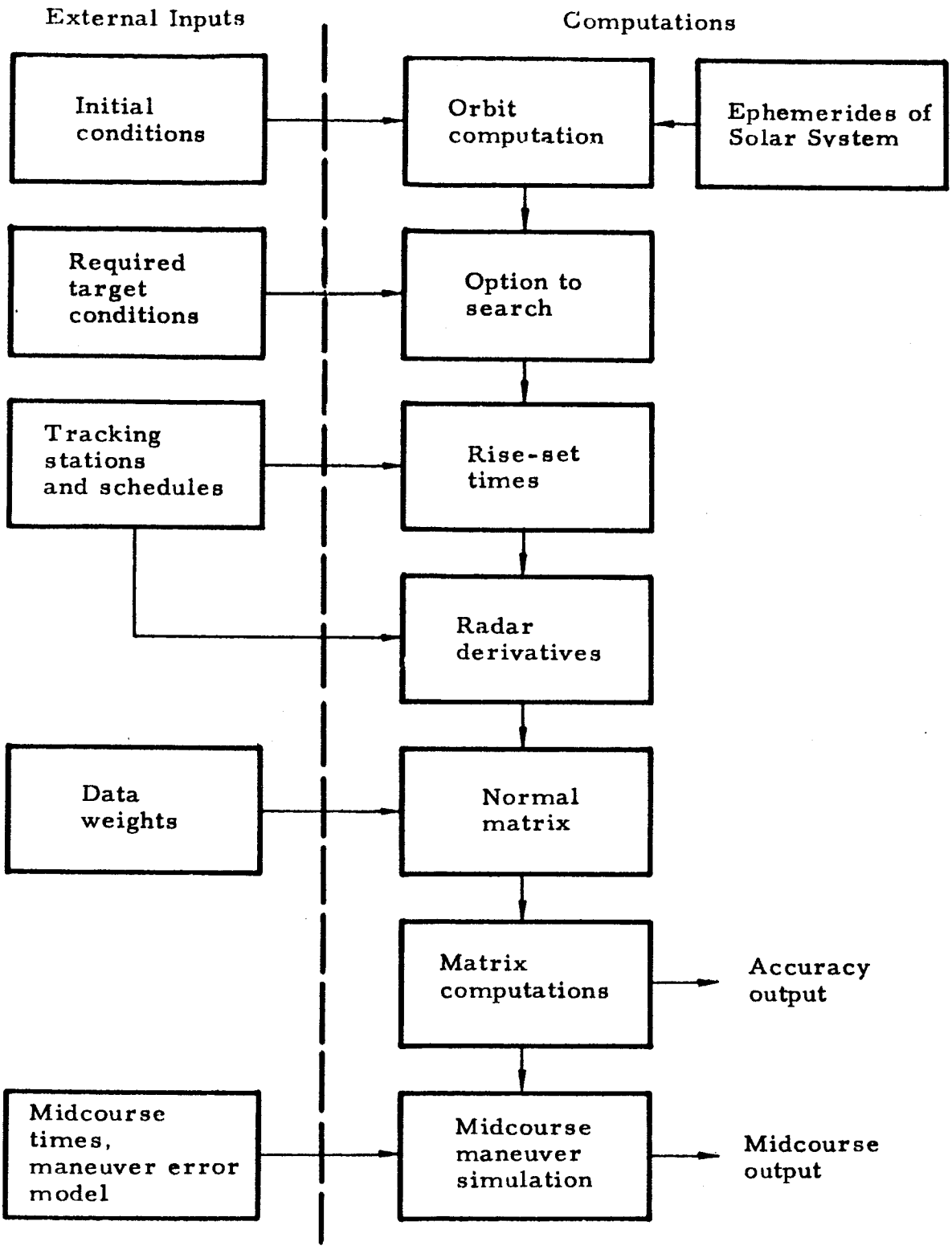

Figure 5-1. General Block Diagram

primary attracting centers, a succession of conics are matched together at the boundaries of the sphere of action for the various bodies. Such a procedure removes the necessity for any integration of the equations of motion. The computation scheme for orbits and variations is shown in Figure 5-2.

In addition, the ephemerides for the pertinent celestial bodies are computed from Kepler formulas using mean orbital elements which include secular variation terms but not periodic ones. A provision is made to accept osculating elements at a fixed epoch if higher accuracy is required. However, in most instances, the tracking accuracy should not be critically affected by small deviations in the positions of the celestial bodies from their actual position.

2. Search Routine

One required program input is a set of initial orbit conditions yielding approximately the desired final conditions at the target body. These input conditions will normally be obtained from one of the standard lunar or interplanetary trajectory design programs available. To allow for differences in computational models used by TAPP and other programs, a search routine is provided in TAPP to achieve a required set of final conditions. This is accomplished by a differential correction process on the initial conditions. Given an initial vector, x_o, which yields a reasonably close value of the required final vector b; the routine computes the differential coefficient matrix, $\left(\frac{\partial b}{\partial x_o}\right)$, and finds the correction vector

$$\delta x_o = \left(\frac{\partial b}{\partial x_o}\right)^{-1} \left[b \text{ (required)} - b \text{ (computed)}\right]$$

The new value $x_1 = x_o + \delta x_o$ are used to compute the new values b_1. The process is repeated until the required conditions are achieved. The search may be carried out by varying the injection conditions at the earth or the velocity at infinity on the escape hyperbola.

3. Rise and Set Times

To insure that the simulated observation times correspond realistically with the given orbit and tracking stations, visibility times from each station are computed over the period of interest.

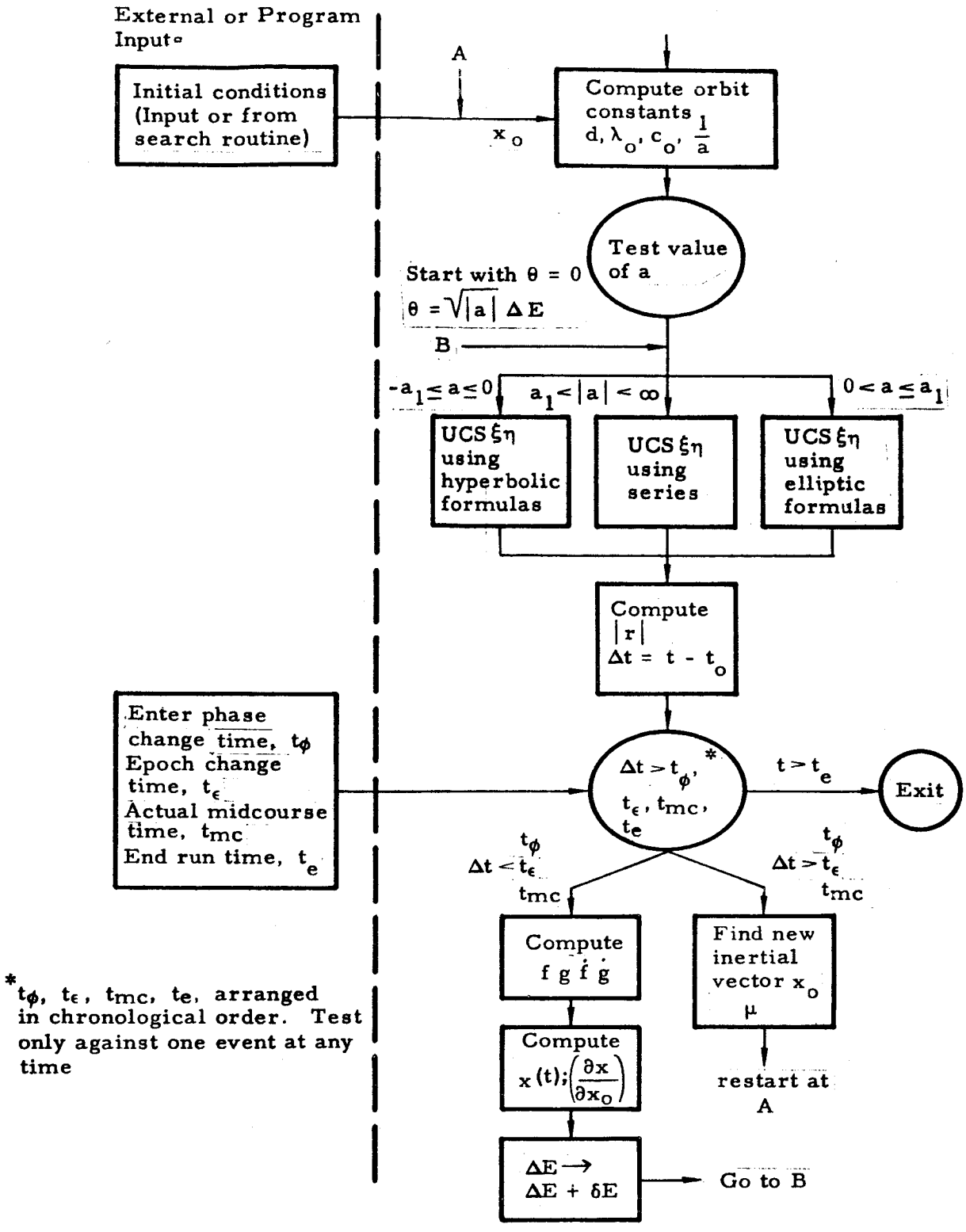

Figure 5-2. Orbit and Variational Equation Block Diagram

This is accomplished in the program by computing the elevation angle, E, from the tracker at prescribed intervals over the span of tracking. In particular, we compute

$$\delta = \sin E - \sin \gamma_o = \frac{R_s \cdot \rho}{|R_s| \, |\rho|} - \sin \gamma_o$$

where

R_s is the position vector of the station

ρ is the vector from station to spacecraft

γ_o is the minimum elevation before visibility is said to occur (usually different from zero)

The spacecraft is visible from a given station if $\delta \geq 0$. The rise-set intervals are found by interpolating for the times at which δ changes sign.

In case of lunar and deep space vehicles, the spacecraft has a slow angular rate with respect to the earth after the initial day or two. Since the station coordinates have a period of one sidereal day, the rise-set times on the n^{th} day are reasonable first approximations to the rise-set times on the $n + 1$st day. This fact is used to speed the determination of rise and set times over a long trajectory time span.

In anticipation of lunar satellites, the rise-set routine also finds the occultation times of the spacecraft by the moon. Only visible, non-occulted times are used in simulated observations.

4. Radar Derivatives

The radar derivatives are the regression coefficients appearing in the least squares estimation of x_o. In the present program they are obtained by use of the differentiation chain rule. Let R_i be the i^{th} radar observation; t the time of the observation; x(t) the position and velocity at time t; and x_o the value of x at the epoch, t_o;* then in matrix notation, $\left(\frac{\partial R_i}{\partial x_o}\right)$ is

*For illustrative purposes, we are considering x_o to be the initial condition vector. However, x_o may, in general, include physical constants elements as well.

$$\left(\frac{\partial R_i}{\partial x_o}\right) = \left(\frac{\partial R_i}{\partial x}\right)\left(\frac{\partial x}{\partial x_o}\right)$$

where

$\left(\frac{\partial R_i}{\partial x}\right)$ is the (1 x 6) matrix of derivatives of R_i with respect to x(t). It is obtained directly from the definitions of $R_i(x)$ by differentiation.

$\left(\frac{\partial x}{\partial x_o}\right)$ is the (6 x 6) variational matrix for the change $\delta x(t)$ due to an initial increment δx_o.

Since conic formulas are used to approximate the trajectory, $\left(\frac{\partial x}{\partial x_o}\right)$ is obtained by differentiation of the Kepler formulas.

5. Normal Matrix

Let R be the vector consisting of all the individual observations, R_i. The elements of the matrix $A = \left(\frac{\partial R}{\partial x_o}\right)$ are formed in accordance with a prescribed set of rules which dictate the type and frequency of the simulated tracking data. The normal matrix is then simply

$$A'WA = \left(\frac{\partial R}{\partial x_o}\right)' W \left(\frac{\partial R}{\partial x_o}\right)$$

where a prime denotes transpose, and W is the diagonal matrix of final weights assigned to the observations. W is computed in accordance with a set of rules which relate it to the noise moment matrix M. The matrix M will, in turn, be typically computed from Table 5-1.

6. Tracking Accuracy Output

The covariance matrix of the impact vector (or some appropriate substitute) is the criterion of tracking accuracy. To elaborate on its computation, we define the notations:

$\hat{R}$ - m vector of actual observations including noise

x_{ot} - n vector of true orbital parameters to be estimated

x_o - initial estimate of x_{ot}

Table 5-1. Typical Noise Model for Terrestrial Tracker

Data Type	Noise Source	σ (typical values)	σ (typical values)
angular	readout error	0.003	<10 seconds
measurements	antenna deflections	0.007	~5 hours
(each type)	jitter	0.01	<10 seconds
doppler shift	oscillator drift	$\left(\frac{\dot{f}}{f}\right) R$	T
	round off	$\frac{C}{2\sqrt{3\,fT}}$	<10 seconds
range	clock error	$K_C R$	1 hour
	systems error	5 meters	5 hours
	round off	10 meters	<10 seconds

R is the slant range

T is the counting interval

$(\dot{f}/f)$ is the percentage drift rate

C is the velocity of light

K_C = constant

p - q vector of parameters (usually physical constants) which affect the values of the computed observations but which are not being estimated

$R = R(x_o, p)$ - m vector of computed values of the observables based on the initial values, x_o and p

Γ_o - covariance matrix of the initial estimate, x_o

Λ_p - covariance matrix of the vector p (assumed given)

A - m x n matrix of partial derivatives, $\left(\frac{\partial R}{\partial x_o}\right)$

P - m x q matrix of partial derivatives, $\left(\frac{\partial R}{\partial p}\right)$

W - m x m diagonal matrix of final least squares weights

In most of the following, we absorb $\sqrt{W}$ into A and P matrices, i.e.,

$$A'WA \longrightarrow A'A \qquad \sqrt{W}A \longrightarrow A$$

$$A'WP \longrightarrow A'P \qquad \sqrt{W}P \longrightarrow P$$

In performing the least squares fit, we hold the vector p fixed but include the effects of its uncertainty in computing the covariance matrix of impact errors. In general, the p vector will include quantities such as mass of the earth, moon, station loaction, velocity of light, etc. The errors in x_o, p, and the noise on the observations are assumed to be independent of each other for the present.

If the assumed values of p coincides with the true values, p_t, then the least squares estimate of x_{ot} is the value x_{ls} which minimizes the weighted sum

$$S = \left[\hat{R} - R(x_o, p_t) - A(x_{ls} - x_o)\right]' W \left[\hat{R} - R(x_o, p_t) - A(x_{ls} - x_o)\right]$$

If, in addition, x_o is an a priori estimate of x_{ot} with covariance matrix Γ_o, then the combined least squares and a priori estimate, $\tilde{x}_o$, is obtained

from the equation*

$$\tilde{x}_o = x_o + K A' \left[\hat{R} - R(x_o, p_t) \right] \qquad (5.1)$$

$$K = (A'A + \Gamma_o^{-1})^{-1}$$

A small increment $\delta p = p - p_t$ will yield a slightly different estimate, $\hat{x}_o$, where

$$\hat{x}_o = x_o + K A' \left[\hat{R} - R(x_o\, p) - P\, \delta p \right] \qquad (5.2)$$

If $\delta\hat{x}_o = \hat{x}_o - x_{ot}$ and $\delta x_o = x_o - x_{ot}$, we obtain from (5.2)

$$\delta\hat{x}_o = \delta x_o + K A' \left[\hat{R} - R(x_{ot}, p_t) - A\, \delta x_o - P\, \delta p \right] \qquad (5.3)$$

$$= K \left[A'\, \delta R - A'P\, \delta p + \Gamma_o^{-1}\, \delta x_o \right]$$

---

* If $\Gamma_o = 0$ (no a priori knowledge), the estimate of x_{ot} reduces to x_{ls} where

$$x_{ls} = x_o + (A'A)^{-1} A' \left[R - R(x_o, p_t) \right] \qquad (5.1a)$$

which is the usual formula based on a least squares criterion. Equation (5.1) combines the a priori estimate with the least squares estimate, all into one operation. As shown in Reference [17], it is equivalent to finding the least squares fit as in (5.1a), and then combining with the a priori estimate in accordance with the formula

$$\tilde{x}_o = \left[\Lambda_{ls}^{-1} + \Gamma_o^{-1} \right]^{-1} \left[\Lambda_{ls}^{-1}\, x_{ls} + \Gamma_o^{-1}\, x_o \right] \qquad (5.1b)$$

where Λ_{ls} is the covariance matrix of x_{ls}. The methods are equivalent and the covariance matrix of $\tilde{x}_o$ is given by the first term of (5.4) if one assumes that there are no errors in p.

The covariance matrix of the estimate is

$$\Lambda_o = \overline{\delta\hat{x}_o \, \delta\hat{x}_o'} = K\left[J + A' P \Lambda_p P' A\right] K \tag{5.4}$$

$$J = A' N A + \Gamma_o^{-1} \tag{5.5}$$

where the bar denotes an enxemble average and Λ_p is the a priori covariance matrix of p; N is the product of the diagonal matrix of the variances on the noise and the weighting matrix W. The matrix, A, always has included in it the factor $\sqrt{W}$; otherwise an additional factor of W would appear in (5.5). Figure 5-3 is a flow diagram of the orbit determination simulation.

The differential errors in the impact vector, $b = b(x_o, p)$ are related linearly to $\delta\hat{x}_o$ and δp. We have

$$\delta b = \lambda \, \delta\hat{x}_o + \mu \delta p$$

where

$$\lambda = \left(\frac{\partial b}{\partial x_o}\right)$$

$$\mu = \left(\frac{\partial b}{\partial p}\right)$$

$$\nu = -KA' P$$

The covariance matrix of b is

$$\Lambda_b = \overline{\delta b \, \delta b'} = \overline{(\lambda \, \delta\hat{x}_o + \mu\delta p)(\lambda \, \delta\hat{x}_o + \mu\delta p)'}$$

$$= \lambda \, KJK\lambda' + (\mu + \lambda \nu) \, \Lambda_p \, (\mu + \lambda\nu)' \tag{5.6}$$

λ and μ are the usual explicit partial derivatives of b with respect to x_o and p respectively. $\delta b = \lambda\nu\delta p$ is an additional error term in b due to an error in $\hat{x}_o$ arising from an incremental change δp.

Equation (5.6) is the formula for finding Λ_b when δx_o and δp are independent. Since Λ_b is the criterion which measures the tracking accuracy,

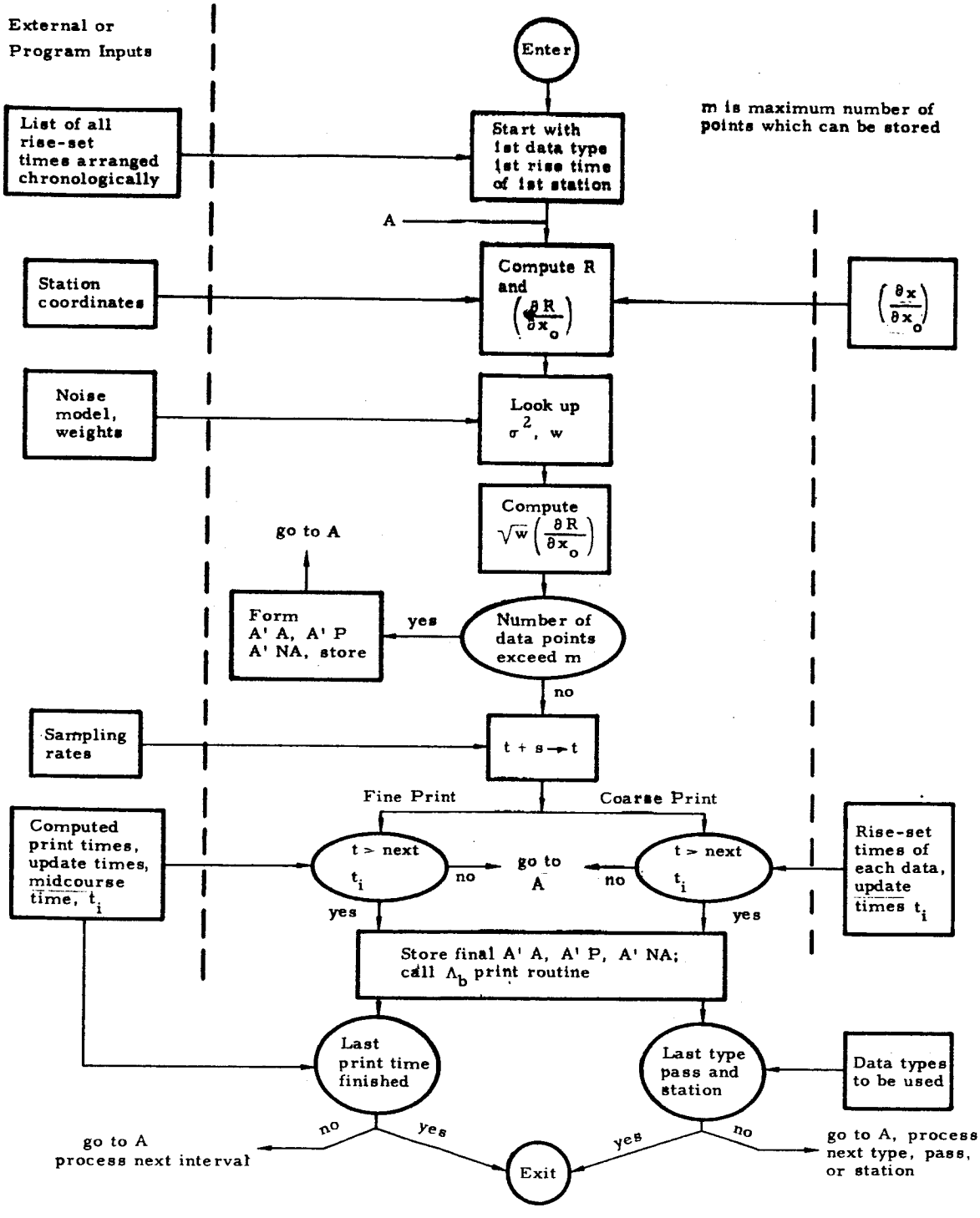

Figure 5-3. Data Processor Block Diagram

much of the remainder of this write-up deals with the details and options pertaining to its computation from hypothetical observations.

As shown in Figure 5-4, the impact parameter b is a vector consisting of the two components of the miss vector, $\bar{m} = \begin{pmatrix} m_1 \\ m_2 \end{pmatrix}$ and the total flight time, t_f.

$$b = \begin{bmatrix} m_1 \\ m_2 \\ t_f \end{bmatrix}$$

m_1 and m_2 define a plane which will be called the impact parameter plane. $\Lambda_b = \overline{\delta b\, \delta b'}$ is a 3 x 3 matrix whose upper left hand 2 x 2 is given by $\Lambda_m = \overline{\delta m\, \delta m'}$. We rewrite this as

$$\Lambda_m = \begin{bmatrix} \sigma_1^2 & \rho\sigma_1\sigma_2 \\ \rho\sigma_1\sigma_2 & \sigma_2^2 \end{bmatrix} \tag{5.7}$$

The quadratic form $\delta m'\, \Lambda_m^{-1}\, \delta m$ = constant describes a dispersion ellipse of constant probability in the (m_1, m_2) plane. Λ_m may be diagonalized by means of an orthogonal transformation to new variables M where

$$M = Um$$

so that

$$\Lambda_M = U\Lambda_m U' = \begin{pmatrix} \lambda_1 & 0 \\ 0 & \lambda_2 \end{pmatrix} \tag{5.8}$$

U is a rotation from the m_1 axis to the major axis of the dispersion ellipse. The angle of rotation is θ where (assume $\sigma_1 \geq \sigma_2$)

$$\theta = \frac{1}{2} \tan^{-1} \frac{2\rho\sigma_1\sigma_2}{\sigma_1^2 - \sigma_2^2} \tag{5.9}$$

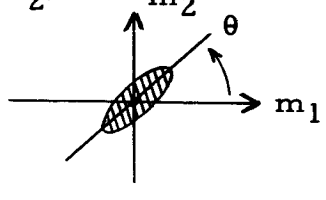

The quantities Λ_b, Λ_M, and θ are computed at various stages of the simulation as an indication of the tracking accuracy.

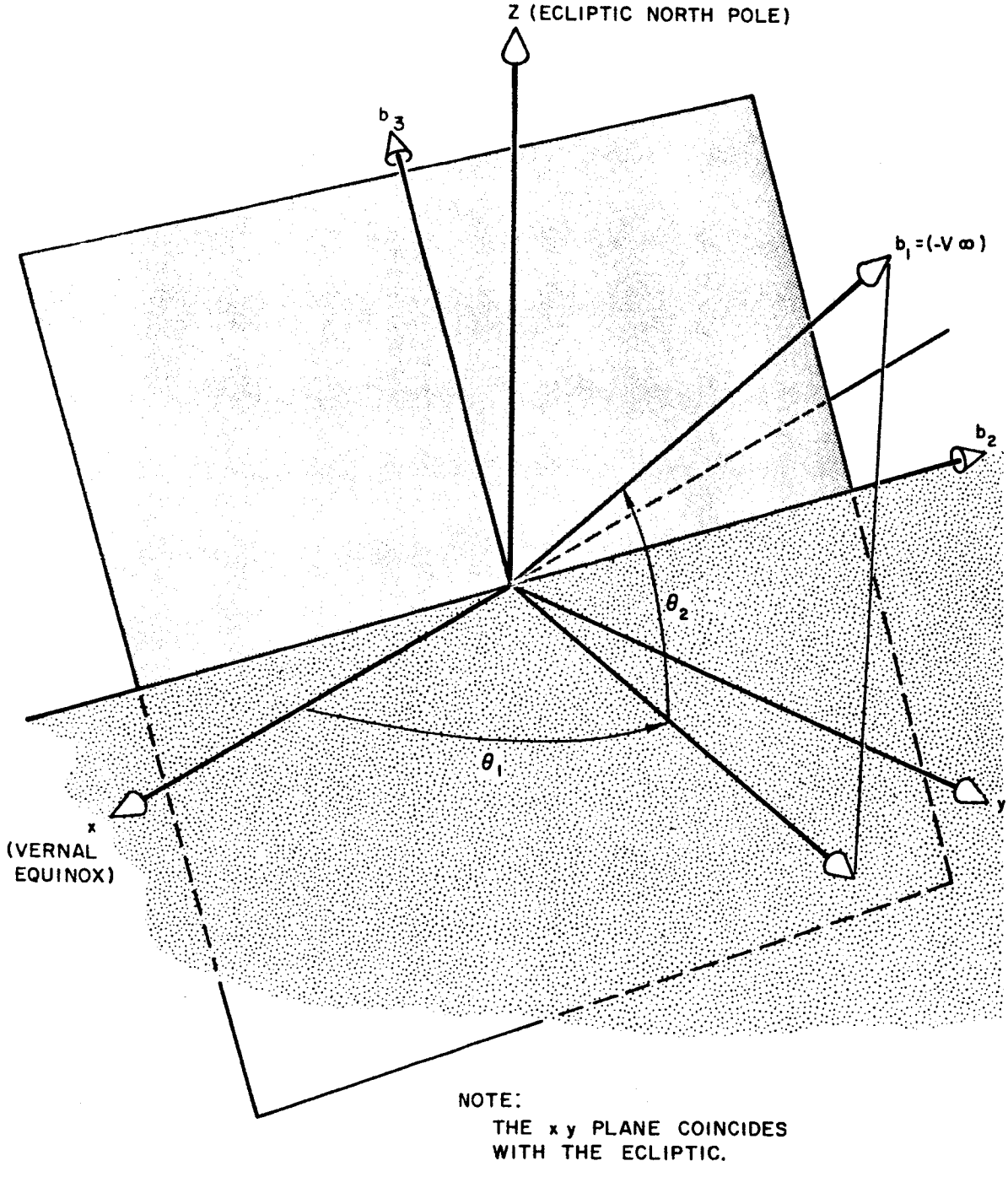

Figure 5-4. Illustration of the B-Plane Coordinate System

7. Midcourse Maneuvers

Another use of the program is to simulate the errors of a midcourse velocity correction. This is done by supplementing Λ_b with an error covariance matrix due to the imperfect execution of the maneuver. Since the maneuver system errors and the tracking noise are assumed to be independent, the covariance matrices from the two sources add directly. The program may be instructed to perform either a hypothetical or an actual maneuver.

The difference between them is that in the first case the correction velocity errors are not propagated into the future. Their effects on Λ_b are computed at the time of the hypothetical maneuver and are dropped for further calculations. The object is to display the effects on Λ_b of the maneuver errors at various points along the orbit as the amount of tracking and the error coefficients vary in time.

In contrast, the simulation of an actual midcourse implies that the maneuver errors are permanently implanted in the orbit as they always are in real life. All computations of Λ_b after the maneuver will have included in them the errors arising from the performance of the maneuver. In both cases we assume that the mean of the midcourse velocity magnitude is zero so that the orbit remains unaltered from the nominal even though the errors are added on. This a a valid procedure if everything is linear, i.e., the error coefficients do not change rapidly in the vicinity of the nominal. The program may be required to perform a series of hypothetical maneuvers but only one actual one at this time.*

a. Hypothetical Maneuvers (abbreviated hm)

Usually, a sequence of the hypothetical maneuvers are called for along an orbit. To illustrate the effect of the i^{th} point, use the symbols:

Λ_{bi} = covariance matrix of b just prior to the i^{th} hm

Λ_{ai} = covariance matrix of b just after the i^{th} hm

*TAPP Mod II, under development, will have a multiple midcourse maneuver capability.

Λ_e = covariance matrix of velocity errors due to imperfect execution of the required maneuver. Λ_e is a 3 x 3 matrix but may be used as a partitioned 6 x 6 matrix $\Lambda_e = \begin{pmatrix} 0 & 0 \\ 0 & \Lambda_e \end{pmatrix}$

x_i = (r_i, v_i) - the spacecraft position and velocity vector with respect to the force center at t_i, the time of the i^{th} hm

Λ_i = covariance matrix of x_i due to tracking

x_o = position and velocity at the initial epoch, t_o, of the phase during which the maneuver occurs

Λ_o = covariance matrix of x_o due to tracking only

A straightforward way of computing Λ_{bi} is to update the epoch to the i^{th} hm; compute Λ_i due to tracking; Λ_{bi} is just $\Lambda_{bi} = \left(\frac{\partial b}{\partial x_i}\right) \Lambda_i \left(\frac{\partial b}{\partial x_i}\right)'$.

Λ_{ai} is found by replacing Λ_i by $\Lambda_i + \Lambda_e$ in Λ_{bi}. However, frequent updating involves some tedious matrix manipulations if physical constants are involved. A somewhat simpler scheme is used for hm's in the present program by keeping the epoch at t_o. At t_i compute

$$\Lambda_{oi} = \left(\frac{\partial x_o}{\partial v_i}\right) \Lambda_e \left(\frac{\partial x_o}{\partial v_i}\right)'$$

after which

$$\Lambda_{ai} = \Lambda_{bi} + \left(\frac{\partial b}{\partial x_o}\right) \Lambda_{oi} \left(\frac{\partial b}{\partial x_o}\right)' = \left(\frac{\partial b}{\partial x_o}\right) (\Lambda_o + \Lambda_{oi}) \left(\frac{\partial b}{\partial x_o}\right)'$$

(neglecting physical constant errors in this case)

For computational purposes, $\left(\frac{\partial x_o}{\partial v_i}\right)$ is obtained from $\left(\frac{\partial x_i}{\partial x_o}\right)^{-1}$ in which $x_i = (r_i, v_i)$ i.e.

$$\left(\frac{\partial x_o}{\partial x_i}\right) = \left(\frac{\partial x_i}{\partial x_o}\right)^{-1} = \left[\begin{array}{c} \frac{\partial x_o}{\partial r_i} \\ \hline \frac{\partial x_o}{\partial v_i} \end{array}\right]$$

b. Actual Maneuvers

After an actual maneuver, the epoch is moved to the time of the maneuver. Calling the new point (t_o, x_o) with a priori covariance matrix Λ_o, then

$$\Lambda_a = \left(\frac{\partial b}{\partial x_o}\right) (\Lambda_o + \Lambda_e) \left(\frac{\partial b}{\partial x_o}\right)'$$

If more tracking data is added after t_o, then the effects of the new data can be incorporated into the covariance matrix of x_o by the formula

$$\tilde{\Lambda}_o = K J K$$

where

$$K = \left[(\Lambda_o + \Lambda_e)^{-1} + A_1' A_1\right]^{-1}$$

$$J = A_1' N_1 A_1 + (\Lambda_o + \Lambda_e)^{-1}$$

A_1 and N_1 are quantities referring to the new data having meanings which correspond to A and N in (5.5). The covariance matrix for b is then simply

$$\Lambda_a = \left(\frac{\partial b}{\partial x_o}\right) \tilde{\Lambda}_o \left(\frac{\partial b}{\partial x_o}\right)'$$

The program also covers the more complicated case where physical constant uncertainties are considered.

•REFERENCES

FORMAL TECHNICAL REPORTS

1. Steiner, P. "Lunar Powered Flight." Space Technology Laboratories, Inc., 8976-0004-RU-000, 10 August 1961.

2. Penzo, P.A., I. Kliger and C.C. Tonies. "Computer Program Guide: Analytic Lunar Return Program." Space Technology Laboratories, Inc., 8976-0005-MU-000, 23 August 1961.

3. Magness, T.A., P.A. Penzo, P. Steiner and W.H. Pace. "Trajectory and Guidance Considerations for Two Lunar Return Missions Employing Radio Command Midcourse Guidance." Space Technology Laboratories, Inc., 8976-0007-RU-000, 29 September 1961.

4. Penzo, P.A. "An Analysis of Moon-to-Earth Trajectories," Space Technology Laboratories, Inc., 8976-0008-RU-000, 30 October 1961.

5. Magness, T.A. and J.B. McGuire. "Statistics of Orbit Determination - Correlated Observations." Space Technology Laboratories, Inc., 8976-6001-RU-000, 15 December 1961.

6. Magness, T.A. and J.B. McGuire. "Statistics of Orbit Determination - Weighted Least Squares." Space Technology Laboratories, Inc., 8976-6002-RU-000, 15 January 1962.

7. Wong, L., A.S. Liu, M.C. Fujisaki and O. Senda. "Computer Program Guide: Tracking Accuracy Prediction Program (TAPP Mod I)." Space Technology Laboratories, Inc., 8976-6005-NU-000, 8 February 1962.

INFORMAL MEMORANDA

8. White, J.F. "Parametric Evaluation of Powered Flight from the Moon." Space Technology Laboratories, Inc., 9861.2-4, 2 March 1961.

9. Penzo, P.A. "Analytic Lunar Return Program - I." Space Technology Laboratories, Inc., 9861.3-13, 6 March 1961.

10. Ireland, R.O., T.A. Magness and J.B. McGuire. "Effects of Uncertainties in Physical Constants on Ranger Mission." Space Technology Laboratories, Inc., 9861.5-11, 17 March 1961.

11. Magness, T.A., and J.B. McGuire. "Comparison of Least Squares and Minimum Variance Regression Analysis, Part I - Theoretical Analysis." Space Technology Laboratories, Inc., 9861.5-20, 30 March 1961.

12. Skidmore, L. J. "Midcourse Guidance Techniques and Error Analysis for Moon-to-Earth Spacecraft." Space Technology Laboratories, Inc., 9861.5-17, 31 March 1961.

13. Steiner, P. "Lunar Launch Error Analysis - I: Basic Theory." Space Technology Laboratories, Inc., 9861.5-19, 31 March 1961.

14. Magness, T.A. and J.B. McGuire. "Statistics of Orbit Determination - I: Physical Constants." Space Technology Laboratories, Inc., 9861.5-22, 14 April 1961.

15. Magness, T.A. "Correlation and Data Density Simulation." Space Technology Laboratories, Inc., 9861.5-23, 19 April 1961.

16. Wong, L. "Analytic Tracking Program." Space Technology Laboratories, Inc., 9861.5-24, 24 April 1961.

17. Magness, T.A. "Statistics of Orbit Determination - A Priori Estimates." Space Technology Laboratories, Inc., 9861.5-25, 26 April 1961.

18. Penzo, P.A. "Addition of a Moon-to-Earth Search Routine to the Encke Program." Space Technology Laboratories, Inc., 9861.3-26, 5 May 1961.

19. McGuire, J.B. "Variational Equations - Part I." 20 May 1961.

20. Tompkins, E.H. "SSAS Preliminary Briefing Charts for Moon-to-Earth Flights." Space Technology Laboratories, Inc., 9861.0-15, 12 June 1961.

21. Wong, L. and T. Liu. "Partial Derivatives for Analytic Tracking Accuracy Prediction Program." Space Technology Laboratories, Inc., 9861.5-29, 13 June 1961.

22. Magness, T.A. "Spectral Theory of Regression Analysis." Space Technology Laboratories, Inc., 9861.5-28, 16 June 1961. Revised and Expanded, 16 June 1961.

23. Penzo, P.A., I. Kliger and C.C. Tonies. "Production Report on Analytic Lunar Return Program." Space Technology Laboratories, Inc., 9861.0-16, 12 July 1961.

24. Magness, T.A. and J.B. McGuire. "On the Comparison of Least Squares and Minimum Variance." Space Technology Laboratories, Inc., 9861.5-31, 21 July 1961.

25. Skidmore, L.J. and P.A. Penzo. "Monte Carlo Simulation of Midcourse Guidance Schemes for Lunar Return Flights." Space Technology Laboratories, Inc., 9321.4-120, 25 July 1961.

26. Magness, T.A. and J.B. McGuire. "Orbit Determination by Filtering." Space Technology Laboratories, Inc., 9861.5-34, 16 August 1961.

27. Penzo, P.A. "A Preliminary Investigation of Circumlunar Trajectories." Space Technology Laboratories, Inc., 9861.3-76, 6 September 1961.

28. Penzo, P.A. "Modifications and Additions to the Analytic Lunar Program." Space Technology Laboratories, Inc., 9861.3-75, 6 September 1961.

29. Penzo, P.A. "A Graphical Addendum to the Moon-to-Earth Trajectory Analysis." Space Technology Laboratories, Inc., 9861.3-106, 21 November 1961.

30. Penzo, P.A. "Modifications in the Lunar and Lunar Return Programs to Implement the Lunar Fly-by Return Propulsion Study." Space Technology Laboratories, Inc., 9861.3-115, 12 December 1961.

31. Pace, W.H., Jr. "Monte Carlo Simulation of Midcourse Guidance for TAPP-II." Space Technology Laboratories, Inc., 9861.5-55, 1 March 1962.

GENERAL REFERENCES

32. Egorov, V.A. "Some Problems Relating to the Dynamics of Flight to the Moon," Proc. VIII Int'l. Astronaut. Federation Cong., Springer Verlag Wien, 1958.

33. Grenander, U. and M. Rosenblatt. "Statistical Analysis of Stationary Time Series," John Wiley and Sons, New York, 1957.

34. Hoel, P.G. "Asymptotic Efficiency in Polynomial Estimation," Annals of Mathematical Statistics, 32, pp 1042-1047 (December 1961).

35. Lass, H. and C. Solloway. "On An Integral Arising in the Theory of Midcourse Maneuvers," Jet Propulsion Laboratory Technical Memo No. 312-150.

36. Smith, G.L. and S.F. Schmidt. "The Application of Statistical Filter Theory to Optimal Trajectory Determination On-Board a Circumlunar Vehicle," paper presented at the American Astronautical Society Meeting, San Francisco, 3 August 1961.

37. Herrick, S. "Positions, Velocities, Ephemerides Referred to the Dynamical Center," Astrodynamical Report No. 7, AFOSR TN-60-773, July 1960.